R. & M. No. 3676

MINISTRY OF DEFENCE
AERONAUTICAL RESEARCH COUNCIL
REPORTS AND MEMORANDA

The Theoretical Treatment of Slowly Oscillating Part-Span Control Surfaces in Subsonic Flow

By H. C. Garner and Doris E. Lehrian
Aerodynamics Division N.P.L.

LONDON: HER MAJESTY'S STATIONERY OFFICE
1971
PRICE £2·60 NET

The Theoretical Treatment of Slowly Oscillating Part-Span Control Surfaces in Subsonic Flow

By H. C. Garner and Doris E. Lehrian
Aerodynamics Division N.P.L.

Reports and Memoranda No. 3676*
October, 1969

Summary.

To first order in frequency, subsonic lifting-surface theory is applied to arbitrary configurations of a thin wing and a trailing-edge control. The discontinuities in flow direction at the hinge line and part-span boundaries are surmounted by independent consideration of smooth equivalent slopes in the chordwise and spanwise directions; the combined equivalent incidences depend on the aerodynamic quantities to be evaluated. The present method yields satisfactory values for lift, pitching and rolling moments, hinge moment and the associated spanwise distributions, but does not determine the complete load distribution due to an oscillating control.

Illustrative examples cover four planforms, namely, rectangular and cropped delta wings for which there are experimental data on hinge moment, an untapered swept wing that has been studied by electrical analogue, and a tapered swept wing to be the subject of future experiments. The solutions for each planform are tabulated and plotted as functions of control chord, control span or Mach number and are examined from the standpoint of numerical convergence with respect to the number of chordwise collocation points. Consideration is given to the transformed aerodynamic problem on the reversed wing by application of the reverse-flow theorem, and these alternative numerical results strengthen confidence in the present method and give some indication of the likely accuracy. The optimum central rounding of swept edges is discussed together with many other refinements of numerical technique.

A broad conclusion is that significant wing forces can be calculated to at least two-figure accuracy. The approximations in the method are such that the true theoretical values of hinge moment are likely to be within 2 per cent of the calculated stiffness derivative and within 10 per cent of the calculated damping, provided that there is due attention to the choice of equivalent incidences. Comparisons with wind-tunnel data tend to show larger discrepancies, which can be reconciled with rough predictions from charts based on two-dimensional static tests. A simple empirical correction to the theoretical hinge-moment damping is suggested, which reproduces the available experimental data within ± 10 per cent.

LIST OF CONTENTS

* Replaces N.P.L. Aero Report 1303—A.R.C. 31 490.

LIST OF CONTENTS—*continued*

Section

LIST OF TABLES

Tables

LIST OF TABLES—*continued*

LIST OF ILLUSTRATIONS

Figure

---

1. *Introduction.*

The aerodynamic problem to be considered is that of a hinged control surface extending streamwise from the hinge to the trailing edge and of arbitrary spanwise extent. The main wing surface is at rest in a uniform subsonic airstream and the control surface is oscillating with small amplitude. There is a requirement for a theoretical method of calculating the aerodynamic loading that would occur in linearized potential flow, but it is recognized that in practice the influence of boundary layers is paramount; in consequence, such a theoretical method should be a prelude to semi-empirical development. The paucity of relevant theoretical and experimental data must therefore be overcome as a matter of some urgency.

The theoretical treatment for a general frequency of oscillation is discussed in Refs. 1 and 2. The crux of the problem is the discontinuity in flow direction where the control surface adjoins the main wing. By means of the reverse-flow theorem, Davies[1] formulates a smooth mode of oscillation that gives smooth generalized forces identical to those resulting from the oscillating control; in other words, he formulates smooth 'equivalent slopes' that can replace the true discontinuous downwash condition in the original problem. The second author[2] has successfully developed and applied the principles of Ref. 1 to determine lift and pitching moment; she has also examined the consequence of using the same 'equivalent slopes' to evaluate hinge moments, for which the force mode is no longer smooth, and finds evidence of large inconsistencies without the possibility of assessing accuracy. It is therefore essential to consider an alternative approach to the calculation of load distribution or hinge moment, the latter being of special importance in flutter prevention.

A feature of Refs. 1 and 2 is that, apart from the linear dependence on frequency of the downwash out

of phase with the control deflection, the equivalent slopes are little affected by changes in frequency within its practical range. It is therefore considered that an attack on the low-frequency problem will have wider applications. The relevant background to the treatment of slowly oscillating lifting surfaces is provided in Refs. 3 to 6. Multhopp's[3] steady subsonic theory is extended to slow pitching oscillations in Ref. 4, which has been further developed in Ref. 5 by the first author and Fox; the numerical technique has been improved so that up to four terms in the chordwise loading and the same number of solving points in the chordwise direction can be used without loss of accuracy (Section 2). Applications of the reverse-flow theorem are discussed in Ref. 6, in Section 5.2 of which the present authors formulate the lift and pitching moment due to control oscillations in terms of theoretical solutions for the reversed wing. These results for lift and pitching moment provide an important check on the approach to equivalent slopes adopted in the present report, where chordwise and spanwise discontinuities are considered separately (Sections 3 and 4). The combined procedure in Section 5.1 can be shown to be successful for lift and pitching moment; being applicable to spanwise loading and hinge moments as well, it can be used to determine these with some confidence.

The rectangular, untapered swept, tapered swept, and cropped delta wings, for which illustrative calculations have been made, are chosen specifically to allow comparisons with results from other sources. By electrical analogy Enselme[7] has obtained the steady spanwise loading on the untapered swept wing with part-span controls. The tapered swept wing with outboard half-span controls is chosen partly because oscillatory experiments on this configuration are planned at the N.P.L., but also because it has been the subject of theoretical investigation, both in Ref. 2 and by Woodcock[8]. The rectangular wing with full-span control has been tested at low speeds, and Molyneux and Ruddlesden[9] give experimental values of the oscillatory hinge moment. For the cropped delta wing with full-span control the hinge moment has been measured by Bratt[10], and these tests include the upper range of subsonic Mach number. The discussion of results for each of the four wings (Section 6) includes the effects of part-span, and in the cases of the tapered swept and cropped delta wings the spanwise distribution of hinge-moment damping is considered.

The question of accuracy is difficult; apart from two-dimensional theory and slender-wing or classical lifting-line theory from which the equivalent slopes are derived, no exact solutions are available for comparison with the present method. Convergence with respect to the number of chordwise variables can be considered, and inconsistencies can be revealed by procedures involving the reverse-flow theorem (Appendix). The problem of control hinge-moment is further complicated by the different criteria of accuracy demanded by the theoretician and the practical aerolastician. The present objective is to achieve sufficient theoretical accuracy that, after suitable experimental data have been acquired, semi-empirical adaptation of the method will seem worth while. In the meantime the simplest form of empirical correction to damping derivatives is suggested in Section 7 with supporting evidence from measurements of hinge moment.

2. *Low-Frequency Lifting-Surface Theory.*

The present investigation is essentially the application of Ref. 5 to the evaluation of aerodynamic derivatives associated with a control surface. The symbols relating to planform geometry are given in Fig. 1a, which also defines the mode of control rotation. The boundary condition to be satisfied by the upward component of velocity takes the usual form

$$\frac{w}{U} = \mathscr{R}\left[\left(\frac{\partial z}{\partial x}+\frac{i\omega z}{U}\right)e^{i\omega t}\right], \tag{1}$$

where ω is the circular frequency of oscillation and the mode is

$$z = -\theta_0(x-x_0) \text{ for pitching about } x = x_0 \tag{2}$$

or for control rotation* about the hinge $x = x_h(y)$

$$\left.\begin{aligned} z &= -\xi_0(x-x_h) \text{ on the starboard control surface} \\ z &= -\varepsilon\,\xi_0(x-x_h) \text{ on the port control surface} \\ z &= 0 \text{ elsewhere on the planform} \end{aligned}\right\} \tag{3}$$

with $\varepsilon = \pm 1$ corresponding to symmetry or antisymmetry. In order to apply Ref. 5, the leading and trailing edges of the planform are, if necessary, rounded to have continuous curvature. As discussed in Section 6 of Ref. 11, the central rounding of swept planforms needs care; for uniform sweepback and straight taper the leading edge and chord over the range $|y| < y_i$ are modified to become respectively

$$\left.\begin{aligned} x_l(y) &= x_l(y_i) f(\lambda) \\ c(y) &= c_r + \{c(y_i) - c_r\} f(\lambda) \end{aligned}\right\}, \tag{4}$$

where $\lambda = |y|/y_i$. In Ref. 5

$$f(\lambda) = \lambda + \tfrac{1}{6}(1-\lambda)^6 \text{ and } y_i = s \sin\frac{\pi}{m+1}\,; \tag{5}$$

however, as discussed in Section 6.2, there are advantages in following Ref. 12 and taking

$$f(\lambda) = \tfrac{1}{3} + \lambda^2 - \tfrac{1}{3}\lambda^3\,. \tag{6}$$

Both shapes of rounding will be used, but for general formulation it is immaterial whether equation (5) or (6) is chosen.

Given a smooth planform, the load distribution can be taken as

$$\Delta p = \tfrac{1}{2}\rho U^2\, \mathscr{R}\left[l(x,y) \exp\left(i\omega t + \frac{i\omega M^2 x}{\beta^2 U} \right) \right] \tag{7}$$

with the usual expression

$$\begin{aligned} l(x,y) = \frac{8s}{\pi c(y)} \Big[& \gamma(y) \cot\tfrac{1}{2}\phi + 4\mu(y)\,(\cot\tfrac{1}{2}\phi - 2\sin\phi) + \\ & + \kappa(y)\,(\cot\tfrac{1}{2}\phi - 2\sin\phi - 2\sin 2\phi) + \\ & + \lambda(y)\,(\cot\tfrac{1}{2}\phi - 2\sin\phi - 2\sin 2\phi - 2\sin 3\phi) \Big], \end{aligned} \tag{8}$$

where $\gamma(y)$, $\mu(y)$, ... are complex and the angular co-ordinate ϕ is given by

$$x = x_l(y) + \tfrac{1}{2}\, c(y)\,(1-\cos\phi)\,. \tag{9}$$

---

*ξ_0, the amplitude of control rotation relative to the stream direction, corresponds to a true rotation through the larger angle $\xi_{0T} = \xi_0 \sec \Lambda_h$ about a swept hinge.

The spanwise distribution of each function $\gamma(y), \mu(y), \ldots$ is represented by Multhopp's interpolation polynomial from Appendix IV of Ref. 3

$$g(\theta) = (-1)^{\frac{1}{2}(m+1)} \sum_{n=-u}^{u} g(\theta_n) \frac{(-1)^{n-1} \sin\theta_n \sin(m+1)\theta}{(m+1)(\cos\theta - \cos\theta_n)}, \tag{10}$$

where $y = s\cos\theta$, $y_n = s\cos\theta_n = s\sin\dfrac{n\pi}{m+1}$, m is an odd integer and $u = \frac{1}{2}(m-1)$. Thus, if N represents the number of functions $\gamma(y), \mu(y), \ldots$, the quantity $l(x, y)$ involves mN unknowns

$$\gamma(y_n) = \gamma_n, \mu(y_n) = \mu_n, \ldots (n = 0, \pm 1, \ldots \pm u). \tag{11}$$

With the aid of equation (1) the integral relation between w/U and l to first order in frequency from equation (5) of Ref. 5 becomes

$$\left(\frac{\partial z}{\partial x} + \frac{i\omega z}{U}\right)\left(1 - \frac{i\omega M^2 x}{\beta^2 U}\right) = \frac{\beta^2}{8\pi} \int_{-\infty}^{x} \iint_{S} \frac{l(x', y')\, dx'\, dy'}{[(x_0 - x')^2 + \beta^2(y - y')^2]^{3/2}} \left\{1 + \frac{i\omega(x_0 - x)}{\beta^2 U}\right\} dx_0, \tag{12}$$

where for a subsonic Mach number M, $\beta^2 = 1 - M^2$ and S denotes the area of the planform. It remains to satisfy equation (12) at the mN collocation points $(x, y) = (x_{pv}, y_v)$ given by

$$\left.\begin{aligned} x_{pv} &= x_l(y_v) + \tfrac{1}{2}c(y_v)(1 - \cos\phi_p) \\ &= x_{lv} + \tfrac{1}{2}c_v(1 - \cos\phi_p) \\ \phi_p &= 2\pi p/(2N+1) \qquad (p = 1, 2, \ldots N) \\ y_v &= s\sin\frac{v\pi}{m+1} \qquad (v = 0, \pm 1, \ldots \pm u) \end{aligned}\right\}, \tag{13}$$

which are illustrated in Fig. 1b. The resulting linear simultaneous equations will determine the unknowns indicated in equation (11).

To evaluate equation (12), the integrations with respect to x_0 and x' are carried out analytically in terms of the influence functions in equations (12) and (13) of Ref. 5. The final spanwise integral takes the form

$$\left(\frac{\partial z}{\partial x} + \frac{i\omega z}{U}\right)\left(1 - \frac{i\omega M^2 x}{\beta^2 U}\right) = \frac{1}{2\pi} \int_{-s}^{s} \left\{H_1(x, y, y') - \frac{i\omega\bar{c}}{\beta^2 U} H_2(x, y, y')\right\} \frac{s\, dy'}{(y - y')^2}, \tag{14}$$

where the geometric mean chord $\bar{c}$ is used as reference length and the functions H_1 and H_2 are linear in $\gamma(y'), \mu(y'), \ldots$ and are defined in equations (11) of Ref. 5. The polynomial (10) is then fitted to H_1 and H_2, but to achieve adequate representation the odd integer m is usually increased to

$$\bar{m} = q(m+1) - 1, \tag{15}$$

where q is an even integer. By mathematical integration for each collocation point equation (14) becomes

$$\left\{\bar{H}_1(x_{pv}, y_v) - \frac{i\omega\bar{c}}{\beta^2 U}\bar{H}_2(x_{pv}, y_v)\right\} -$$

$$-\sum_{n=-\bar{u}}^{\bar{u}}{}' a_{v\bar{n}}\left\{H_1(x_{pv}, y_v, y_{\bar{n}}') - \frac{i\omega\bar{c}}{\beta^2 U}H_2(x_{pv}, y_v, y_{\bar{n}}')\right\}$$

$$= -\frac{1}{b_{vv}}\left(\frac{\partial z}{\partial x} + \frac{i\omega z}{U}\right)_{pv}\left(1 - \frac{i\omega M^2 x_{pv}}{\beta^2 U}\right), \tag{16}$$

where the functions $\bar{H}_1$ and $\bar{H}_2$ are defined in equations (18) to (21) of Ref. 5, $\bar{u} = \frac{1}{2}(\bar{m}-1)$, Σ' denotes that $(\bar{n}-qv)$ takes odd values only and

$$\left.\begin{aligned} b_{vv} &= \tfrac{1}{4}(\bar{m}+1)\sec\frac{v\pi}{m+1} \\ a_{v\bar{n}} &= \frac{4\cos\dfrac{v\pi}{m+1}\cos\dfrac{\bar{n}\pi}{\bar{m}+1}}{(\bar{m}+1)^2\left(\sin\dfrac{v\pi}{m+1} - \sin\dfrac{\bar{n}\pi}{\bar{m}+1}\right)^2} \end{aligned}\right\}. \tag{17}$$

Unless $q = 1$, the summation Σ' in equation (16) involves only odd values of $\bar{n}$ corresponding to sections

$$y_{\bar{n}}' = s\sin\frac{\bar{n}\pi}{\bar{m}+1} \tag{18}$$

that are intermediate to the collocation sections in the last of equations (13). Each of the quantities $\gamma(y_{\bar{n}}')$, $\mu(y_{\bar{n}}')$, ... is therefore expressed in terms of unknowns in equation (11) by use of the polynomial (10). Each collocation point yields a linear boundary condition to be satisfied by the complex unknowns.

It is convenient to write the mN equations in matrix form

$$\left(\mathbf{A} - \frac{i\omega\bar{c}}{\beta^2 U}\mathbf{B}\right)L = h, \tag{19}$$

where $\mathbf{A}$ and $\mathbf{B}$ are real square matrices of order mN, L is the complex column matrix of unknowns and h is a column matrix of the right-hand sides from equation (16). The inverse of equation (19) is

$$L = \left(\mathbf{A}^{-1} + \frac{i\omega\bar{c}}{\beta^2 U}\mathbf{A}^{-1}\mathbf{B}\mathbf{A}^{-1}\right)h + 0(\omega^2). \tag{20}$$

By equation (2) the elements of h to first order in frequency for pitching motion about $x = x_0$ are written as

$$h = \frac{\theta_0}{b_{vv}}\left[\alpha_1 + \frac{i\omega\bar{c}}{U}\left\{\frac{\beta^2 - M^2}{\beta^2}\alpha_2 - \frac{x_0}{\bar{c}}\alpha_1\right\}\right]_{pv} \tag{21}$$

with

$$\alpha_1 = 1 \quad \text{and} \quad \alpha_2 = x/\bar{c}\,.$$

Equations (20) and (21) combine to give

$$L = \theta_0 \left[L_1 + \frac{i\omega\bar{c}}{U} \left\{ \frac{\beta^2 - M^2}{\beta^2} L_2 + \frac{1}{\beta^2} L_3 - \frac{x_0}{\bar{c}} L_1 \right\} \right], \tag{22}$$

where

$$\left.\begin{aligned} &L_r = \mathbf{A}^{-1} h_r \\ &h_r \text{ has elements } \alpha_{rpv}/b_{vv} \\ &h_3 = \mathbf{B} L_1 \end{aligned}\right\}.$$

Similarly, by equation (3) for the mode of symmetrical control rotation to first order in frequency parameter

$$h = \frac{\xi_0}{b_{vv}} \left[\alpha_{1f} + \frac{i\omega\bar{c}}{U} \left\{ \frac{\beta^2 - M^2}{\beta^2} \alpha_{2f} - \frac{M^2}{\beta^2} \alpha_{4f} \right\} \right]_{pv} \tag{23}$$

with

$$\left.\begin{aligned} &\alpha_{1f} = 1 \\ &\alpha_{2f} = \frac{x - x_h(y)}{\bar{c}} \\ &\alpha_{4f} = x_h(y)/\bar{c} \end{aligned}\right\} \quad \text{on the control surface,}$$

$$\alpha_{1f} = \alpha_{2f} = \alpha_{4f} = 0 \text{ elsewhere on the planform.}$$

Then by equations (20) and (23)

$$L = \xi_0 \left[L_{1f} + \frac{i\omega\bar{c}}{U} \left\{ \frac{\beta^2 - M^2}{\beta^2} L_{2f} + \frac{1}{\beta^2} L_{3f} - \frac{M^2}{\beta^2} L_{4f} \right\} \right], \tag{24}$$

where

$$\left.\begin{aligned} &L_{rf} = \mathbf{A}^{-1} h_{rf} \\ &h_{rf} \text{ has elements } (\alpha_{rf})_{pv}/b_{vv} \\ &h_{3f} = \mathbf{B} L_{1f} \end{aligned}\right\}.$$

Let l_r and l_{rf} denote the distributions $l(x, y)$ from equation (8) after the elements (11) of L_r and L_{rf} respectively have been substituted in equation (10) to give polynomials $\gamma_r(y), \mu_r(y), \gamma_{rf}(y)$ and so on. Then by equations (7) and (22) for pitching motion

$$\Delta p = \tfrac{1}{2}\rho U^2 \theta_0 \mathscr{R} \left[\left\{ l_1 + \frac{i\omega\bar{c}}{U} \left(\frac{M^2 x}{\beta^2 \bar{c}} l_1 + \frac{\beta^2 - M^2}{\beta^2} l_2 + \frac{1}{\beta^2} l_3 - \frac{x_0}{\bar{c}} l_1 \right) \right\} e^{i\omega t} \right]. \tag{25}$$

The aerodynamic coefficients and derivatives for wing forces associated with equation (25) are defined in equations (33) and (39) of Ref. 5. Hinge moments† involve the integrals

$$\left.\begin{aligned} -I_{hr} &= \frac{\beta}{S_f \bar{c}_f}\iint_{S_f} l_r(x-x_h)\,dx\,dy \\ -I^*_{hr} &= \frac{\beta}{S_f \bar{c}_f}\iint_{S_f} \frac{x}{\bar{c}}\, l_r(x-x_h)\,dx\,dy \end{aligned}\right\}. \tag{26}$$

where S_f and $\bar{c}_f$ are the plan area and geometric mean chord of the starboard control surface. With the definition

$$\text{Hinge moment} = \rho U^2 S_f \bar{c}_f \mathscr{R}\left[\left\{h_\theta + \frac{i\omega\bar{c}}{U} h_{\dot\theta}\right\}\theta_0\, e^{i\omega t}\right] \tag{27}$$

it follows from equation (25) that

$$\left.\begin{aligned} -h_\theta &= \frac{1}{2\beta}\left(-I_{h1}\right) \\ -h_{\dot\theta} &= \frac{1}{2\beta}\left[\frac{M^2}{\beta^2}\left(-I^*_{h1}\right)+\frac{\beta^2-M^2}{\beta^2}\left(-I_{h2}\right)+\frac{1}{\beta^2}\left(-I_{h3}\right)-\frac{x_0}{\bar{c}}\left(-I_{h1}\right)\right] \end{aligned}\right\}. \tag{28}$$

Similarly by equations (7) and (24) for an oscillating control

$$\Delta p = \tfrac{1}{2}\rho U^2 \xi_0 \mathscr{R}\left[\left\{l_{1f}+\frac{i\omega\bar{c}}{U}\left(\frac{M^2 x}{\beta^2\bar{c}}\, l_{1f}+\frac{\beta^2-M^2}{\beta^2}\, l_{2f}+\frac{1}{\beta^2}\, l_{3f}-\frac{M^2}{\beta^2}\, l_{4f}\right)\right\} e^{i\omega t}\right]. \tag{29}$$

Then we write for lift, rolling moment and pitching moment

$$\left.\begin{aligned} I_{Lrf} &= \frac{\pi\beta A}{m+1}\sum_{n=-u}^{u} \gamma_{rfn}\cos\frac{n\pi}{m+1} \\ -I_{lrf} &= \frac{\pi\beta A}{4(m+1)}\sum_{n=-u}^{u} \gamma_{rfn}\sin\frac{2n\pi}{m+1} \\ -I^*_{lrf} &= \frac{\pi\beta A}{4(m+1)}\sum_{n=-u}^{u}\frac{1}{\bar{c}}\left\{\gamma_{rfn}(x_{ln}+\tfrac{1}{4}c_n)-\mu_{rfn}c_n\right\}\sin\frac{2n\pi}{m+1} \\ -I_{mrf} = I^*_{Lrf} &= \frac{\pi\beta A}{m+1}\sum_{n=-u}^{u}\frac{1}{\bar{c}}\left\{\gamma_{rfn}(x_{ln}+\tfrac{1}{4}c_n)-\mu_{rfn}c_n\right\}\cos\frac{n\pi}{m+1} \\ -I^*_{mrf} &= \frac{\pi\beta A}{m+1}\sum_{n=-u}^{u}\frac{1}{\bar{c}^2}\left\{\gamma_{rfn}(x_{ln}^2+\tfrac{1}{2}x_{ln}c_n+\tfrac{1}{8}c_n^2)-\mu_{rfn}(2x_{ln}c_n+\tfrac{3}{4}c_n^2)+\kappa_{rfn}(\tfrac{1}{16}c_n^2)\right\}\cos\frac{n\pi}{m+1} \end{aligned}\right\}, \tag{30}$$

†As for the mode in equation (3), the convention is to use streamwise distances and ignore the factor $\cos\Lambda_h$ in the true definition of hinge moment H_T.

and for hinge moments

$$\left.\begin{aligned} -I_{hrf} &= \frac{\beta}{S_f \bar{c}_f}\int\int_{S_f} l_{rf}(x-x_h)\,dx\,dy \\ -I^*_{hrf} &= \frac{\beta}{S_f \bar{c}_f}\int\int_{S_f} \frac{x}{\bar{c}} l_{rf}(x-x_h)\,dx\,dy \end{aligned}\right\}. \tag{31}$$

With the definitions

$$\left.\begin{aligned} \text{Lift} &= \rho U^2 S \mathscr{R}\left[\left\{-z_\xi - \frac{i\omega\bar{c}}{U} z_{\dot\xi}\right\} \xi_0 e^{i\omega t}\right] \\ \text{Pitching moment} &= \rho U^2 S \bar{c} \mathscr{R}\left[\left\{ m_\xi + \frac{i\omega\bar{c}}{U} m_{\dot\xi}\right\} \xi_0 e^{i\omega t}\right] \\ \text{Rolling moment} &= 2\rho U^2 S s \mathscr{R}\left[\left\{ l_\xi + \frac{i\omega\bar{c}}{U} l_{\dot\xi}\right\} \xi_0 e^{i\omega t}\right] \\ \text{Hinge moment} &= \rho U^2 S_f \bar{c}_f \mathscr{R}\left[\left\{ h_\xi + \frac{i\omega\bar{c}}{U} h_{\dot\xi}\right\} \xi_0 e^{i\omega t}\right] \end{aligned}\right\} \tag{32}$$

it follows from equation (29) that these control derivatives are obtained as

$$\left.\begin{aligned} -z_\xi &= \frac{1}{2\beta}\left(I_{L1f}\right) \\ -z_{\dot\xi} &= \frac{1}{2\beta}\left[\frac{M^2}{\beta^2} I^*_{L1f} + \frac{\beta^2-M^2}{\beta^2} I_{L2f} + \frac{1}{\beta^2} I_{L3f} - \frac{M^2}{\beta^2} I_{L4f}\right] \end{aligned}\right\}, \tag{33}$$

$$\left.\begin{aligned} -m_\xi &= -\frac{x_0}{\bar{c}}\left(-z_\xi\right) + \frac{1}{2\beta}\left(-I_{m1f}\right) \\ -m_{\dot\xi} &= -\frac{x_0}{\bar{c}}\left(-z_{\dot\xi}\right) + \frac{1}{2\beta}\left[\frac{M^2}{\beta^2}\left(-I^*_{m1f}\right) + \frac{\beta^2-M^2}{\beta^2}\left(-I_{m2f}\right) + \frac{1}{\beta^2}\left(-I_{m3f}\right) - \frac{M^2}{\beta^2}\left(-I_{m4f}\right)\right] \end{aligned}\right\}, \tag{34}$$

$$\left.\begin{aligned} -l_\xi &= \frac{1}{2\beta}\left(-I_{l1f}\right) \\ -l_{\dot\xi} &= \frac{1}{2\beta}\left[\frac{M^2}{\beta^2}\left(-I^*_{l1f}\right) + \frac{\beta^2-M^2}{\beta^2}\left(-I_{l2f}\right) + \frac{1}{\beta^2}\left(-I_{l3f}\right) - \frac{M^2}{\beta^2}\left(-I_{l4f}\right)\right] \end{aligned}\right\}, \tag{35}$$

$$\left.\begin{aligned} -h_\xi &= \frac{1}{2\beta}\left(-I_{h1f}\right) \\ -h_{\dot\xi} &= \frac{1}{2\beta}\left[\frac{M^2}{\beta^2}\left(-I^*_{h1f}\right) + \frac{\beta^2-M^2}{\beta^2}\left(-I_{h2f}\right) + \frac{1}{\beta^2}\left(-I_{h3f}\right) - \frac{M^2}{\beta^2}\left(-I_{h4f}\right)\right] \end{aligned}\right\}. \tag{36}$$

In the case of a model with reflection-plane symmetry, coefficients are required for the half-wing rolling or 'bending' moment and we define

$$\left.\begin{aligned} -I_{brf} &= \beta A \int_0^1 \gamma_{rf}\,\eta\,d\eta = \frac{\pi\beta A}{2(m+1)} \sum_{n=0}^{u} b_n \gamma_{rfn} \\ -I^*_{brf} &= \beta A \int_0^1 \int_{x_l}^{x_t} \frac{x}{\bar{c}} \frac{l_{rf}}{4s} \eta\,dx\,d\eta \\ &= \frac{\pi\beta A}{2(m+1)} \sum_{n=0}^{u} \frac{b_n}{\bar{c}} \left\{ \gamma_{rfn} \left(x_{ln} + \tfrac{1}{4} c_n \right) - \mu_{rfn} c_n \right\} \end{aligned}\right\}, \tag{37}$$

where for $m = 15$ the factors b_n are given by

$$\begin{aligned} b_0 &= 0{\cdot}03994, \quad b_1 = 0{\cdot}37332, \quad b_2 = 0{\cdot}71033, \quad b_3 = 0{\cdot}92235, \\ b_4 &= 1{\cdot}00084, \quad b_5 = 0{\cdot}92339, \quad b_6 = 0{\cdot}70738, \quad b_7 = 0{\cdot}38256. \end{aligned}$$

The bending-moment derivatives $-b_\xi$ and $-b_{\dot{\xi}}$ are then given by equations (35) with the quantities $-I_{brf}$ and $-I^*_{brf}$ from equations (37) in place of $-I_{lrf}$ and $-I^*_{lrf}$. The table at the end of the List of Symbols gives the conversion factors required when the true control angle ξ_T and true hinge moment H_T are used in place of those based on streamwise distance.

The preceding remarks on the application of low-frequency lifting-surface theory to control derivatives have side-stepped certain matters that call for clarification and will be considered in more detail later on. The question of central rounding in equations (4) to (6) is discussed for the swept wings in Sections 6.2 and 6.3, where the hinge line has also to be considered. It is basic to the problem of control rotation that the incidences α_{1f}, α_{2f} and α_{4f} in equation (23) are discontinuous; although the loading from equations (7) to (10) becomes inapplicable, the objective is to modify the incidences so that these equations yield integrated forces to the desired accuracy. Chordwise and spanwise discontinuities are considered separately in Sections 3 and 4, and by synthesis in Section 5.1 smooth equivalent incidences α_{1e}, α_{2e} and α_{4e} are used in place of the discontinuous ones. It is not entirely satisfactory that such a procedure changes the quantity α_{3f} implicit in equation (24) to $\alpha_{3e} = b_{vv} h_{3e}$, because $h_{3e} = \mathbf{B} L_{1e}$ no longer involves the true L_{1f}. It will appear, moreover, that, while α_{1e}, α_{2e} and α_{4e} will vary according as lift or hinge moment is to be calculated, the quantity α_{3e} remains unchanged (Section 6.1). Some justification can be made by numerical example with the aid of checks on lift by the reverse-flow theorem (Section 5.3). Clarification is also necessary in respect of the double integrals for hinge moment in equations (26) and (31); the numerical procedure for their evaluation is formulated and discussed in Section 5.2.

3. *Chordwise Equivalent Slopes.*

In the incidences α_{rf} of equation (23), two types of chordwise singularity occur at the hinge, namely a discontinuity in α_{1f} or α_{4f} and a discontinuous gradient of α_{2f}. The chordwise incidences are treated independently on the basis of two-dimensional steady theory[13] for incompressible flow, so that they may be replaced by smooth equivalent slopes that give the same forces as the exact solutions. This treatment was proposed in Ref. 14 for the calculation of steady forces on wings with flaps and was subsequently used by Multhopp in Appendix II of Ref. 3. An extension to control surfaces oscillating at low frequency was considered in Ref. 15. In these references the application is to incompressible flow, but by the Prandtl-Glauert rule the principles also apply to linearized subsonic flow.

At any section, the incidences can be written as

$$\left.\begin{aligned} \alpha_{1f} &= \alpha_1(X) \\ \alpha_{2f} &= \left(\frac{c}{\bar{c}}\right)\alpha_2(X) \\ \alpha_{4f} &= \left(\frac{x_h}{\bar{c}}\right)\alpha_1(X) \end{aligned}\right\}, \tag{38}$$

where

$$\left.\begin{aligned} \alpha_r(X) &= 0 && \text{when } 0 \leqslant X < (1-E) \\ &= [X+E-1]^{r-1} && \text{when } (1-E) < X \leqslant 1 \end{aligned}\right\}. \tag{39}$$

with $X = \left(\frac{x-x_l}{c}\right)$ and $E = \left(\frac{x_t-x_h}{c}\right)$

The two-dimensional load distributions $l_r(X)$ corresponding to $\alpha_r(X)$ are known exactly. When $r = 1$, the analysis in Ref. 13 leads to the formula

$$l_1(X) = \frac{4}{\pi}\left[(\pi-\phi_h)\cot\tfrac{1}{2}\phi + 2\sum_{j=1}^{\infty}\left(\frac{\sin j\phi \sin j\phi_h}{j}\right)\right],$$

where

$$\left.\begin{aligned} \phi &= \cos^{-1}(1-2X) \\ \phi_h &= \cos^{-1}(2E-1) \end{aligned}\right\}; \tag{40}$$

this series for $l_1(X)$ can be expressed as

$$l_1(X) = \frac{4}{\pi}\left[(\pi-\phi_h)\cot\tfrac{1}{2}\phi + ln\left|\frac{\sin\tfrac{1}{2}(\phi+\phi_h)}{\sin\tfrac{1}{2}(\phi-\phi_h)}\right|\right] \tag{41}$$

where ln denotes the natural logarithm, and in this form the load distribution is obviously singular at $\phi = \phi_h$. Similarly for $r = 2$, the formula for the loading in Appendix II of Ref. 15 gives in the present notation

$$l_2(X) = \frac{2}{\pi}\left[\left\{(\pi-\phi_h)\cos\phi_h + \sin\phi_h\right\}\cot\tfrac{1}{2}\phi + (\pi-\phi_h)\sin\phi - (\cos\phi-\cos\phi_h)\,ln\left|\frac{\sin\tfrac{1}{2}(\phi+\phi_h)}{\sin\tfrac{1}{2}(\phi-\phi_h)}\right|\right]. \tag{42}$$

Thus, for $r = 1$ and $r = 2$, specified forces can be determined by exact integration of the respective distributions in equations (41) and (42).

The control-surface problem is to be solved by the lifting-surface method of Section 2 with N chordwise terms. When $N = 4$, for example, we consider the two-dimensional loading with the first N' terms from equation (8); apart from a few special examples in Sections 6.1 and 6.4, the standard procedure is to take $N' = N$.

Then

$$l(X)=\frac{4}{\pi}[\gamma_e \cot \tfrac{1}{2}\phi+4\,\mu_e(\cot \tfrac{1}{2}\phi-2\sin\phi)+\kappa_e(\cot \tfrac{1}{2}\phi-2\sin\phi-2\sin 2\phi)+$$

$$+\lambda_e(\cot \tfrac{1}{2}\phi-2\sin\phi-2\sin 2\phi-2\sin 3\phi)], \tag{43}$$

and the corresponding two-dimensional incidence is

$$\alpha_e(X)=\frac{1}{\pi}[\gamma_e+4\,\mu_e(1+2\cos\phi)+\kappa_e(1+2\cos\phi+2\cos 2\phi)+\lambda_e(1+2\cos\phi+2\cos 2\phi+2\cos 3\phi)]. \tag{44}$$

The coefficients γ_e, μ_e, κ_e, λ_e are chosen so that the smooth load distribution $l(X)$ in equation (43) gives specified forces, of number $N = 4$, that are identical to those due to the exact loading in equation (41) for $r = 1$ or in equation (42) for $r = 2$. In Sections 3.1 and 3.2 respectively, two distinct types of equivalent slopes are formulated, namely

$$\left.\begin{aligned}\alpha_e(X) &= \sigma_r(X,E)\\ \alpha_e(X) &= \tau_r(X,E)\end{aligned}\right\}\ (r=1,2)\ ; \tag{45}$$

for σ_r only wing forces are specified, whilst for τ_r one of these is replaced by hinge moment.

3.1. *Wing Forces.*

For the purpose of calculating wing forces due to the control motion, it seems appropriate to take equivalent slopes σ_r. Thus, for the four-term formula in equation (44), the coefficients γ_e, μ_e, κ_e, λ_e are chosen so that equation (43) produces the exact lift $(C_L)_r$ and first three moments $(C_m)_r$, $(C_{mm})_r$ and $(C_{mmm})_r$. Referred to the quarter-chord axis,

$$\left.\begin{aligned}&\int_0^1 l(X)\,dX \equiv (C_L)_r\\ &\int_0^1 (\tfrac{1}{4}-X)\,l(X)\,dX \equiv (C_m)_r\\ &\int_0^1 (\tfrac{1}{4}-X)^2\,l(X)\,dX \equiv (C_{mm})_r\\ &\int_0^1 (\tfrac{1}{4}-X)^3\,l(X)\,dX \equiv (C_{mmm})_r\end{aligned}\right\}. \tag{46}$$

Substituting $l(X)$ from equation (43) and integrating, we obtain the set of equations in matrix notation

$$\begin{bmatrix} 2 & 0 & 0 & 0 \\ 0 & 2 & 0 & 0 \\ 1 & -4 & 1 & 0 \\ -1 & 12 & -2 & 1 \end{bmatrix} \begin{bmatrix} \gamma_e \\ \mu_e \\ \kappa_e \\ \lambda_e \end{bmatrix} = \begin{bmatrix} (C_L)_r \\ (C_m)_r \\ 8(C_{mm})_r \\ 32(C_{mmm})_r \end{bmatrix}. \tag{47}$$

Inversion of the matrix gives

$$\left.\begin{aligned} \gamma_e &= \tfrac{1}{2}(C_L)_r \\ \mu_e &= \tfrac{1}{2}(C_m)_r \\ \kappa_e &= [8(C_{mm})_r + 2(C_m)_r - \tfrac{1}{2}(C_L)_r] \\ \lambda_e &= [32(C_{mmm})_r + 16(C_{mm})_r - 2(C_m)_r - \tfrac{1}{2}(C_L)_r] \end{aligned}\right\}. \tag{48}$$

To complete the formulation of the slopes σ_1, the distribution $l_1(X)$ of equation (41) is substituted in equation (46) to give

$$\left.\begin{aligned} (C_L)_1 &= 2\,C_\gamma \\ 8(C_m)_1 &= -C_\mu \\ 8(C_{mm})_1 &= [C_\gamma + \tfrac{1}{4}\,C_\mu + C_\kappa] \\ 32(C_{mmm})_1 &= [-C_\gamma - \tfrac{3}{4}\,C_\mu - 2\,C_\kappa - C_\lambda] \end{aligned}\right\}, \tag{49}$$

where

$$\left.\begin{aligned} C_\gamma &= [(\pi - \phi_h) + \sin\phi_h] \\ \tfrac{1}{4}C_\mu &= [\sin\phi_h - \tfrac{1}{2}\sin 2\phi_h] \\ C_\kappa &= [-\tfrac{1}{2}\sin 2\phi_h + \tfrac{1}{3}\sin 3\phi_h] \\ C_\lambda &= [\tfrac{1}{3}\sin 3\phi_h - \tfrac{1}{4}\sin 4\phi_h] \end{aligned}\right\}. \tag{50}$$

The four-term formula for σ_1 is then completely determined by $\alpha_e(X)$ from equations (44), (48), (49) and (50). Similarly, when $r = 2$, equations (42) and (46) give

$$\left.\begin{aligned} (C_L)_2 &= D_\gamma \\ 16(C_m)_2 &= -D_\mu \\ 16(C_{mm})_2 &= [D_\gamma + \tfrac{1}{4}\,D_\mu + D_\kappa] \\ 64(C_{mmm})_2 &= [-D_\gamma - \tfrac{3}{4}\,D_\mu - 2D_\kappa - D_\lambda] \end{aligned}\right\}, \tag{51}$$

where

$$\left.\begin{aligned} D_\gamma &= [(\pi - \phi_h)(\tfrac{1}{2} + \cos\phi_h) + \sin\phi_h + \tfrac{1}{4}\sin 2\phi_h] \\ \tfrac{1}{4}\,D_\mu &= [\tfrac{1}{2}(\pi - \phi_h) + \tfrac{1}{4}\sin\phi_h + \tfrac{1}{4}\sin 2\phi_h - \tfrac{1}{12}\sin 3\phi_h] \\ D_\kappa &= [\tfrac{1}{4}\sin\phi_h - \tfrac{1}{12}\sin 2\phi_h - \tfrac{1}{12}\sin 3\phi_h + \tfrac{1}{24}\sin 4\phi_h] \\ D_\lambda &= [-\tfrac{1}{12}\sin 2\phi_h + \tfrac{1}{24}\sin 3\phi_h + \tfrac{1}{24}\sin 4\phi_h - \tfrac{1}{40}\sin 5\phi_h] \end{aligned}\right\} \tag{52}$$

and equations (44), (48), (51) and (52) determine σ_2. It remains to evaluate σ_1 and σ_2 at the $N = 4$ collocation positions $\phi = \phi_p$ defined in equation (13).

If we consider N (or $N' < 4$, the formulation of σ_r again starts from equations (43) and (44); only the first N terms are retained, and the unknown coefficients satisfy the first N conditions in equation (48). According as $r = 1$ or $r = 2$, the first N formulae in equations (49) and (50) or in equations (51) and (52) are used. Then, the equivalent slopes σ_r are determined by equation (44) with $\lambda_e = 0$ when $N = 3$ and $\kappa_e = \lambda_e = 0$ when $N = 2$.

The formulae for σ_r are obtained as functions of the chordwise positions ϕ and ϕ_h defined by equation (40) in terms of X and E. In Fig. 2a, values of the slopes σ_1 when $E = 0{\cdot}25$ are plotted for $N = 2, 3$ and 4 respectively as linear, quadratic and cubic functions of X. These three curves differ most in the range $0 < X < 0{\cdot}2$: the $N = 4$ curve gives the steepest gradient at $X = 0{\cdot}75$, the position of the discontinuity in the exact incidence shown by the dotted lines.

The boundary condition of equation (23) is to be satisfied at the collocation positions $\phi = \phi_p$ ($p = 1, 2 \ldots N$) defined in equation (13). Values of the slopes σ_r at the positions ϕ_p are denoted as σ_{rp}. In Tables 1 and 2, the values of σ_{1p} and σ_{2p} respectively are tabulated for $p = 1(1)N$ corresponding to each value $N = 2, 3$ and 4 with $E = 0{\cdot}05(0{\cdot}05)0{\cdot}75$. In Fig. 3a, for a rectangular wing at $M = 0$ with full-span control (E = constant), values of the lift damping derivative $-z_{\dot{\xi}}$ are plotted against E ($\leqslant 0{\cdot}5$). It is noted that, when $M = 0$, the contributions to $-z_{\dot{\xi}}$ from equation (33) reduce to the terms L_{L2f} and I_{L3f} corresponding respectively to solutions for α_{2f} and α_{3f}, the latter being derived from the solution for α_{1f}. The effect of using equivalent slopes σ_{1p} and σ_{2p}, for $N = 4$, is shown by the curve in Fig. 3a, whilst the exact boundary conditions at the collocation points give the dashed lines with breaks in $-z_{\dot{\xi}}$ at $E = 0{\cdot}03$ and at $E = 0{\cdot}25$. The fictitious discontinuities occur whenever a collocation point coincides with the hinge position, that is if $E = \frac{1}{2}(1 + \cos \phi_p)$; the equivalent slopes overcome this difficulty.

3.2. *Control Hinge Moment.*

Equation (45) indicates that in the calculation of the hinge-moment derivatives for control motion, the equivalent slopes τ_r replace σ_r from Section 3.1. In the four-term formula for τ_r, the unknown coefficients γ_e, μ_e, κ_e, λ_e of equation (44) are chosen to satisfy the first three conditions in equation (46) together with the following condition for the exact two-dimensional hinge moment

$$\frac{1}{E^2} \int_{X_h}^{1} (X - X_h)\, l(X)\, dX = (-C_h)_r \tag{53}$$

where $X_h = 1 - E$. With $l(X)$ from equation (43), this condition becomes

$$\tfrac{1}{2}\left[\gamma_e A_\gamma + \mu_e A_\mu + \kappa_e A_\kappa + \lambda_e A_\lambda\right] \equiv (-C_h)_r, \tag{54}$$

where after integration

$$\left.\begin{aligned}
(\pi E^2)\, A_\gamma &= \left[(\pi - \phi_h)(2\cos\phi_h - 1) + 2\sin\phi_h - \tfrac{1}{2}\sin 2\phi_h\right] \\
(\pi E^2)\, A_\mu &= 4\left[-(\pi - \phi_h) + \tfrac{1}{2}\sin\phi_h - \tfrac{1}{2}\sin 2\phi_h - \tfrac{1}{6}\sin 3\phi_h\right] \\
(\pi E^2)\, A_\kappa &= \left[\tfrac{1}{2}\sin\phi_h + \tfrac{1}{6}\sin 2\phi_h - \tfrac{1}{6}\sin 3\phi_h - \tfrac{1}{12}\sin 4\phi_h\right] \\
(\pi E^2)\, A_\lambda &= \left[\tfrac{1}{6}\sin 2\phi_h + \tfrac{1}{12}\sin 3\phi_h - \tfrac{1}{12}\sin 4\phi_h - \tfrac{1}{20}\sin 5\phi_h\right]
\end{aligned}\right\}. \tag{55}$$

Therefore, in place of the matrix equation (47), γ_e, μ_e, κ_e, λ_e are now determined by

$$\begin{bmatrix} 2 & 0 & 0 & 0 \\ 0 & 2 & 0 & 0 \\ 1 & -4 & 1 & 0 \\ A_\gamma & A_\mu & A_\kappa & A_\lambda \end{bmatrix} \begin{bmatrix} \gamma_e \\ \mu_e \\ \kappa_e \\ \lambda_e \end{bmatrix} = \begin{bmatrix} (C_L)_r \\ (C_m)_r \\ 8(C_{mm})_r \\ 2(-C_h)_r \end{bmatrix} \tag{56}$$

with the formulae for $(C_L)_r$, $(C_m)_r$ and $(C_{mm})_r$ given by equations (49) to (52) for $r = 1$ and $r = 2$. The respective formulae for $(-C_h)_r$ are determined from equation (53) with $l_r(X)$ from equation (41) or (42); then after integration,

$$\left.\begin{aligned} [2\pi E^2(-C_h)_1] &= [(\pi-\phi_h)^2(2\cos\phi_h-1)+2(\pi-\phi_h)\sin\phi_h+\sin^2\phi_h] \\ [2\pi E^2(-C_h)_2] &= [(\pi-\phi_h)^2\cos^2\phi_h+(\pi-\phi_h)\sin 2\phi_h+\sin^2\phi_h] \end{aligned}\right\} . \tag{57}$$

Unless $A_\lambda = 0$, the matrix on the left-hand side of equation (56) is non-singular and the coefficients γ_e, μ_e, κ_e, λ_e can be determined for a specified value of E and $r = 1$ or 2. The equivalent slopes $\alpha_e(X) = \tau_r$ are then given by equation (44). It is important to know the values of E for which $A_\lambda = 0$ and the matrix is singular. The formula for A_λ in equation (55) can be rearranged as

$$(15\pi)A_\lambda = 8\sin\phi_h(1-\cos\phi_h)(6\cos\phi_h-1), \tag{58}$$

which only vanishes in the range $0 < E < 1$ if

$$\cos\phi_h = (2E-1) = \tfrac{1}{6}. \tag{59}$$

Hence, for $E = 0{\cdot}58\dot{3}$ it is not possible to obtain τ_r when $N = 4$. It should be emphasized that this singularity has no basis in a physical sense and arises solely from the loading functions used and their failure to represent the exact boundary conditions of equation (3).

If equivalent slopes τ_r are required for N (or N') < 4, then $\alpha_e(X)$ is represented by the first N terms of equation (44). The unknown coefficients are chosen to give correctly the forces $(C_L)_r$ and $(-C_h)_r$ when $N = 2$ or the forces $(C_L)_r$, $(C_m)_r$ and $(-C_h)_r$ when $N = 3$. In neither case can the matrix of order N replacing the left-hand side of equation (56) become singular in the range $0 < E < 1$, because both A_μ and A_κ remain non-zero; hence the equivalent slopes τ_r are never singular when $N = 2$ or $N = 3$. The difference between the slopes τ_2 when $N = 2, 3$ and 4 is illustrated in Fig. 2b by the distributions for $E = 0{\cdot}25$ plotted as continuous functions of X. Comparison with the exact incidence for $r = 2$ from equation (39) shows a progressive approximation towards it as N increases. Values of τ_{1p} and τ_{2p} at the collocation positions $p = 1(1)N$ are tabulated for $N = 2, 3$ and 4 with $E = 0{\cdot}05(0{\cdot}05)0{\cdot}75$ in Tables 3 and 4 respectively.

The importance of the equivalent slopes τ_r, chosen to satisfy the two-dimensional hinge moment, is illustrated in Fig. 3b. For a rectangular wing with full-span constant-chord control, the equivalent slopes σ_{1p} that satisfy wing forces only and the special equivalent slopes τ_{1p} are applied to give alternative solutions ($N = 4$) for the hinge-moment derivative $-h_\xi$. The results for a range of control-chord ratio E from 0·05 to 0·50 are plotted in Fig. 3b and show large differences when $E < 0{\cdot}25$. Whilst the solutions with τ_{1p} indicate a small change in $-h_\xi$ as E varies, those with σ_{1p} indicate a rapid variation, particularly for small E, which will be seen to be erroneous in Section 6.1.

4. *Spanwise Equivalent Slopes.*

For a part-span control surface, it is readily seen from equation (23) that the incidences α_{rf} have span-

wise discontinuities at the sections where the control surface adjoins the wing. After the chordwise discontinuities within the control span have been removed by means of the equivalent slopes σ_r or τ_r from Section 3, there remain spanwise discontinuities in the value and, in general, in the spanwise gradient of σ_r and τ_r. Both types of discontinuity are treated by the use of spanwise equivalent slopes. As for the different chordwise slopes σ_r in Section 3.1 and τ_r in Section 3.2, we determine in Sections 4.1 and 4.2 spanwise slopes that are appropriate respectively to the calculation of wing forces and of sectional loads or hinge moments; the numerical procedure for the combined equivalent slopes is outlined in Section 5.1.

For an outboard control, the two types of spanwise discontinuity are represented by distributions of incidence

$$\left.\begin{aligned} \alpha_t(\eta) &= \varepsilon\,[\,|\eta| - \eta_a]^{t-1} && -1 \leqslant \eta \leqslant -\eta_a \\ &= 0 && -\eta_a < \eta < \eta_a \\ &= +[\eta - \eta_a]^{t-1} && \eta_a \leqslant \eta \leqslant 1 \end{aligned}\right\}, \tag{60}$$

where $t = 1$ or 2 and, as in Fig. 1a, $y_a = s\eta_a$ locates the spanwise discontinuities; the symbol $\varepsilon = \pm 1$ according as the control motion is symmetrical or antisymmetrical with respect to y. Controls of arbitrary span can be handled by superposition.

4.1. *Wing Forces.*

The smooth spanwise slopes, which give correctly the wing forces such as lift and rolling moment corresponding to the incidence $\alpha_t(\eta)$, can be formulated directly However, there is a simpler treatment on the reverse-flow basis, as suggested by Davies[1], and this approach and some applications are considered in detail in Section 4.3 of Ref. 6.

In the present context, the spanwise equivalent slopes are represented as

$$\alpha_e(\eta) = \sum_{k=1}^{m} \left[E_{tk} \left(\frac{\sin k\theta}{\sin \theta} \right) \right], 0 \leqslant \theta \leqslant \pi, \tag{61}$$

where $\eta = \cos\theta$ and the odd integer m defines the collocation sections in equation (13); the unknown coefficients E_{tk} are chosen to satisfy the m conditions corresponding to the exact wing forces in the spanwise modes η^{k-1}, $k = 1(1)m$. By equations (5), (42) and (44) of Ref. 6, the reverse-flow relation between the incidences $\alpha_e(\eta)$ and $\alpha_t(\eta)$ becomes

$$\int\int_S \alpha_e(\eta)\, \bar{l}(x, y)\, dx\, dy = \int\int_S \alpha_t(\eta)\, \bar{l}(x, y)\, dx\, dy, \tag{62}$$

where $\bar{l}(x, y)$ is a smooth lift distribution over the wing in reverse flow. This loading can be represented by the series of equation (8) with ϕ replaced by $(\pi - \phi)$ to give the correct leading-edge and trailing-edge singularities for the reversed flow. It follows, by transforming to the non-dimensional parameters ϕ and η and integrating with respect to ϕ, that equation (62) reduces to

$$\int_{-1}^{1} \alpha_e(\eta)\, \bar{\gamma}(\eta)\, d\eta = \int_{-1}^{1} \alpha_t(\eta)\, \bar{\gamma}(\eta)\, d\eta. \tag{63}$$

Substitution of $\alpha_t(\eta)$ and $\alpha_e(\eta)$ from equations (60) and (61) gives

$$\sum_{k=1}^{m}\left[E_{tk}\int_{0}^{\pi}\sin k\theta\,\bar{\gamma}(\eta)\,d\eta\right]=\oint(|\cos\theta|-\cos\theta_a)^{t-1}\,\bar{\gamma}(\eta)\sin\theta\,d\theta\,, \tag{64}$$

where $\eta_a=\cos\theta_a$

and the integral $\oint$ denotes $\int_{0}^{\theta_a}+\varepsilon\int_{\pi-\theta_a}^{\pi}$.

The spanwise distribution of circulation $\bar{\gamma}(\eta)$ can be defined by equation (10) but is more conveniently expressed as

$$\bar{\gamma}(\eta)=\sum_{j=1}^{m}\left[K_j\sin j\theta\right]. \tag{65}$$

When this series is inserted into both sides of equation (64), a set of m equations is obtained by identifying the terms of each coefficient K_j. Thus,

$$\sum_{k=1}^{m}\left[E_{tk}\int_{0}^{\pi}\sin k\theta\sin j\theta\,d\theta\right]=\oint(|\cos\theta|-\cos\theta_a)^{t-1}\sin j\theta\sin\theta\,d\theta\,, \tag{66}$$

whence

$$E_{tk}=\frac{2}{\pi}\oint(|\cos\theta|-\cos\theta_a)^{t-1}\sin k\theta\sin\theta\,d\theta\,. \tag{67}$$

Then, for $t=1$,

$$E_{1k}=\frac{1}{\pi}\left[\frac{\sin(k-1)\theta}{(k-1)}-\frac{\sin(k+1)\theta}{(k+1)}\right]_{0}^{\theta_a}+\frac{\varepsilon}{\pi}\left[\frac{\sin(k-1)\theta}{(k-1)}-\frac{\sin(k+1)\theta}{(k+1)}\right]_{\pi-\theta_a}^{\pi}$$

$$=\frac{1}{\pi}\left[1-\varepsilon(-1)^k\right]\left[\frac{\sin(k-1)\theta_a}{(k-1)}-\frac{\sin(k+1)\theta_a}{(k+1)}\right]. \tag{68}$$

Similarly, for $t=2$,

$$E_{2k}=-E_{1k}\cos\theta_a+\frac{1}{2\pi}\left[1-\varepsilon(-1)^k\right]\left[\frac{\sin(k-2)\theta_a}{(k-2)}-\frac{\sin(k+2)\theta_a}{(k+2)}\right]. \tag{69}$$

In equations (68) and (69), $\varepsilon=1$ for the symmetrical case gives $E_{tk}=0$ for even k, whilst $\varepsilon=-1$ for the antisymmetrical case gives $E_{tk}=0$ for odd k. The spanwise equivalent slopes $\alpha_e(\eta)$ to represent $\alpha_t(\eta)$ of equation (60) follow immediately from equation (61) with equation (68) or (69), and respectively, we write

$$\alpha_e(\eta)=\Omega_t(\eta,\eta_a)\text{ for }t=1,2\,. \tag{70}$$

The boundary condition of equation (23) is to be satisfied at the m collocation sections $\eta = \eta_\nu = \sin\dfrac{\nu\pi}{m+1}$, where Ω_t is denoted as $\Omega_{t\nu}$; both $\Omega_{1\nu}$ and $\Omega_{2\nu}$ are illustrated in Fig. 4 for the outboard control $\eta_a = 0{\cdot}5$ in symmetrical deflection. The values of $\Omega_{1\nu}$, plotted against η_ν in Fig. 4a, show that $m = 7$ gives a very smooth but inadequate representation of the exact discontinuous incidence $\alpha_1(\eta)$, whilst with $m = 15$ the values lie very close to $\alpha_1(\eta)$ and show a steep gradient in the neighbourhood of η_a. For $\Omega_{2\nu}$ in Fig. 4b, on the other hand, the values for both $m = 7$ and $m = 15$ closely represent the discontinuity in gradient defined by $\alpha_2(\eta)$. In all the numerical examples we take $m = 15$, and the corresponding values of $\Omega_{t\nu}$ ($t = 1, 2$) are listed in Tables 5 and 6, for the symmetrical and antisymmetrical cases respectively, with η_a ranging from 0 to 0·85.

The importance of using smooth spanwise slopes in place of $\alpha_t(\eta)$ of equation (60) is illustrated in Fig. 5a, by the values of the lift derivative $-z_\xi$ for outboard controls on a rectangular wing in incompressible flow. Collocation solutions ($m = 15$, $N = 3$) with local chordwise equivalent slopes $\sigma_{1p}\alpha_1(\eta_\nu)$, having spanwise discontinuities, give the dashed lines that are discontinuous whenever η_a coincides with a collocation section. This difficulty is overcome if we use $\sigma_{1p}\Omega_{1\nu}$, whence the continuous curve of $-z_\xi$ is obtained.

4.2. *Spanwise Loading and Hinge Moment.*

The construction of special spanwise equivalent slopes, for use in the calculation of local loads and hinge moments, is quite distinct from that of $\Omega_{t\nu}$ in Section 4.1. Here we work from analytical treatments of spanwise discontinuities, following Multhopp's[16] lifting-line theory for wings of large aspect ratio and De Young's[17] theory for low aspect ratios. By applying either of these theories it is possible to represent the discontinuous incidence $\alpha_t(\eta)$ of equation (60) by a smooth equivalent distribution $\Psi_t(\eta, \eta_a)$ that gives the circulation correctly at all the collocation sections η_ν. The local values $\Psi_{t\nu}(\eta_a)$ from the two theories are identical and therefore likely to apply to wings of arbitrary aspect ratio.

In the low-aspect-ratio theory of Ref. 17, the boundary conditions along an unswept trailing edge relate the local incidence to the spanwise distribution of circulation $2Us\gamma(\eta)$ by the integral equation

$$\alpha(\eta) = \frac{1}{\pi}\int_{-1}^{1}\frac{1}{(\eta-\eta')}\frac{d\gamma(\eta')}{d\eta'}\,d\eta' . \tag{71}$$

Thus $\gamma(\eta)$ depends only upon the incidence at the trailing edge and is independent of such chordwise details as the position of the control hinge. De Young takes the incidence distribution $\alpha_1(\eta)$ of equation (60) and satisfies equation (71) by an infinite series for $\gamma(\eta)$. A more direct mathematical analysis, as used to treat equation (1) of Ref. 18, is to invert the integral equation; by this means equation (71) yields

$$\gamma(\eta) = -\frac{1}{\pi}\int_{-1}^{1}\alpha(\eta')\,ln\left|\frac{\sin\frac{1}{2}(\theta-\theta')}{\sin\frac{1}{2}(\theta+\theta')}\right|d\eta' , \tag{72}$$

where $\eta = \cos\theta$ and $\eta' = \cos\theta'$. By equation (72) we can determine the circulation $\gamma_t(\eta)$ corresponding to $\alpha_t(\eta)$ of equation (60) with $t = 1$ or $t = 2$. Hence

$$\gamma_1(\eta) = \frac{1}{\pi}\left[(\cos\theta_a-\cos\theta)\,ln\left|\frac{\sin\frac{1}{2}(\theta-\theta_a)}{\sin\frac{1}{2}(\theta+\theta_a)}\right| - \varepsilon(\cos\theta_a+\cos\theta)\,ln\left|\frac{\cos\frac{1}{2}(\theta-\theta_a)}{\cos\frac{1}{2}(\theta+\theta_a)}\right| + (1+\varepsilon)\,\theta_a\sin\theta\right] \tag{73}$$

and

$$\gamma_2(\eta) = -\frac{1}{2\pi}\left[(\cos\theta_a - \cos\theta)^2 \, ln \left|\frac{\sin\frac{1}{2}(\theta-\theta_a)}{\sin\frac{1}{2}(\theta+\theta_a)}\right| - \varepsilon(\cos\theta_a + \cos\theta)^2 \, ln \left|\frac{\cos\frac{1}{2}(\theta-\theta_a)}{\cos\frac{1}{2}(\theta+\theta_a)}\right| + \right.$$

$$\left. + (1+\varepsilon)(2\,\theta_a \cos\theta_a - \sin\theta_a)\,\mathrm{sln}\,\theta - (1-\varepsilon)(\tfrac{1}{2}\,\theta_a)\sin 2\theta\right]. \tag{74}$$

With $\varepsilon = +1$ or -1, respectively for symmetrical or antisymmetrical deflection, equation (73) agrees with the closed expression derived for the deflected outboard control from the infinite series in Ref. 17.

In the lifting-surface method of Section 2, the smooth distribution $\gamma(\eta)$ is expressed in terms of the values γ_n in equation (11) by the polynomial of equation (10). An alternative form for this distribution in Ref. 3 is

$$\gamma(\eta) = \frac{2}{(m+1)} \sum_{n=-u}^{u} \left[\gamma(\eta_n) \sum_{\lambda=1}^{m} (\sin\lambda\theta_n \sin\lambda\theta)\right], \tag{75}$$

where m is an odd integer and $u = \frac{1}{2}(m-1)$. The unique smooth incidence distribution consistent with equations (71) and (75) is

$$\alpha_e(\eta) = \frac{2}{(m+1)} \sum_{n=-u}^{u} \left[\gamma(\eta_n) \sum_{\lambda=1}^{m} \left(\sin\lambda\theta_n \int_0^{\pi} \frac{\lambda\cos\lambda\theta'}{(\cos\theta' - \cos\theta)}\, d\theta'\right)\right]$$

$$= \frac{2}{(m+1)} \sum_{n=-u}^{u} \left[\gamma(\eta_n) \sum_{\lambda=1}^{m} \left(\frac{\lambda \sin\lambda\theta_n \sin\lambda\theta}{\sin\theta}\right)\right]. \tag{76}$$

At the collocation sections $\eta = \eta_v$, it can be shown that

$$\alpha_e(\eta_v) = 2\,b_{vv}\left[\gamma(\eta_v) - \sum_{n=u}^{u}{}' \left\{a_{vn}\,\gamma(\eta_n)\right\}\right], \tag{77}$$

where Σ' denotes that $(v-n)$ takes odd values only and the coefficients b_{vv} and a_{vn} are defined by equations (17) with $\bar{m} = m$ and $\bar{n} = n$. Substitution of the values of $\gamma_t(\eta_n)$ from equation (73) or (74) into equation (77) defines the equivalent slopes

$$\alpha_e(\eta_v) = \Psi_{tv}(\eta_a) \qquad \text{for } t = 1 \text{ or } 2\,. \tag{78}$$

It is important to recognize that there is no restriction in aspect ratio although Ψ_{tv} has been derived on the basis of low-aspect-ratio theory. It can be shown that precisely the same spanwise equivalent slopes follow from the rigorous application of Multhopp's[16] lifting-line theory for part-span controls, whatever the aspect ratio. The circulation is proportional to $\alpha_t(\eta) - \alpha_i(\eta)$ where the induced incidence $\alpha_i(\eta)$ is given by equation (71) with a factor $\frac{1}{2}$ inserted on the right-hand side. The invariance of Ψ_{tv} follows from the condition that $\alpha_i(\eta)$ must contain the same singularities as $\alpha_t(\eta)$ of equation (60) to ensure a smooth distribution of circulation.

Values of the spanwise slopes $\Psi_{tv}(t = 1, 2)$ appropriate to $m = 15$ are tabulated in Tables 5 and 6 respectively for symmetrical ($\varepsilon = 1$) and antisymmetrical ($\varepsilon = -1$) spanwise loading, with the control-

span parameter varying from 0 to 0·85. A diagram similar to Fig. 4 would show that Ψ_{1v} and Ψ_{2v} are close to the corresponding exact incidences. The effect of using the spanwise equivalent slopes Ψ_{1v}, rather than the slopes Ω_{1v} of Section 4.1, in the calculation of the steady spanwise loading $\gamma(\eta)$ is illustrated in Fig. 5b for the rectangular wing with symmetrical constant-chord outboard controls $\eta_a = 0{\cdot}25$ and $\eta_a = 0{\cdot}85$. The solution with equivalent incidences $\sigma_{1p}\Omega_{1v}$ is plotted as circles, whilst the incidences $\sigma_{1p}\Psi_{1v}$ give the more precise curve of γ against η. The former is a poorer representation of the loading in the neighbourhood of $\eta = \eta_a$. When $\eta_a = 0{\cdot}85$, $\gamma(\eta)$ is plotted for twice the control deflection ($\xi = 2$ radians) and the difference between the solutions with Ω_{1v} and Ψ_{1v} is more obvious. From these comparisons the spanwise equivalent slopes Ψ_{1v} give a more satisfactory representation of the spanwise loading due to the control deflection.

5. *Numerical Procedures.*

The major part of the numerical work has been carried out on a KDF 9 computer by the Algol program of Ref. 5, and this has restricted the calculations to at most four chordwise terms. With $m = 15$ throughout, there is the further restriction $q \leqslant 6$ when $N = 4$; thus, by equation (15), a maximum of $\bar{m} = 95$ spanwise integration points is used. The program includes an automatic routine for incorporating the planform rounding of equation (5); however, most of the present calculations use equation (6) instead, in which case all the necessary values of the leading-edge ordinate x_l and chord c have to be inserted numerically. The other input data that require preliminary calculation are the smooth equivalent incidences α_{1e}, α_{2e} and α_{4e} which will vary according as lift or hinge moment is required. In general, these will involve the chordwise and spanwise equivalent slopes of Sections 3 and 4 respectively, and the technique of combining them is discussed in Section 5.1.

The output data from the Algol program include column matrices L_r ($r = 1, 2, 3$) and L_{rf} ($r = 1, 2, 3, 4$) for pitching and control rotation respectively, from which the load distributions in equations (25) and (29) can be obtained; the output also gives values of the lift, pitching-moment and rolling-moment coefficients from equations (33) of Ref. 5 and from the present equations (30). The 'bending' moment coefficients in equation (37) are easily computed, but the hinge-moment coefficients in equations (26) and (31) are calculated by a procedure of interpolation and integration described in Section 5.2. Then all the aerodynamic derivatives from equations (39) of Ref. 5 and from the present equations (28) and (33) to (36) are simple to evaluate.

Other numerical procedures explicitly related to applications of the reverse-flow theorem are explained in Section 5.3. Again, the hinge moments present the greatest difficulties, while the wing forces are evaluated more simply without resort to equivalent incidences.

5.1. *Combined Equivalent Slopes.*

The most general application of the chordwise and spanwise equivalent slopes, from Sections 3 and 4 respectively, occurs for a tapered swept wing and part-span control. The spanwise variation in the wing chord $c(y)$ or in the control hinge-line $x_h(y)$ obviously affects the incidences α_{rf} for $r = 2$ or $r = 4$ in equation (38). Furthermore, at each section, equation (39) is replaced by the local chordwise equivalent slopes σ_{rp} or τ_{rp} corresponding to the control-chord ratio $E = c_f(y)/c(y)$; the spanwise variation of these slopes with E over the control span is denoted as $\sigma_{rp}(E)$ or $\tau_{rp}(E)$. In the calculation of wing forces, when the slopes $\sigma_{rp}(E)$ are used, the incidences α_{rf} for $r = 1, 2$ and 4 are therefore replaced along each line $p =$ constant by the spanwise distributions

$$\left.\begin{aligned} \alpha_{rp}(\eta) &= \varepsilon[f_r(\eta)\,\sigma_{rp}(E)] && -1 \leqslant \eta \leqslant -\eta_a \\ &= 0 && -\eta_a < \eta < \eta_a \\ &= +[f_r(\eta)\,\sigma_{rp}(E)] && \eta \leqslant \eta \leqslant 1 \end{aligned}\right\}, \tag{79}$$

where $\varepsilon = \pm 1$ according as the control deflection is symmetrical or antisymmetrical, $\sigma_{4p}(E) \equiv \sigma_{1p}(E)$ and, by equations (38),

$$\left.\begin{aligned} f_1(\eta) &= 1 \\ f_2(\eta) &= c(y)/\bar{c} \\ f_4(\eta) &= x_h(y)/\bar{c} \end{aligned}\right\} \tag{80}$$

In order to treat the spanwise singularities in $\sigma_{rp}(\eta)$ at $\eta = \pm\eta_a$, equation (79) is divided into three distributions. We consider

$$\left.\begin{aligned} \alpha_I &= [f_r(\eta_a)\,\sigma_{rp}(E_a)]\,\alpha_1(\eta) \\ \alpha_{II} &= \left(\frac{d}{d\eta}\left[f_r(\eta)\,\sigma_{rp}(E)\right]\right)_{\eta=\eta_a} \alpha_2(\eta) \end{aligned}\right\}, \quad -1 \leqslant \eta \leqslant 1, \tag{81}$$

where the spanwise singularities in α_I and α_{II} are respectively defined by the incidence $\alpha_t(\eta)$ of equation (60) with $t = 1$ and $t = 2$. In equation (81), we require the value of $\alpha_{rp}(\eta)$ and its gradient $\alpha'_{rp}(\eta)$ at $\eta = \eta_a$; the latter is determined numerically as indicated in the next paragraph. Thus, given the distributions α_I and α_{II} from equation (81), the residual of the incidence $\alpha_{rp}(\eta)$ is determined as the distribution

$$\alpha_{III} = [\alpha_{rp}(\eta) - \alpha_I - \alpha_{II}] \quad , \quad -1 \leqslant \eta \leqslant 1, \tag{82}$$

which is zero for $|\eta| \leqslant \eta_a$. Since $c(y)$ and $x_h(y)$ are smooth functions, so is $\alpha_{III}(\eta)$. The procedure then is to replace $\alpha_t(\eta)$ in equation (81) by the spanwise equivalent slopes Ω_{tv} for $t = 1$ and $t = 2$ from Section 4.1. The resulting sets of equivalent values at the collocation sections η_v are then added to the actual values of the residual incidence $(\alpha_{III})_v$ from equation (82). Thus, the combined equivalent incidences are

$$(\alpha_{re})_{pv} = (\alpha_{III})_v + [f_r(\eta_a)\,\sigma_{rp}(E_a)]\,\Omega_{1v} + \left(\frac{d}{d\eta}\left[f_r(\eta)\,\sigma_{rp}(E)\right]\right)_{\eta=\eta_a} \Omega_{2v} \tag{83}$$

$$= \alpha_{rp}(\eta_v) + \alpha_{rp}(\eta_a)\,[\Omega_{1v} - \alpha_1(\eta_v)] + \alpha'_{rp}(\eta_a)\,[\Omega_{2v} - \alpha_2(\eta_v)] \tag{84}$$

in terms of $\alpha_{rp}(\eta)$ from equation (79).

The above procedure is illustrated in Fig. 6 for equation (79) with $r = 1$, $p = 1$ and spanwise symmetry ($\varepsilon = 1$). Here the curve of $\alpha = \alpha_{1p}(\eta) = \sigma_{1p}(E)$ against $\eta \geqslant \eta_a$ corresponds to $p = 1$ in the solution ($m = 15$, $N = 3$) for the cropped delta wing with outboard control $\eta_a = 0{\cdot}5$. This example shows the large variation in $\sigma_{11}(E)$ as E increases from 0·25 to 1. When this distribution is divided into three parts, according to equations (81) and (82), we obtain the three spanwise distributions labelled ①, ② and ③ in Fig. 6. The third distribution is smooth, but the first two distributions are proportional to the exact incidences $\alpha_t(\eta)$ shown as broken lines in Figs. 4a and 4b and replaced by the values Ω_{tv}. The spanwise gradient in the second of equations (81) is estimated by means of a polynomial in η through $\sigma_{1p}(E_a)$ and the values $\sigma_{1p}(E_v)$ at the four collocation sections η_v, $v = 1(1)4$, two on either side of the position $\eta = \eta_a = 0{\cdot}5$. At the sections $\eta_1 = 0{\cdot}195$ and $\eta_2 = 0{\cdot}383$ we must use the values of σ_{1p} appropriate to an extended control as indicated by the smooth dotted curve in Fig. 6. Once the gradient is determined by differentiating the polynomial for $\sigma_{1p}(E)$ and putting $\eta = \eta_a$, the combined equivalent incidences $(\alpha_{1e})_{pv}$ for $p = 1$ and $v = 0(1)7$ are calculated from equation (84) and plotted as circles in Fig. 6. The procedure for other values of r allows for the spanwise variation of both $\sigma_{rp}(E)$ and $f_r(\eta)$ in equation (79).

The formulation of the equivalent incidences $(\alpha_{re})_{pv}$, by equations (79) to (84), also applies if we replace

the chordwise slopes $\sigma_{rp}(E)$ by $\tau_{rp}(E)$ or the spanwise slopes Ω_{tv} by Ψ_{tv}. The combination of chordwise and spanwise slopes is selected according to the aerodynamic requirements in the following table.

	Equivalent Slopes	
	Chordwise	Spanwise
Wing forces	σ_{rp}	Ω_{tv}
Spanwise loading	σ_{rp}	Ψ_{tv}
Hinge moment	τ_{rp}	Ψ_{tv}

For hinge moment, therefore, equation (84) is replaced by

$$(\alpha_{re})_{pv} = \alpha_{rp}(\eta_v) + \alpha_{rp}(\eta_a)\,[\Psi_{1v} - \alpha_1(\eta_v)] + \alpha'_{rp}(\eta_a)\,[\Psi_{2v} - \alpha_2(\eta_v)] \tag{85}$$

$$\left.\begin{aligned} \text{with } \alpha_{rp}(\eta) &= \varepsilon\,[f_r(\eta)\,\tau_{rp}(E)] && -1 \leqslant \eta \leqslant -\eta_a \\ &= 0 && -\eta_a < \eta < \eta_a \\ &= +[f_r(\eta)\,\tau_{rp}(E)] && \eta_a \leqslant \eta \leqslant 1 \end{aligned}\right\},$$

where $r = 1, 2$ or 4, $\varepsilon = \pm 1$, $\tau_{4p}(E) \equiv \tau_{1p}(E)$ and $f_r(\eta)$ is defined by equation (80).

The procedure simplifies in a number of cases. For a symmetrical full-span control, $\Omega_{tv} = \Psi_{tv} = 1$ at any collocation section η_v. When the control chord ratio E is constant across the control span we always have zero gradient and $\alpha_{II} = 0$ for $r = 1$, but this only remains true for $r = 2$ if the wing chord is also constant or for $r = 4$ if the control hinge line is unswept. Thus for a rectangular wing with constant-chord control, the last term in equation (84) or (85) vanishes and for each r the combined equivalent slopes simplify to give

$$(\alpha_{re})_{pv} = [f_r\,\sigma_{rp}(E)\,\Omega_{1v}] \qquad \text{for wing forces} \tag{86}$$

or

$$(\alpha_{re})_{pv} = [f_r\,\tau_{rp}(E)\,\Psi_{1v}] \qquad \text{for hinge moment} \tag{87}$$

where $f_1 = f_2 = 1$ and $f_4 = 1 - E$.

5.2. *Integration of Hinge Moment.*

The hinge moment on the control surface due to low-frequency pitching motion or control rotation is determined by equations (26) to (28) or by equations (31), (32) and (36). In each case, the double integrals are to be evaluated over the starboard area S_f bounded by the hinge line $x_h(y)$ and the trailing edge $x_t(y)$ with the range of y for outboard and inboard controls defined respectively as $y_a \leqslant y \leqslant s$ and $0 \leqslant y \leqslant y_f$; this definition holds for both symmetrical and antisymmetrical modes of oscillation. When an inboard or full-span control is swept, there arises the question of the kinked hinge line at $y = 0$; formerly in the calculation of Ref. 2 the actual hinge line was retained throughout the calculation while the planform was rounded. It now seems more appropriate to use a rounded hinge line consistent with the planform rounding either from equation (5) or from equation (6), as will be discussed in Section 6.3.

The procedure for integration of the hinge moment will be formulated in detail for the derivatives $-h_\xi$ and $-h_{\dot\xi}$ due to control rotation. These can be expressed in terms of the local hinge-moment distributions across the control span, $-h_{\xi L}$ and $-h_{\dot\xi L}$, as defined by the integrals

$$\left.\begin{aligned} -h_\xi &= \left(\frac{s}{s_f}\right)\int (-h_{\xi L})\, d\eta \\ -h_{\dot\xi} &= \left(\frac{s}{s_f}\right)\int (-h_{\dot\xi L})\, d\eta \end{aligned}\right\}, \tag{88}$$

where the control span and range of integration are defined for outboard and inboard controls respectively as

$$\left.\begin{aligned} s_f &= s(1-\eta_a), \quad \int = \int_{\eta_a}^{1} \\ \text{and} \qquad & \\ s_f &= s\,\eta_f, \quad \int = \int_{0}^{\eta_f} \end{aligned}\right\}. \tag{89}$$

By identifying equation (88) with the formulae for $-h_\xi$ and $-h_{\dot\xi}$ from equations (31) and (36) where $S_f = s_f \bar{c}_f$, it follows that

$$-h_{\xi L} = \frac{1}{2\bar{c}_f^2}\int_{x_h}^{x_t} (x-x_h)\, l_{1f}\, dx \tag{90}$$

and

$$-h_{\dot\xi L} = \frac{1}{2\bar{c}_f^2}\int_{x_h}^{x_t} (x-x_h)\left[\frac{x}{\bar{c}}\frac{M^2}{\beta^2}\, l_{1f} + \frac{\beta^2-M^2}{\beta^2}\, l_{2f} + \frac{1}{\beta^2}\, l_{3f} - \frac{M^2}{\beta^2}\, l_{4f}\right] dx\,. \tag{91}$$

In accord with the table after the List of Symbols $-h_{\xi L}$ and $-h_{\dot\xi L}$ require the factor $\cos^2 \Lambda_h$ when the control angle and hinge moment are defined truly in planes normal to the hinge line. In the present method, the load distributions l_{1f}, l_{2f} and l_{4f} are determined for the equivalent incidences α_{re} from equation (85), but l_{3f} is obtained from an incidence α_{3e} involving the matrix $\mathbf{BA}^{-1}$ in the notation of equation (24). When $N = 4$, $l_{rf}(x, y)$ is represented by the real spanwise distributions $\gamma_{rf}(y)$, $\mu_{rf}(y)$, $\kappa_{rf}(y)$ and $\lambda_{rf}(y)$ together with the four associated chordwise functions of ϕ in equation (8). Then equation (90) reduces to

$$-h_{\xi L} = \frac{A}{4}\left(\frac{\bar{c}}{\bar{c}_f}\right)^2 F_1(\eta), \tag{92}$$

where in general

$$F_r(\eta) = \left(E^2\frac{c}{\bar{c}}\right)\left[\gamma_{rf}(y)\, A_\gamma + \mu_{rf}(y)\, A_\mu + \kappa_{rf}(y)\, A_\kappa + \lambda_{rf}(y)\, A_\lambda\right]; \tag{93}$$

the chordwise integrals A_γ, A_μ, A_κ, A_λ are expressed analytically in terms of $\phi_h = \cos^{-1}(1-2E)$ by equations (55). For $-h_{\dot\xi L}$ in equation (91), the first term in the square bracket requires additional functions B_γ, B_μ, B_κ, B_λ defined by the integrals

$$P_q(\phi_h) = \int_{\phi_h}^{\pi} [\cos(q-1)\phi + \cos q\phi](\cos\phi_h - \cos\phi)^2 d\phi\,, \quad q = 1(1)4\,; \tag{94}$$

after integration, we obtain the set of functions

$$\left.\begin{aligned}
(\pi E^2)B_\gamma &= P_1 = [(\pi-\phi_h)(1-\cos\phi_h+\tfrac{1}{2}\cos 2\phi_h)-\tfrac{3}{4}\sin\phi_h+\tfrac{3}{4}\sin 2\phi_h-\tfrac{1}{12}\sin 3\phi_h]\\
(\pi E^2)B_\mu &= 4P_2 = [(\pi-\phi_h)(1-4\cos\phi_h)-3\sin\phi_h+\tfrac{2}{3}\sin 2\phi_h-\tfrac{1}{3}\sin 3\phi_h-\tfrac{1}{12}\sin 4\phi_h]\\
(\pi E^2)B_\kappa &= P_3 = [\tfrac{1}{4}(\pi-\phi_h)-\tfrac{1}{12}\sin\phi_h+\tfrac{1}{6}\sin 2\phi_h+\tfrac{1}{24}\sin 3\phi_h-\tfrac{1}{48}\sin 4\phi_h-\tfrac{1}{120}\sin 5\phi_h]\\
(\pi E^2)B_\lambda &= P_4 = [-\tfrac{1}{12}\sin\phi_h-\tfrac{1}{48}\sin 2\phi_h+\tfrac{1}{24}\sin 3\phi_h+\tfrac{1}{60}\sin 4\phi_h-\tfrac{1}{120}\sin 5\phi_h-\tfrac{1}{240}\sin 6\phi_h]
\end{aligned}\right\}\,. \tag{95}$$

Values of the eight functions A_γ, A_μ, A_κ, A_λ and B_γ, B_μ, B_κ, B_λ are tabulated for $E = 0{\cdot}05(0{\cdot}05)0{\cdot}75$ in Table 7. Thus, equation (91) can be evaluated from the expression

$$-h_{\xi L} = \frac{A}{4}\left(\frac{\bar{c}}{\bar{c}_f}\right)^2\left[\frac{M^2}{\beta^2}F_1^*(\eta)+\frac{\beta^2-M^2}{\beta^2}F_2(\eta)+\frac{1}{\beta^2}F_3(\eta)-\frac{M^2}{\beta^2}F_4(\eta)\right], \tag{96}$$

where $F_r(\eta)$ is defined by equation (93) and

$$F_1^*(\eta) = \left(\frac{x_h}{\bar{c}}\right)F_1(\eta)+\left(E^2\frac{c^2}{\bar{c}^2}\right)\left[\gamma_{1f}(y)B_\gamma+\mu_{1f}(y)B_\mu+\kappa_{1f}(y)B_\kappa+\lambda_{1f}(y)B_\lambda\right]. \tag{97}$$

The values of $-h_{\xi L}$ and $-h_{\dot{\xi} L}$ at the collocation sections $y_n = s\eta_n$ within the control span are determined by equations (92) and (96) respectively with the values of $\gamma_{rfn} = \gamma_{rf}(y_n)$, $\mu_{rfn} = \mu_{rf}(y_n)$, ... from the collocation solution inserted into equations (93) and (97); in general, the planform data x_h, E and c and the functions $A_\gamma, \ldots B_\lambda$ will all vary with η_n

To determine $-h_{\xi L}$ and $-h_{\dot{\xi} L}$ at the extremity of the control span, we require the values of $F_r(\eta)$ for $r = 1(1)4$ and $F_1^*(\eta)$ at $\eta = \eta_a$ (or η_f). In general, η_a does not coincide with a collocation section and the values of $\gamma_{rf}(y_a)$, $\mu_{rf}(y_a)$, ... must therefore be obtained by interpolation. Except for $r = 3$, it is necessary to simulate the singularity in spanwise loading associated with deflection of the starboard outboard control; each distribution $\gamma_{rf}(y)$, $\mu_{rf}(y)$, ... is represented by a four-term equation

$$G(\eta) = \left[\sum_{k=1}^{3}\left(a_k\eta^{k-1}\sqrt{1-\eta^2}\right)+a_4\gamma_1(\eta)\right], \tag{98}$$

where the distribution

$$\gamma_1(\eta) = \frac{1}{\pi}\left[\theta_a\sin\theta+(\cos\theta_a-\cos\theta)\ln\left|\frac{\sin\frac{1}{2}(\theta-\theta_a)}{\sin\frac{1}{2}(\theta+\theta_a)}\right|\right] \tag{99}$$

is defined by equation (73) with $\varepsilon = 0$. For an inboard control, it follows by superposition that equations (98) and (99) apply with θ_a replaced by $\theta_f = \cos^{-1}\eta_f$. When $r = 3$, equation (99) is no longer appropriate to the interpolation and the last term in equation (98) is replaced by $a_4\eta^3\sqrt{1-\eta^2}$. The arbitrary coefficients a_k, $k = 1(1)4$, are chosen for each r and each distribution γ_{rfn}, μ_{rfn}, ..., so that $G(\eta_n)$ is satisfied at the four collocation sections η_n, two on either side of the position η_a (or η_f). The interpolation is illustrated for $-h_{\xi L}$ on an outboard control in Fig. 7 by the simple case of a rectangular wing with constant-

chord control. For $m = 15$, the interpolated value at $\eta_a = 0{\cdot}45$ involves the values at $\eta = \eta_n$ for $n = 1(1)4$, as indicated by the 'range for interpolation' in Fig. 7.

To complete the evaluation of $-h_\xi$ and $-h_{\dot\xi}$, we require a numerical procedure for the spanwise integration of equation (88). Basically, we apply Simpson's rule to the integrations with respect to the angular parameter $\theta = \cos^{-1}\eta$ over each double interval

$$\theta_n \leqslant \theta \leqslant \theta_{n+2}\left[\theta_n = \frac{\pi}{2} - \frac{n\pi}{m+1}\right], \tag{100}$$

where the integer n is even. Thus the integration over the greater part of the control span is effected in terms of the local hinge-moment coefficients $-h_{\xi L}$ and $-h_{\dot\xi L}$ at the collocation sections η_n, but there remains a divided interval requiring special integration factors appropriate to the value η_a (or η_f). On an outboard control, this interval is denoted as $\eta_a \leqslant \eta \leqslant \eta_b$ where η_b is the outer end of the double interval that overlaps the position η_a; η_b may or may not be the collocation section nearest to η_a and we have to consider both cases. By assuming a quadratic function of θ through the values of $-h_{\xi L}$ and $-h_{\dot\xi L}$ at η_a and the two nearest collocation sections within the control span, equations (88) are integrated over the range $\eta_a \leqslant \eta \leqslant \eta_b$. In the example of Fig. 7 for $m = 15$ and $\eta_a = 0{\cdot}45$, the shaded areas denote the three ranges for integration; $-h_\xi$ is calculated by using Simpson's rule over the two double intervals $\eta_4 \leqslant \eta \leqslant \eta_6$ and $\eta_6 \leqslant \eta \leqslant \eta_8$, whilst over the divided interval $\eta_a \leqslant \eta \leqslant \eta_4$, the integrand is represented in terms of the values of $-h_{\xi L}$ at $\eta = \eta_a$, η_3 and η_4. Thus, for the outboard control $\eta_a = 0{\cdot}45$,

$$-h_\xi = \frac{\pi}{(m+1)(1-\eta_a)}\left\{-h_{\xi L}(\eta_a)\, I_a (1-\eta_a^2)^{\frac{1}{2}} + \sum_{n=3}^{7}\left[-h_{\xi L}(\eta_n)\, I_n \cos\left(\frac{n\pi}{m+1}\right)\right]\right\} \tag{101}$$

where $I_a = 0{\cdot}10665$, $I_3 = 1{\cdot}14365$, $I_4 = 0{\cdot}70582$,

$I_5 = 1{\cdot}33333$, $I_6 = 0{\cdot}66667$, $I_7 = 1{\cdot}33333$.

The other case arises when the numerical integration procedure for $m = 15$ is applied to an outboard control $\eta_a = 0{\cdot}25$; there are three double intervals and the divided interval $\eta_a \leqslant \eta \leqslant \eta_2$ is represented by the values of $-h_{\xi L}$ at $\eta = \eta_a$, η_2 and η_3. The derivative $-h_\xi$ is then given by equation (101) with the summation from $n = 2$ to $n = 7$ and

$$I_a = 0{\cdot}30708 \ , \qquad I_2 = 0{\cdot}77464 \ , \qquad I_3 = 1{\cdot}29805 \ , \qquad I_4 = 0{\cdot}66667$$

and I_5 to I_7 as given above. These numerical procedures have been found satisfactory in the present applications. Improved accuracy could be obtained over the divided interval from $\eta = \eta_a$ to $\eta = \eta_b = \cos\theta_b$, if an additional interpolation were made for the position $\theta = \frac{1}{2}(\theta_a + \theta_b)$ to permit the application of Simpson's rule.

A similar numerical procedure is used to evaluate the hinge-moment derivatives $-h_\theta$ and $-h_{\dot\theta}$ from equations (26) and (28) corresponding to pitching motion. Instead of equations (98) and (99), it is appropriate to use the smooth interpolation polynomial

$$G(\eta) = \sum_{k=1}^{4}\left(a_k \eta^{k-1}\sqrt{1-\eta^2}\right) \tag{102}$$

to evaluate each spanwise distribution at $\eta = \eta_a$. To the local hinge moments we again apply the spanwise integration procedure illustrated in equation (101).

5.3. *Applications of Reverse Flow.*

The reverse-flow theorem is applied in Section 5 of Ref. 6 to low-frequency oscillations in the pitching and symmetrical control-rotation modes. Expressions are derived on the basis of Multhopp's low-frequency theory for the lift and pitching-moment derivatives, which are given for the two modes respectively by equations (71) and (77) of Ref. 6. Both sets of formulae are in terms of the same load distributions, $l_r(\bar{x}, \bar{y})$, $r = 1(1)5$, appropriate to solutions for the 'reversed wing' in simple modes. With the coordinate system $(\bar{x}, \bar{y})$ defined by

$$\left.\begin{aligned} \bar{x} &= c_r - x \\ \bar{y} &= -y \end{aligned}\right\}, \tag{103}$$

these solutions are referred to the origin at $\bar{y} = 0$ on the leading edge of the reversed wing. Thus, each distribution $\bar{l}_r(\bar{x}, \bar{y})$ is represented by equation (8) with a bar inserted over each symbol in the square brackets; the corresponding collocation solutions for the reversed wing follow the principles of Section 2 with respective incidences

$$\left.\begin{aligned} \bar{\alpha}_1 &= 1 \\ \bar{\alpha}_2 &= \bar{x}/\bar{c} \\ \bar{\alpha}_3 &= b_{vv}\,\bar{\mathbf{B}}\bar{\mathbf{A}}^{-1}(\bar{\alpha}_1/b_{vv}) \\ \bar{\alpha}_4 &= (\bar{x}/\bar{c})^2 \\ \bar{\alpha}_5 &= b_{vv}\,\bar{\mathbf{B}}\bar{\mathbf{A}}^{-1}(\bar{\alpha}_2/b_{vv}) \end{aligned}\right\}. \tag{104}$$

where $\bar{\mathbf{A}}$ and $\bar{\mathbf{B}}$ are the matrices from the collocation solution for the reversed wing, analogous to those in equation (19).

For pitching motion, equations (38) of Ref. 5 give the lift and pitching-moment derivatives in terms of the force coefficients $\bar{I}_{Lr}$ with $r = 1(1)5$, $-\bar{I}_{m1}$ and $-\bar{I}_{m2}$ for the reversed wing. A straightforward application of the Algol program[5] to the reversed wing gives the seven coefficients as output, and the pitching derivatives follow immediately.

The program also outputs the values of the spanwise loading coefficients $\bar{\gamma}(\bar{y}_n)$, $\bar{\mu}(\bar{y}_n)$, ... which define the distributions $\bar{l}_r(\bar{x}, \bar{y})$. In the present notation, the formulae from equation (77) of Ref. 6 for the lift derivatives due to control rotation become

$$\left.\begin{aligned} -z_\xi &= \frac{1}{S}\int\int_{S_f} \bar{l}_1\, d\bar{x}\, d\bar{y} \\ \text{and} \\ -z_{\dot{\xi}} &= \frac{1}{S}\int\int_{S_f}\left[\frac{M^2\,\bar{x}_h}{\beta^2\,\bar{c}}\bar{l}_1 - \left(\frac{\beta^2 - M^2}{\beta^2}\right)\left(\frac{\bar{x}-\bar{x}_h}{\bar{c}}\right)\bar{l}_1 - \frac{M^2}{\beta^2}\bar{l}_2 + \frac{1}{\beta^2}\bar{l}_3\right] d\bar{x}\, d\bar{y} \end{aligned}\right\}, \tag{105}$$

where $\bar{x}_h(\bar{y}) = c_r - x_h(y)$, the wing area $S = 2s\bar{c}$ and the starboard control-surface area $S_f = s_f\,\bar{c}_f$ is bounded by the control span, the leading edge $\bar{x}_l(\bar{y})$ and the hinge line $\bar{x}_h(\bar{y})$ on the reversed-wing planform. Likewise, the formulae for the pitching-moment derivatives can be written as

$$\left[m_\xi - z_\xi\left(\frac{c_r - x_0}{\bar{c}}\right)\right] = \frac{1}{S}\int_{S_f}\int \bar{l}_2\, d\bar{x}\, d\bar{y}$$

and

$$\left[m_\xi - z_\xi\left(\frac{c_r - x_o}{\bar{c}}\right)\right] = \frac{1}{S}\int_{S_f}\int \left[\frac{M^2}{\beta^2}\frac{\bar{x}_h}{\bar{c}}\bar{l}_2 - \left(\frac{\beta^2 - M^2}{\beta^2}\right)\left(\frac{\bar{x} - \bar{x}_h}{\bar{c}}\right)\bar{l}_2 - \frac{M^2}{\beta^2}\bar{l}_4 + \frac{1}{\beta^2}\bar{l}_5\right] d\bar{x}\, d\bar{y} \Bigg\}. \quad (106)$$

To evaluate equations (105) and (106), the integrals are transformed to the non-dimensional parameters $\bar{\phi}$ and $\bar{\eta}$ defined by

$$\left.\begin{aligned} \bar{x} &= \bar{x}_l(\bar{y}) + \tfrac{1}{2}\, c(\bar{y})\,[1 - \cos\bar{\phi}] \\ \text{and} \qquad \bar{y} &= s\bar{\eta} \end{aligned}\right\}, \quad (107)$$

where by equations (103) and planform symmetry

$$\bar{x}_l(\bar{y}) = c_r - [x_l(y) + c(y)].$$

Since $\bar{x}_h(\bar{y}) = c_r - x_h(y)$ gives $\bar{\phi}_h = \pi - \phi_h$, we need to consider chordwise integrals of the two types

$$Q_r(\bar{\eta}) = \frac{c}{4\bar{c}}\int_0^{\pi-\phi_h} \bar{l}_r \sin\bar{\phi}\, d\bar{\phi}\,, \qquad r = 1(1)5\,, \quad (108)$$

and

$$R_r(\bar{\eta}) = \frac{c}{4\bar{c}}\int_0^{\pi-\phi_h} (\cos\bar{\phi} - \cos\bar{\phi}_h)\,\bar{l}_r \sin\bar{\phi}\, d\bar{\phi}, r = 1, 2\,. \quad (109)$$

When the loading $\bar{l}_r(\bar{x}, \bar{y})$ is expressed as the series with $N = 4$ chordwise terms in equation (8) with bars inserted, equation (108) becomes

$$Q_r(\bar{\eta}) = \frac{A}{\pi}\left[\bar{\gamma}_r(\bar{y})\, C_\gamma + \bar{\mu}_r(\bar{y})\, C_\mu + \bar{\kappa}_r(\bar{y})\, C_\kappa + \bar{\lambda}_r(\bar{y})\, C_\lambda\right], \quad (110)$$

where the chordwise integrals C_γ, C_μ, C_κ and C_λ correspond to the four chordwise functions associated with $\bar{\gamma}$, $\bar{\mu}$, $\bar{\kappa}$ and $\bar{\lambda}$ respectively; these integrals are defined analytically as functions of the hinge-line parameter ϕ_h by equations (50). Similarly, equation (109) reduces to

$$R_r(\bar{\eta}) = \frac{A}{\pi}\left[\bar{\gamma}_r(\bar{y})\, D_\gamma + \bar{\mu}_r(\bar{y})\, D_\mu + \bar{\kappa}_r(\bar{y})\, D_\kappa + \bar{\lambda}_r(\bar{y})\, D_\lambda\right], \quad (111)$$

where the functions D_γ, D_μ, D_κ and D_λ are defined in terms of ϕ_h by equations (52). It follows that the derivatives of equations (105) and (106) can be expressed in terms of the spanwise functions $Q_r(\bar{\eta})$, $r = 1(1)5$, from equation (110), $R_1(\bar{\eta})$ and $R_2(\bar{\eta})$ from equation (111). Hence, for an outboard control, equations (105) reduce to the integrals

$$-z_{\xi} = \int_{\eta_a}^{1} Q_1 \, d\bar{\eta}$$

and

$$-z_{\dot{\xi}} = \int_{\eta_a}^{1} \left[\frac{M^2}{\beta^2} \frac{\bar{x}_h}{\bar{c}} Q_1 + \left(\frac{\beta^2 - M^2}{\beta^2} \right) \left(\frac{c}{2\bar{c}} \right) R_1 - \frac{M^2}{\beta^2} Q_2 + \frac{1}{\beta^2} Q_3 \right] d\bar{\eta} \Bigg\} \quad . \qquad (112)$$

Similarly, equations (106) become

$$\left[m_{\xi} - z_{\xi} \left(\frac{c_r - x_0}{\bar{c}} \right) \right] = \int_{\eta_a}^{1} Q_2 \, d\bar{\eta}$$

and

$$\left[m_{\dot{\xi}} - z_{\dot{\xi}} \left(\frac{c_r - x_0}{\bar{c}} \right) \right] = \int_{\eta_a}^{1} \left[\frac{M^2}{\beta^2} \frac{\bar{x}_h}{\bar{c}} Q_2 + \left(\frac{\beta^2 - M^2}{\beta^2} \right) \left(\frac{c}{2\bar{c}} \right) R_2 - \frac{M^2}{\beta^2} Q_4 + \frac{1}{\beta^2} Q_5 \right] d\bar{\eta} \Bigg\} \quad . \qquad (113)$$

To complete the evaluation of the lift and pitching-moment derivatives, the values $\bar{\gamma}_r(\bar{y}_n)$, $\bar{\mu}_r(\bar{y}_n)$, ... from the collocation solutions are inserted into equations (110) and (111). In general, $\bar{\eta} = \eta_a$ does not coincide with a collocation section $\bar{\eta}_n$ and the interpolation polynomial of equation (102) is used to obtain the necessary values of $\bar{\gamma}_r(y_a)$, $\bar{\mu}_r(y_a)$, ... Then the numerical procedure of Section 5.2 is applied to the spanwise integration of equations (112) and (113), whereby each derivative is expressed in terms of the values of its respective integrand at $\bar{\eta} = \eta_a$ and at the collocation sections $\bar{\eta} = \bar{\eta}_n$ within the control span. This will incorporate any spanwise variation with $\bar{\eta}$ of the planform data $\bar{x}_h(\bar{y})$, $c(\bar{y})$ and also $\phi_h = \cos^{-1}(1-2E)$ through the eight functions C_{γ}, ... D_{λ}, which are defined by equations (50) and (52) and tabulated for $E = 0{\cdot}05(0{\cdot}05)0{\cdot}75$ in Table 8.

Application of the reverse-flow approach to the calculation of hinge moment due to symmetrical control rotation is considered in detail in the Appendix. From equations (A.2) to (A.4), we see that the problem of singularities in both the force and upwash modes persists into the reversed-wing formulation. The singularities in upwash are treated numerically by using appropriate chordwise and spanwise equivalent slopes, combined according to the procedure of Section 5.1. Altogether, the calculation of hinge moment to first order in frequency requires five additional reversed-wing solutions for the steady load distributions $\bar{l}_{re}(\bar{x}, \bar{y})$ due to equivalent incidences $\bar{\alpha}_{re}$ for $r = 2,5,6,7,8$. The following table indicates the actual incidences that each $\bar{\alpha}_{re}$ replaces and the chordwise and spanwise equivalent slopes from the Appendix.

r	$\bar{\alpha}_{re}$ to replace	Chordwise slopes; special condition	Spanwise slopes
2	$(\bar{x}-\bar{x}_h)/\bar{c}$ on S_f	ε ; hinge moment	Ψ_{tv}
5	Equation (104) with $\bar{\alpha}_{2f}$	δ ; N$^{\text{th}}$ wing force	Ω_{tv}
6	$(\bar{x}-\bar{x}_h)/\bar{c}$ on S_f	ζ ; hinge reaction	Ψ_{tv}
7	$[(\bar{x}-\bar{x}_h)/\bar{c}]^2$ on S_f	ψ ; hinge reaction	Ψ_{tv}
8	$(\bar{x}_h/\bar{c})(\bar{x}-\bar{x}_h)/\bar{c}$ on S_f	ζ ; hinge reaction	Ψ_{tv}

Each of the chordwise slopes is chosen on a two-dimensional basis to satisfy conditions for the first $(N-1)$ wing forces and the special aerodynamic quantity listed above; the 'hinge reaction' of equation (A.18), arising from the lift force on the control, gives a distinct condition relevant only to the reverse-flow formulation of hinge moment. The four types of chordwise slope are indicated by equations (A.16) when $N = 4$. Equation (A.15) in conjunction with equations (A.19) to (A.21) leads to the slopes ε and δ, whereas the slopes ζ and ψ are determined by equation (A.15) with equations (A.22) to (A.24). In the case of a part-span control, the spanwise equivalent slopes Ω_{tv} and Ψ_{tv} of Sections 4.1 and 4.2 are selected according to the above table.

In equation (A.26), the hinge-moment derivatives are expressed in terms of the five load distributions $\bar{l}_{re}(\bar{x}, \bar{y})$ over the reversed wing by

$$\left.\begin{aligned} -h_\xi &= \frac{\bar{c}}{2 S_f \bar{c}_f} \iint_{S_f} \bar{l}_{6e}\, d\bar{x}\, d\bar{y} \\ \text{and} \\ -h_{\dot{\xi}} &= \frac{\bar{c}}{2 S_f \bar{c}_f} \iint_{S_f} \left[-\left(\frac{\beta^2 - M^2}{\beta^2}\right)\left(\frac{\bar{x}-\bar{x}_h}{\bar{c}}\right)\bar{l}_{2e} + \frac{1}{\beta^2}\bar{l}_{5e} + \frac{M^2}{\beta^2}\left(\frac{\bar{x}_h}{\bar{c}}\bar{l}_{6e} - \bar{l}_{7e} - \bar{l}_{8e}\right)\right] d\bar{x}\, d\bar{y} \end{aligned}\right\}. \quad (114)$$

For an outboard control, it can be shown that equations (114) reduce to

$$\left.\begin{aligned} -h_\xi &= \frac{1}{1-\eta_a}\left(\frac{\bar{c}}{\bar{c}_f}\right)^2 \int_{\eta_a}^{1} Q_{6e}\, d\bar{\eta} \\ \text{and} \\ -h_{\dot{\xi}} &= \frac{1}{1-\eta_a}\left(\frac{\bar{c}}{\bar{c}_f}\right)^2 \int_{\eta_a}^{1} \left[\left(\frac{\beta^2 - M^2}{\beta^2}\right)\left(\frac{c}{2\bar{c}}\right)R_{2e} + \frac{1}{\beta^2}Q_{5e} + \frac{M^2}{\beta^2}\left(\frac{\bar{x}_h}{\bar{c}}Q_{6e} - Q_{7e} - Q_{8e}\right)\right] d\bar{\eta} \end{aligned}\right\}, \quad (115)$$

where the spanwise functions Q_{re} and R_{2e} are determined by equations (110) and (111) with modified subscript. The evaluation of the spanwise integrals in equations (115) is effected by the numerical procedure for hinge moment in Section 5.2. Thus, formulae for $-h_\xi$ and $-h_{\dot{\xi}}$ are obtained in terms of the spanwise loading coefficients $\bar{\gamma}_{re}(\bar{y}_n), \bar{\mu}_{re}(\bar{y}_n), \ldots$ together with the corresponding values of $C_\gamma, \ldots D_\lambda$ at the collocation sections $\bar{y}_n = s\bar{\eta}_n$. To determine the values of the integrands at the lower limit of integration in equations (115), the interpolation procedure of Section 5.2 is applied to the spanwise loading coefficients; the polynomial of equations (98) and (99) is used, except for Q_{5e} when the smooth polynomial of equation (102) is more appropriate.

The evaluation of control derivatives by the reverse-flow approach must be regarded with some reservations. For the indirect derivatives as well as for the hinge-moment derivatives, the calculations involve the integration of loading over the control area and this includes the leading-edge of the reversed wing, the region where collocation solutions are least reliable. In the case of the lift and pitching-moment derivatives in equations (105) and (106), there is no further difficulty since the reversed-wing solutions correspond to the simple modes of equations (104): the derivatives, so obtained, provide an important check that is independent of equivalent incidences. On the other hand, the derivatives $-h_{\dot{\xi}}$ and $-h_{\ddot{\xi}}$ involve the special equivalent-incidence procedures and rather more lengthy computation from equations (114) than from equations (88) to (91) in direct flow. A further disadvantage is the greater extent to which

indeterminate chordwise equivalent slopes can arise, especially for compressible flow; as shown by equations (A.25), singularities occur when $N = 3$ if $E = 0{\cdot}375$, and for three values $E = 0{\cdot}196$, $0{\cdot}417$ and $0{\cdot}637$ when $N = 4$. These limitations restrict the reverse-flow procedure to the role of providing alternative values of hinge moment in particular examples only. The simplest applications for a rectangular wing at $M = 0$ (Section 6.1) illustrate the difficulties associated with singular solutions. In compressible flow the tapered swept wing with outboard control (Section 6.3) provides an example in which the range of E excludes any singularities in the equivalent slopes.

6. *Illustrative Calculations.*

Numerical applications have been made to the four planforms defined in Fig. 8. The examples have been chosen to demonstrate all aspects of the present method, and in each case to allow comparison with experimental or theoretical results from other sources. The principal objective is to evaluate the hinge-moment derivatives to reasonable accuracy, and their convergence with respect to the number of chordwise terms ($N = 2, 3$ and 4) is examined for each wing.

The two untapered wings of aspect ratio 4 are considered with a wide range of control chord and span, but the calculations are restricted to incompressible flow and to constant values of the chord ratio $E = c_f/c$ over the control span. The results for the rectangular wing in Section 6.1 are mainly concerned with full-span controls and concentrate on the effect of E and the implications of the reverse-flow theorem in relation to chordwise equivalent slopes. The untapered swept wing is chosen partly because its spanwise loading due to part-span controls has been obtained by an electrical analogue[7] of the steady flow, and partly to illustrate the effect of sweepback. The calculations for Section 6.2, restricted to steady flow, show the influence on spanwise loading of the artificial central rounding in equations (4) to (6) by comparison with the analogue results for inboard controls. Stiffness derivatives for zero and 45-deg sweepback are compared for inboard and outboard controls over the whole range of span.

The two tapered wings in Fig. 8 are considered in compressible flow, and the complete sets of pitching derivatives are calculated including the hinge moment from equations (27) and (28). Both wings have control surfaces with fixed hinge lines, a spanwise variation of E and a range of span; they therefore involve the most general procedure for combining chordwise and spanwise equivalent slopes (Section 5.1). On the cropped delta wing, in particular, E has an extreme variation from $\frac{1}{7}$ at the root to 1 at the tip, and the influence of Mach number is studied. The tapered swept wing has been treated theoretically for small frequency in Ref. 8, and derivatives from that source for an oscillating outboard control are compared with the present calculations; a further important check on the wing forces from the present equivalent slopes is obtained by application of the reverse-flow theorem to slowly oscillating control surfaces, as formulated in Section 5.3. Two other special investigations for this wing are included in Section 6.3. Antisymmetrical, as well as symmetrical, control deflections are considered, and both rolling and hinge moments in the case of antisymmetrical ailerons are compared with the corresponding theoretical quantities when reflection-plane symmetry is assumed, as in a half-model experiment. The need to round the central region of a swept wing introduces the further question of rounding the swept hinge line in the full-span case, and the importance of this is examined. For the tapered swept wing in Section 6.3 and the cropped delta wing in Section 6.4 the spanwise distributions of hinge-moment stiffness and damping are illustrated, together with the effect of Mach number on the latter wing.

The ultimate objective is to adapt the present method to include some allowance for aerofoil section and boundary layers. There are insufficient experimental data to establish a practicable semi-empirical scheme, but measured hinge-moment derivatives are available in Refs. 9 and 10 for the rectangular and cropped delta wings. Sections 6.1 and 6.4 include relevant comments on the discrepancies between these measurements and the present theoretical results. Section 7 suggests a simple means whereby a known discrepancy in the stiffness derivative can be utilized to estimate a rather smaller discrepancy in the damping derivative.

6.1. *Rectangular Wing.*

The rectangular wing of moderately large aspect ratio $A = 4$ with control surfaces of constant chord does not introduce much interaction between chordwise and spanwise characteristics. The smooth equivalent incidences for part-span controls are easily determined from the appropriate equation (86) or (87), and as a further simplification the flow is taken to be incompressible. Only control oscillation is considered, and the six derivatives of lift, mid-chord pitching moment and hinge moments have been calculated from equations (32) to (36) by the present method with $m = 15, q = 6$ and $N \leqslant 4$. The various results from direct and reverse flow in Tables 9 to 12 serve to clarify many basic features of the theory. The discussion of the derivatives for part-span controls in Tables 10 and 11 is partly delayed until Section 6.2; we now concentrate on full-span controls, and especially on the effect of chord ratio E. The particular aspect ratio with $E = 0{\cdot}2$ enables us to make comparison between the theoretical hinge moments and the wind-tunnel measurements of Molyneux and Ruddlesden[9].

The dependence of the lift-damping $-z_{\dot{\xi}}$ on E with its changing sign near $E = 0{\cdot}4$ is illustrated by the curve in Fig. 3a. From the results in Table 9, $-z_{\dot{\xi}}$ and the stiffness derivatives $-z_{\xi}$ and $-m_{\xi}$ are less sensitive than $-m_{\dot{\xi}}$ to the number of chordwise terms N. Even so, the curves of pitching-moment damping against E for $N = 2, 3$ and 4 in Fig. 9 show good convergence, with nearly-indistinguishable curves for $N = 3$ and $N = 4$. Similarly good convergence for part-span controls is found in Table 10, and again $N \geqslant 3$ gives sufficient accuracy. Table 10 also includes a set of results for $E = 0{\cdot}35$, in which the spanwise factors $\Omega_{1\nu}$ for wing forces are replaced by $\Psi_{1\nu}$ that would normally occur in the equivalent incidence for the spanwise distribution of lift or hinge moment. Although the effect on lift and pitching-moment derivatives is quite trivial, the distinction between $\Omega_{1\nu}$ and $\Psi_{1\nu}$ is seen to be significant in the application to spanwise loading in Fig. 5b.

While the lift and pitching moment require equivalent incidences based on σ_{rp} in the present direct-flow method, τ_{rp} is used in the calculation of hinge moment. This applies without question to the stiffness derivative $-h_{\xi}$, as is suggested in Fig. 3b and demonstrated conclusively in Fig. 10. The upper diagram of $-h_{\xi}$ against E shows to large scale the very satisfactory convergence with respect to N, slightly marred when E increases above 0·4 as will be discussed later. By contrast, the small-scale lower diagram of Fig. 10 shows the chaotic picture that emerges when σ_{1p} is used in place of τ_{1p}; only for the larger values of $E > 0{\cdot}4$ is there any semblance of convergence with respect to N, and even for $N = 4$ there is a resulting error in $-h_{\xi}$ of more than 25 per cent when $E = 0{\cdot}2$. The high order of convergence with the special chordwise equivalent slopes τ_{1p} is maintained in Table 11a in the examples by direct flow where the control has part-span from $\eta_a = 0{\cdot}45$ to the tip.

The corresponding situation for the damping derivative $-h_{\dot{\xi}}$ differs in two respects. In the first place, the imaginary part of the boundary condition (1) and the quasi-steady incidence σ_{2f} in equation (23) are continuous at $x = x_h$; therefore the distinction between σ_{2p} and τ_{2p} is less crucial than between σ_{1p} and τ_{1p}. Although the solutions with σ_{2p} in the lower diagram of Fig. 11 show poorer convergence than the recommended ones with τ_{2p} in the upper diagram, the discrepancies between the two for $N = 4$ only becomes appreciable when $E < 0{\cdot}2$. In the second place, the damping $-h_{\dot{\xi}}$ in the second of equations (36) involves the coefficient $-I_{h3f}$ corresponding to the incidence α_{3f} indicated in equation (24) by means of the matrix operation $\mathbf{B}L_{1f}$. The most precarious assumption in the present method is that equivalent incidences α_{1e} can be used to replace L_{1f} by L_{1e} in this particular operation and so derive α_{3e} instead of α_{3f}. It is recommended that, whereas $-I_{h1f}$ (likewise $-I^*_{h1f}$ and $-I_{h4f}$ when $M \neq 0$) is based on τ_{1p} and $\Psi_{1\nu}$, the coefficient $-I_{h3f}$ should involve a different α_{1e} based on σ_{1p} and $\Omega_{1\nu}$. In Table 11b there are a few examples where, instead, the same $\alpha_{1e} = \tau_{1p}\Psi_{1\nu}$ has been used for both $-I_{h1f}$ and $-I_{h3f}$. The convergence of $-h_{\dot{\xi}}$ with respect to N remains fairly satisfactory, but incomplete, whichever $-I_{h3f}$ is used. Except for the smallest control $E = 0{\cdot}15$, the two procedures show smaller differences when $N = 4$ than when $N = 3$ but these discrepancies are quite as significant as the incomplete convergence.

Some support for the recommended procedure for $-I_{h3f}$, based on σ_{1p} and $\Omega_{1\nu}$ can be drawn from the evidence of solutions for the rectangular wing by reverse flow in Table 9. For the damping derivatives $-z_{\dot{\xi}}$ and $-m_{\dot{\xi}}$, in Table 9b, the reverse-flow calculations depend only upon solutions in modes that

involve neither equivalent slopes nor any question of principle concerning α_{3f}. The upper diagrams of Fig. 12 show equally good convergence when $-m_\xi$ and $-m_{\bar{\xi}}$ by direct and reverse flow are plotted against N; in this example of full span and $E = 0{\cdot}25$ the derivatives almost agree to four decimals when $N = 4$. Throughout Table 9 the lift and pitching-moment derivatives agree within 0·005 and 0·001 respectively for all E. This justifies the use of the chordwise equivalent slopes σ_{rp} for wing forces, and in particular the procedure for α_{3e} involving the loading l_{1e} from the equivalent incidence α_{1e}. There is no fundamental reason why the same incidence α_{3e} should not apply as well to hinge moment in direct flow.

As discussed in Section 5.3, the calculation of hinge moments by reverse flow involves additional types of chordwise equivalent slopes and is no simpler than the present method in direct flow. Although the two calculations of $-h_\xi$ and $-h_{\bar{\xi}}$ show fair correlation against N in the lower diagrams of Fig. 12, there are two undesirable features, the disparity in $-h_\xi$ for $N = 4$ to be considered later and the rather slow convergence in $-h_{\bar{\xi}}$. The following table for $\eta_a = 0$ and $E = 0{\cdot}25$ shows that $-I_{h3f}$ is solely responsible for the slow convergence.

N	$-I_{h1f}$	$-I_{h2f}$	$-I_{h3f}$
2	0·7295	0·2549	0·0760
3	0·7363	0·2593	0·1270
4	0·7363	0·2617	0·1559

It is likely that $-I_{h3f}$ would converge more rapidly with respect to N, if only α_{3f} could be obtained from a loading l_{1f} that incorporated the correct mathematical singularities at the hinge. Then by use of an equivalent incidence $-I_{h3f}$ might be calculated as successfully as $-I_{h1f}$ and $-I_{h2f}$ in the table above. Without such precise treatment more chordwise terms are needed and the restriction is one of computation. With $N = 4$, the damping derivative cannot be trusted to much better accuracy than 10 per cent, which in practical terms is marginally adequate.

Although the disparity in $-h_\xi$ for $E = 0{\cdot}25$ and $N = 4$ in Fig. 12 is a mere 1 per cent, the phenomenon can be seen in a more acute form for $E = 0{\cdot}20$ in Table 11a, where by reverse flow for $N = 4$ this derivative is clearly about 8 per cent too high. This raises the numerical difficulty that the chordwise equivalent slopes τ_r are indeterminate whenever the matrix, such as in equation (56), becomes singular. This situation cannot arise for wing forces since in direct flow the matrix, such as in equation (47), is always triangular with non-zero diagonal elements, and in reverse flow there is no problem of singularities in incidence. For hinge moments, however, the chordwise equivalent slopes become increasingly hazardous as N increases, and the critical values of E are listed in the following table.

Singularities in hinge moment		$N = 2$	$N = 3$	$N = 4$	
Direct flow	$-h_\xi$ and $-h_{\bar{\xi}}$	None	None	$E = \frac{7}{12}$	
Reverse flow	$-h_\xi$	None	$E = \frac{3}{8}$	$E = \frac{5 \pm \sqrt{7}}{12}$	$-h_{\bar{\xi}}$ $(M \neq 0)$
	$-h_{\bar{\xi}}(M = 0)$	None	None	$E = \frac{5}{12}$	

The problem is more severe in reverse flow, where with $N = 4$ there is danger near $E = 0{\cdot}196$, 0·417

and 0·637 in compressible flow. In direct flow the chordwise equivalent slopes τ_{1p} or τ_{2p} escape trouble when $N = 3$ and only succumb near $E = 0{\cdot}583$ when $N = 4$. This provides the explanation of the behaviour of $-h_\xi$ for $N = 4$ and $E > 0{\cdot}4$ in the upper diagram of Fig. 10. The small discrepancy of about $1\frac{1}{2}$ per cent at $E = 0{\cdot}5$ will clearly grow as E approaches 0·583. The complete story for $-h_\xi$ and $-h_{\dot\xi}$ in the case of incompressible flow and $N = 4$ is depicted in Fig. 13 over the range $0{\cdot}05 \leqslant E \leqslant 0{\cdot}75$. Because of the weaker singularity in α_{2f} than in α_{1f}, the singularities in $-h_{\dot\xi}$ at $E = 0{\cdot}583$ in direct flow and $E = 0{\cdot}417$ in reverse flow are very localized, and it is only necessary to avoid the critical values of E by ± 2 per cent for the discrepancies to become negligible. For the stiffness derivative the region $0{\cdot}4 < E < 0{\cdot}7$ is fraught with uncertainty, but an estimate over the whole range could be made from a faired curve of the direct-flow results for $0{\cdot}05 \leqslant E \leqslant 0{\cdot}40$ and $0{\cdot}65 \leqslant E \leqslant 0{\cdot}75$ and the reverse-flow results for $0{\cdot}40 \leqslant E \leqslant 0{\cdot}60$. There would be worse confusion for $N > 4$, since the critical conditions would occur at more values of E.

These singularities have no physical aerodynamic significance and are implicit in the present use of equivalent slopes. It is important to consider how to get rid of the difficulty by further approximation. A satisfactory expedient is indicated in Fig. 14, where the first N' terms in the polynomial (44) are used to represent the chordwise equivalent slopes $\tau_{rp}(N' \leqslant N)$. The individual plots of $-h_\xi$ against N for five full-span values of E are analysed for convergence in three ways:

(i) the standard $N' = N$ (full lines),
(ii) fixed $N' = 2$ (long dashed lines),
(iii) fixed $N = 4$ and variable N'.

In all these respects the convergence is good, except when $E = 0{\cdot}05$ and 0·50. The small value of E slows down convergence with respect to N, but not to any serious extent: the large value of E is approaching the critical value for the singularity in τ_{1p}, but the result for $N' = 3$, $N = 4$ is quite reliable and is the best substitute for the standard $N = 4$ solution in these circumstances. This smaller value of N' has negligible effect on the corresponding values of $-h_{\dot\xi}$ in Fig. 14. The results $-h_\xi = 0{\cdot}3456$ and $-h_{\dot\xi} = 0{\cdot}3902$ from Table 12 when $E = 0{\cdot}50$, $N' = 3$ and $N = 4$ compare satisfactorily with the respective quantities 0·3451 and 0·3891 for $N = 4$ by reverse flow from Tables 11a and 11b. The expedient of reducing N' becomes necessary in Section 6.4, when E varies continuously from $\frac{1}{7}$ to 1 along the span.

Experimental data from Ref. 9 for a full-span control of chord ratio $E = 0{\cdot}2$ are included in Figs. 10 and 11. The factor $E^{-2} = 25$ converts H_β and $H_{\dot\beta}$ in Table 3 of Ref. 9 to h_ξ and $h_{\dot\xi}$ in the present notation. Both measured derivatives have smaller magnitude than the best available theoretical values with $N = 4$, the ratios being 0·56 and 0·69 for $-h_\xi$ and $-h_{\dot\xi}$ respectively. These discrepancies are of higher order than any errors from theoretical or experimental technique and are attributable to the combined effects of thickness and viscosity, analysed in steady two-dimensional flow by the first author[19]. Given the aerofoil section, the Reynolds number and the position of boundary-layer transition, the stiffness derivative for low frequency may be determined as one half of the hinge-moment derivative b_2 from charts in Figs. 2a, 4, 5, 10 and 11 of Ref. 19. The 10 per cent thick RAE 101 aerofoil has trailing-edge

$-h_\xi$	Theory	Ref. 9 or Ref. 19		Experiment
		$x_{tr} = 0{\cdot}1c$	$x_{tr} = 0{\cdot}6c$	Theory (thin)
Thin aerofoil	0·461	—	—	0·63 or 0·68
Thick aerofoil	0·406	0·291	0·312	
Thin wing	0·376	—	—	0·56
Thick wing	—	0·212		

angle 2 $\tan^{-1}$ 0·089, the Reynolds number in Ref. 9 is between $0{\cdot}4 \times 10^6$ and $2{\cdot}3 \times 10^6$, but the state of boundary layer is not recorded. Thus the two-dimensional $-h_\xi = -\frac{1}{2}b_2$ has been determined for a representative Reynolds number 10^6 and boundary-layer transition (x_{tr}) alternatively at 0·1 chord and 0·6 chord; the preceding table shows some correlation between the data for the RAE 101 aerofoil and the rectangular wing. The results indicate that, of the 44 per cent discrepancy between thin-wing theory and experiment, 12 per cent due to aerofoil thickness and about 25 per cent due to viscosity can be predicted from two-dimensional considerations. A rough empirical method of bridging the rather smaller discrepancy in $-h_\xi$ is suggested in Section 7.

6.2. *Untapered Swept Wing.*

Although the calculations for this wing are restricted to steady incompressible flow, there are several new features to be considered. Lift, pitching moment and hinge moment due to symmetrical part-span controls, outboard and inboard, are discussed; comparison with results for the rectangular wing of the same aspect ratio 4 shows the influence of 45° sweepback over a range of control span. The introduction of sweepback raises the question about artificial central rounding posed by the alternative shapes in equations (5) and (6). Arguments in favour of the latter are supported by independent evidence from electrical analogue[7] on stiffness derivatives and spanwise loading. The present method has been applied with $m = 15$, $N = 2, 3$ and 4 and $q = 2N$, as was found satisfactory for this planform in Ref. 11. The results, illustrated in Tables 13 to 15, include spanwise distributions of local centre of pressure and hinge moment.

The evaluation of hinge moment is discussed in Section 5.2; the procedure involves the calculation of local hinge moments, defined by $h_{\xi L}$ in equation (92), and subsequent integration over the span of the control. Typical distributions of $-h_{\xi L}$ for the swept wing with outboard and inboard controls ($E = 0{\cdot}25$) are shown in Fig. 15. Results with the outboard control of extent $0{\cdot}45 \leqslant |\eta| \leqslant 1$ ($\eta_a = 0{\cdot}45$) are obtained from solutions with $N = 2, 3$ and 4, and from Fig. 15a it is apparent that insufficiency of chordwise terms leads to an underestimate near the inboard end and an overestimate near the tip, where the convergence of $-h_{\xi L}$ with respect to N is slowest. The corresponding picture for the inboard control of extent $0 \leqslant |\eta| \leqslant 0{\cdot}45$ ($\eta_f = 0{\cdot}45$) in Fig. 15b again shows the most variation at the centre and outboard and with respective tendencies to underestimate and overestimate $-h_{\xi L}$ when N is too small, but the whole distribution seems to converge with respect to N. The relatively large local hinge moment near $\eta = 0$ follows from the expected build-up of loading in the region of the trailing edge which is better represented by the collocation points as N increases. This characteristic of the swept wing is emphasized by comparison with the full curve in Fig. 15b for the rectangular wing with inboard control of the same span and chord. Although, from calculations with $N = 4$, the swept wing gives nearly 20 per cent more hinge moment at $\eta = 0$, the integrated value of the derivative $-h_\xi = 0{\cdot}292$ is 14 per cent below the corresponding value $-h_\xi = 0{\cdot}340$ for the rectangular wing.

For outboard controls the hinge-moment stiffness is some 20 per cent lower for the wing of 45° sweepback. This is shown in the upper diagram of Fig. 16, where the solutions with $N = 3$ for the two wings give similar variations in $-h_\xi$ against η_a; the percentage reduction due to sweepback increases slightly as the span extends further inboard. The remainder of Fig. 16 illustrates by graphs against N the adequate convergence of $-h_\xi$ for both wings with various values of η_a and E. In all cases there is a substantial reduction in $-h_\xi$ due to sweepback. An increase in control chord also reduces $-h_\xi$, since the hinge moment is divided by the product of control area and control chord; this effect is very small for the swept wing with full-span control, but becomes more marked when there is zero sweep or a part-span outboard control.

In the preceding examples for the untapered swept wing the central rounding has been defined according to equation (5), as originally recommended in Ref. 5. Later analysis in Ref. 11 has established certain advantages from increasing the central rounding, for example, by taking equation (6) instead of equation (5) with the same spanwise extent $|y| < y_i$; the central displacement proportional to $f(0)$ is then doubled, and as a result the collocation error is much reduced. However, unless the wing has small

sweep, the doubled rounding introduces a spurious effect of its own. It is shown in Ref. 11, that this rounding error is of the same order of magnitude as the collocation error and that, by chance, in steady flow more accurate results for wings at incidence are achieved with the central rounding of equation (5). Now it may be argued that aerodynamic forces due to the oscillation of trailing-edge controls are unlikely to be influenced much by the doubled rounding of equation (6), since the leading apex is at zero incidence: on the other hand, collocation error from the less gentle shape of equation (5) is likely to persist. There is reason to suppose that accuracy will be gained by changing the shape of rounding from equation (5) to that of equation (6). Tables 13 to 15 contain several illustrations of the changes in aerodynamic loading so produced. In the first place, the results at the foot of Table 14a show that the hinge moments for $E = 0{\cdot}25$, already discussed, are virtually unchanged; Table 14b shows that a 6 per cent decrease in local hinge moment $-h_{\xi L}$ at $\eta = 0$ is offset by smaller increases elsewhere. The lift and pitching moment in Table 13a are increased by about 3 per cent when $\eta_a = 0$ and the control extends to the centreline, but the effect diminishes below 1 per cent for $\eta_a \geqslant 0{\cdot}25$. Table 15 shows that the preferred rounding from equation (6) increases the central lift by as much as 16 per cent, but over the outer part of the span the increment falls to 2 per cent and below. Likewise in Table 13b, the local centre of pressure as a fraction of local chord,

$$X_{cp}(\eta) = \tfrac{1}{4} - \frac{\mu}{\gamma}, \tag{116}$$

is seriously affected in the central region only.

In the absence of exact theoretical results, we look to the analogue experiments in an electric tank for the particular planform. Enselme[7] uses two models of the flow past a lifting surface, in which the electric potential is identified with the perturbation velocity potential and the perturbation acceleration potential respectively. In the velocity-potential analogue, from which we are to take results, there is a tank of liquid with its free surface representing the half plane of the wing and with one wall as the plane of symmetry $y = 0$. The velocity potential is represented by a large number of small electrodes over the planform and by narrow conducting strips in the wake of potential such that the Joukowski condition is satisfied along the trailing edge. The boundary condition at the wing or control surface requires an electric current proportional to local incidence; when this is satisfied, the potentials of the electrodes determine the aerodynamic loading. There are data from the velocity-potential analogue in Figs. 7 to 11 of Ref. 7 that can be compared with the results of the present method. Moreover, in Figs. 7 and 9 of Ref. 7 there are independent results from the acceleration-potential analogue that confirm the lift, pitching moment and spanwise loading from the velocity-potential analogue for full-span and part-span controls.

The data in Fig. 7 of Ref. 7 are converted to the present notation in the plots of $-z_\xi$ and $-m_\xi$ against η_f in Fig. 17. These show distinctly better comparisons with the present method when the central rounding from equation (6) is used in place of that from equation (5). Fig. 17 also illustrates the effect of sweepback which is quite small on lift until the inboard flap extends beyond $\eta = 0{\cdot}4$; but the moment about the mid-root-chord pitching axis is negligible for the rectangular wing when $E = 0{\cdot}25$, while its variation with increasing η_f for the swept wing shows the expected aft movement of centre of pressure. The convergence of $-z_\xi$ and $-m_\xi$ with respect to N in Table 13a is nearly as convincing as for the rectangular wing in Tables 9a and 10a and, from the practical standpoint, leaves little to be desired.

To obtain the spanwise loadings in Table 15 and the values of X_{cp} in Table 13b, the equivalent incidences $\sigma_{1p}(E)\,\Psi_{1\nu}(\eta_a)$ are required. The one comparison between $N = 2$ and $N = 4$ in Table 15a indicates the small effect of N on loading over most of the span. Likewise, for the two cases in Table 13b, solutions for $N = 2, 3$ and 4 show good convergence properties of X_{cp}, except at the centreline and outermost collocation section $\eta = 0{\cdot}9808$, where there are discrepancies of order 0·01. To this order of accuracy there is excellent agreement between the calculated X_{cp} and the analogue data in Fig. 11 of Ref. 7. To

compare spanwise loadings, the quantities γ from Figs. 8 to 10 of Ref. 7 are converted by the factor $\frac{1}{2}$ and used to obtain the plotted analogue results for outboard controls ($E = 0{\cdot}25$) in Fig. 18a and for inboard controls ($E = 0{\cdot}15, 0{\cdot}35$) in Fig. 18b. Note first the good agreement between the present method and the electrical analogue in Fig. 18a when $\eta_a \geqslant 0{\cdot}45$. The agreement is less satisfactory for the remaining broken curves in Fig. 18; however, with the central rounding of equation (5) collocation error is anticipated whenever the control extends close to or includes the centreline. It is gratifying that the full curves, corresponding to the preferred rounding of equation (6) with $y_1/s = \sin[\pi/(m+1)]$, are in so much better agreement with the analogue results.

6.3. *Tapered Swept Wing.*

The planform of aspect ratio 2 and its swept hinge line are defined in Fig. 8; the control chord ratio E varies from 0·232 at the root to 0·326 at the tip. The wing is considered in compressible flow of Mach number $M = 0{\cdot}7806$ such that the reduced aspect ratio $\beta A = 1{\cdot}25$. The same configuration has been used in the related theoretical investigation for general frequency in Ref. 2 with outboard controls $\eta_a = 0, 0{\cdot}25, 0{\cdot}50$ and $0{\cdot}75$. The present results for low frequency therefore include some that were published in Ref. 2 and were calculated prior to the advance in lifting-surface theory in Ref. 5. Certain other improvements in the treatment of control surfaces have subsequently been introduced, especially with regard to equivalent incidences and the artificial rounding of planform and hinge line. Since this particular example is the most general one to be considered and all aspects of Sections 4 and 5 are taken into account, we shall study the numerical significance of the various refinements. Another factor, governing the choice of configuration, is that a half-model of the wing with oscillating control of part-span $0{\cdot}5 < \eta < 1$ is to be tested at the N.P.L. in subsonic and transonic flow. Since this is intended to represent an aileron, it is necessary to examine the effect of the reflection plane on rolling moment and hinge moment by comparing calculations for symmetrical and antisymmetrical spanwise loading.

The pitching derivatives for the tapered swept wing have been discussed in Ref. 11, notably with reference to Fig. 22 of that paper. Checks by reverse flow have revealed quite large discrepancies in $-z_{\dot{\theta}}$ and $-m_{\dot{\theta}}$ when the artificial rounding in equation (5) is used, and these are attributed to collocation error. The doubled rounding from equation (6) virtually eliminates the trouble, but it is necessary to compensate for the effect of rounding or to ensure that this is reasonably small, as is thought to be the case for these particular derivatives in Table 16a. Good convergence with respect to $N(= 2, 3$ or $4)$ is found for both lift and pitching moment and also for $-h_\theta$ and $-h_{\dot{\theta}}$ in Table 16b. These cross derivatives of hinge moment, defined in equations (27) and (28), show a small dependence on the choice of planform rounding, but are more sensitive to the parameter q from equation (15) and to the question of rounding the hinge line. The analysis in Ref. 11 establishes that $q = 6$ often suffices where the original method (with $q = 1$) does not, and that the errors with $q = 1$ tend to increase as N increases; in the present instance 8 per cent of $-h_\theta$ is at stake for the full-span control when $N = 3$. For the untapered swept wing in Section 6.2, the hinge line is rounded to remain parallel to the leading and trailing edges and to preserve the control area. Now, however, the sweepback of the hinge line is unrelated to that of the leading or trailing edge; consistent with equations (4) and (6), we take

$$x_h(y) = x_{hr} + \{x_h(y_i) - x_{hr}\} f(\lambda) \quad \text{over} \quad |y| < y_i, \tag{117}$$

where x_{hr} is the true hinge ordinate at the root, $\lambda = |y|/y_i$,

$$f(\lambda) = \tfrac{1}{3} + \lambda^2 - \tfrac{1}{3}\lambda^3 \text{ and } y_i = s \sin \frac{\pi}{m+1}. \tag{118}$$

This is thought to be preferable to leaving the hinge line straight, and Table 16b shows in the full-span case a reduction of 5 or 6 per cent in the calculated values of $-h_\theta$ and $-h_{\dot{\theta}}$.

The wing forces due to control rotation are included in Tables 17a and 18a. The following table lists the available results for the full-span control and $N = 3$.

Hinge	Planform rounding	q	$-z_\xi$	$-m_\xi$	$-z_{\dot\xi}$	$-m_{\dot\xi}$
Straight	Eqn. (5)	1	0·946	0·595	−0·083	0·110
Straight	Eqn. (5)	6	0·918	0·587	−0·052	0·111
Straight	Eqn. (6)	6	0·942	0·592	−0·079	0·109
Eqn. (117)	Eqn. (6)	6	0·937	0·594	−0·092	0·102

The lift derivatives are more sensitive than those of pitching moment about mid-root-chord. The first set with $q = 1$ is from the original low-frequency data used in Ref. 2. Although the effects of increasing q to 6 and of increasing the central rounding to that of equation (6) largely cancel each other, both are more significant than the influence of the rounded hinge line. A striking result is that, while $-z_\xi$ and $-z_\theta$ are of similar magnitude, the derivative $z_{\dot\xi}$ is only 7 per cent of $-z_{\dot\theta}$ for the pitching axis through mid-root-chord, but it is pertinent that $-z_{\dot\theta}$ passes through zero as the axis traverses the hinge line. Fig. 19 shows the effect of part-span $\eta_a \leqslant \eta \leqslant 1$ on the lift derivatives. Of the three solutions indicated in the legend, the full curves are preferred to the results with the planform rounding of equation (5). It is fortuitous that the $q = 1$ solution lies so close, for its accuracy is impaired not only by the choice of rounding but by the lack of two other refinements; in place of Ω_{1_ν} in equation (84) the spanwise equivalent slopes Ψ_{1_ν} for spanwise loading are used and, furthermore, the gradient term involving Ω_{2_ν} is omitted altogether. The greatest differences in Fig. 19 at $\eta_a = 0$ have already been discussed; some confidence can be placed in the relatively flat curve of $-z_{\dot\xi}$ near $\eta_a = 0$, so as to cast doubt on the original behaviour for $q = 1$, which is now thought to arise from collocation error due to insufficient planform rounding. The revised values of all four wing derivatives with $q = 6$ in Tables 17a and 18a show excellent convergence with respect to N and agreement within 0·003 of the values obtained by Woodcock[8] for $\eta_a = 0{\cdot}5$. Moreover, the checks by means of reverse flow in Tables 17b and 18b are convincing, as illustrated in the graphs of the damping derivatives $-z_{\dot\xi}$ and $-m_{\dot\xi}$ against N in the upper diagrams of Fig. 20.

Corresponding results for hinge moment are less satisfactory as regards reverse-flow checks and convergence with respect to N. The lower diagrams of Fig. 20 are prepared from values of $-h_\xi$ and $-h_{\dot\xi}$ for $\eta_a = 0{\cdot}5$ in Tables 17 and 18. Whilst $-h_\xi$ converges well enough with respect to N in direct flow, the same is not true of the calculations by reverse flow; by contrast, $-h_{\dot\xi}$ satisfies the reverse-flow check to reasonable accuracy, whilst the convergence is rather slow. Although difficulties in $-h_\xi$ with four chordwise terms have been encountered for the rectangular wing in Fig. 13, these do not arise in the relevant range of control chord ratio $0{\cdot}25 < E < 0{\cdot}33$. Without offering an explanation of the discrepancy in $-h_\xi$ obtained by reverse flow, we regard the result as further evidence to discourage the application of reverse-flow principles to hinge moment (Section 5.3), especially when there is the complication of control taper. Unlike that for the rectangular wing in Section 6.1, the rather slow convergence in $-h_{\dot\xi}$ is not primarily due to the hinge-moment coefficient $-I_{h3f}$, as the following table shows.

N	$-I_{h1f}$	$-I_{h2f}$	$-I_{h3f}$	$-I_{h4f}$	$-I^*_{h1f}$
2	0·3164	0·0912	0·0598	0·5617	0·5938
3	0·3706	0·1117	0·0917	0·6619	0·6934
4	0·3792	0·1217	0·1075	0·6786	0·7051

From equation (36) it is seen that the compressibility factors with $\beta = 0{\cdot}625$ ($\beta^{-3} = 4{\cdot}1$) aggravate the

problem, so that the coefficients are needed to better accuracy than for incompressible flow. Nevertheless, the present results with $N = 4$ are probably adequate for semi-empirical use at sub-critical Mach numbers. The comparisons with the values $-h_\xi = 0{\cdot}363$ and $-h_{\bar{\xi}} = 0{\cdot}197$ from Ref. 8 show that the former is unsatisfactory, because in effect the equivalent incidences in Ref. 8 correspond to chordwise slopes σ_{1p} and, as we have seen in Fig. 10, it is essential to use τ_{1p}; as in Fig. 11 with $N = 4$, the use of τ_{2p} in place of σ_{2p} is less critical, and therefore the value of $-h_{\bar{\xi}}$ from Ref. 8 is well within the present uncertainty arising from incomplete convergence.

The dependence of hinge moment on control span is presented in Fig. 21, where the full curves from direct flow are regarded as the best available for $N = 3$ and show how both stiffness and damping decrease in magnitude as η_a increases. Apart from the less accurate results by the reverse-flow method, the only significant differences in $-h_\xi$ arise from the choice of rounding in the full-span case. Another value $-h_\xi = 0{\cdot}481$ for $\eta_a = 0$ in Table 17a shows that the hinge rounding has more effect than planform rounding in this case. The same is probably true of $-h_{\bar{\xi}}$; the large discrepancies between the full curve and the circles in the lower diagram of Fig. 21 arise primarily because, in common with the original calculations with $q = 1$, the solutions corresponding to the planform rounding of equation (5) use the equivalent slopes τ_{1p} or τ_{2p} and Ψ_{1v} throughout. It has been demonstrated in Section 6.1, however, that the combination σ_{1p} and Ω_{1v} should be used in the matrix operation to obtain α_{3e}, even for the purpose of evaluating $-I_{h3f}$, and this procedure has been followed in the calculations with $q = 6$ and the doubled rounding of equation (6) in Table 18a. It may be helpful to set out the refinements leading from the original method to the present standard method in five stages:

(a) to replace $q = 1$ by $q = 6$,

(b) to replace planform rounding of equation (5) by equation (6),

(c) to include spanwise gradient correction Ψ_{2v} in addition to Ψ_{1v},

(d) to replace τ_{1p} by σ_{1p} in the evaluation of $-I_{h3f}$,

(e) to replace Ψ_{1v} and Ψ_{2v} by Ω_{1v} and Ω_{2v} respectively in the evaluation of $-I_{h3f}$.

The following table illustrates the effect of each stage on the hinge-moment damping for $N = 3$ in the case $\eta_a = 0{\cdot}5$, chosen to avoid the complication of rounding the hinge line.

Rounding	q	Slopes for α_{3f}	$-h_{\bar{\xi}}$	Stage
Eqn. (5)	1	τ_{1p}, Ψ_{1v}	0·2113	
Eqn. (5)	6	τ_{1p}, Ψ_{1v}	0·2058	(a)
Eqn. (6)	6	τ_{1p}, Ψ_{1v}	0·2055	(b)
Eqn. (6)	6	τ_{1p}, Ψ_{1v}, Ψ_{2v}	0·2057	(c)
Eqn. (6)	6	σ_{1p}, Ψ_{1v}, Ψ_{2v}	0·1809	(d)
Eqn. (6)	6	σ_{1p}, Ω_{1v}, Ω_{2v}	0·1769	(e)
Eqn. (5)	1	σ_{1p}, Ψ_{1v}	0·1887	

Stage (a) produces a change of about 3 per cent: neither stage (b) nor (c) is really significant, and it seems true in general that the aerodynamic derivatives are not very sensitive to whether the discontinuous

gradient at $\eta = \eta_a$ is included, but the change of spanwise equivalent slope in stage (e) contributes 2 per cent: the large decrease of 12 per cent in $-h_{\dot{\xi}}$ is due to stage (d), and the first and last values of $-h_{\dot{\xi}}$ show that a similar decrease is achieved when σ_{1p} replaces τ_{1p} in the original calculation of $-I_{h3f}$. As in Section 6.1, the derivative by reverse flow, $-h_{\dot{\xi}} = 0{\cdot}1695$, tends to support the method that is now recommended.

The spanwise distributions of hinge moment are formulated in equations (90) and (91) and are illustrated for the part-span case $\eta_a = 0{\cdot}5$ in Figs. 22 and 23. The steady distribution $-h_{\xi L}$, with average value equal to the stiffness derivative $-h_{\xi}$, is plotted against η for $N = 2, 3$ and 4; Fig. 22 shows the largest differences over the inner half of the control span. Referring back to Fig. 15a for the untapered swept wing, we see the same tendency to underestimate $-h_{\xi L}$ over the inner half and to overestimate $-h_{\dot{\xi}L}$ near the tip, if too few chordwise terms are taken. Nevertheless, the distributions with $N = 4$ have probably converged well enough. The full curve of $-h_{\dot{\xi}L}$ in Fig. 23 gives the corresponding distribution of the damping with $N = 4$, and the other three curves represent particular contributions from equation (91). In the first place we consider the quasi-steady problem in which the imaginary part of the boundary condition in equation (1) is treated in isolation; thus by equation (3) and the definition of α_{2f} in equation (23)

$$\alpha = -w/U = (i\omega\bar{c}\,\xi_0/U)\,\alpha_{2f},$$

and equation (96) becomes simply

$$-h_{\dot{\xi}L} = \frac{A}{4}\left(\frac{\bar{c}}{\bar{c}_f}\right)^2 F_2(\eta). \tag{119}$$

This quasi-steady contribution accounts for about half of the damping. Another distinctive term in equation (96), on which the discussion has centred, is the third term in the square brackets associated with the loading l_{3f} and proportional to β^{-2}; in Fig. 23 this second contribution is slightly larger than the quasi-steady part and of opposite sign, so that the remainder of the damping turns out to be rather larger than $-h_{\dot{\xi}L}$. By inspection of equation (96), it can be seen that this third and largest contribution is proportional to $M^2\beta^{-2}$, which stresses the growing importance of numerical accuracy as Mach number increases.

The calculations include cases in which the port and starboard controls oscillate antisymmetrically; the lift and pitching moment vanish identically, but the derivatives of rolling and hinge moment from equations (35) and (36) are required. It is planned to estimate the rolling moments from half-model experiments with the tunnel side-wall, as reflection plane. Since the measured quantity will correspond to a 'bending moment' with force mode proportional to $|\eta|$ and symmetrical spanwise loading, the special derivatives $-b_{\xi}$ and $-b_{\dot{\xi}}$ have been computed from the formulae

$$\left.\begin{aligned} -b_{\xi} &= \frac{1}{2\beta}\left(-I_{b1f}\right) \\ -b_{\dot{\xi}} &= \frac{1}{2\beta}\left[\frac{M^2}{\beta^2}\left(-I^*_{b1f}\right)+\frac{\beta^2-M^2}{\beta^2}\left(-I_{b2f}\right)+\frac{1}{\beta^2}\left(-I_{b3f}\right)-\frac{M^2}{\beta^2}\left(-I_{b4f}\right)\right] \end{aligned}\right\} \tag{120}$$

with the aid of equations (37). The formulae for hinge moment and the method of calculation in Section 5.2 apply to symmetrical and antisymmetrical cases alike. The available derivatives are given in Table 19, and the results for $N = 3$ are plotted in Fig. 24. The ratio $l_{\dot{\xi}}/b_{\dot{\xi}}$ decreases rapidly as η_a decreases, and the value 0·874 for $\eta_a = 0{\cdot}5$ is the correction factor that must be applied to the measured half-wing rolling moment as part of the tunnel-wall constraint. The corresponding ratio of the two values of $h_{\dot{\xi}}$ is 0·966 and shows, as expected, that the starboard hinge moment is less influenced by the sense in which the port control oscillates. The damping derivatives $-l_{\dot{\xi}}$ and $-b_{\dot{\xi}}$ are small, but of opposite sign; unless

measurements of the latter derivative confirm theoretical prediction, no wall correction can be attempted. Provided that $\eta_a \geqslant 0{\cdot}25$, $-h_{\xi}$ is virtually uninfluenced by the reflection plane; in this respect the half-model experiments will be fully representative.

6.4. *Cropped Delta Wing.*

The fourth and last planform, defined in Fig. 8, has the lowest aspect ratio 1·8 and high taper with $c_r = 7c_t$. The full-span control with unswept hinge and constant chord $c_f = c_t$ has been the subject of an oscillatory experimental investigation by Bratt *et al*,[10] who determined the direct hinge-moment derivatives $-h_{\xi}$ and $-h_{\dot{\xi}}$ over a range of Mach number. The present calculations also cover outboard part-span controls. To enable comparisons to be made with the measured derivatives, the theoretical results are obtained for the four Mach numbers 0, 0·553, 0·745 and 0·866 corresponding to equally spaced values of β. An important feature of the planform geometry is the rapid spanwise variation of the chord ratio E from $\frac{1}{7}$ at the root to 1 at the tip. This contains the special value $E = 0{\cdot}58\dot{3}$ for which the chordwise equivalent slopes τ_{rp} are unobtainable when $N = 4$. The expedient of reducing N' from 4 to 3, already discussed in Section 6.1, is successfully applied to the evaluation of the spanwise distribution of hinge moment.

The derivatives for pitching motion about an axis through the mid-root-chord are given in Table 20. The wing derivatives for $M = 0{\cdot}745$ in Table 20a show that the factor q is much less critical than for the tapered swept wing with similar reduced aspect ratio βA; the small effect of increasing q from 1 to 6, with $N = 3$, is thought to be associated with the unswept trailing edge. The results in Table 20a also show remarkable convergence with respect to N for all the derivatives $-z_{\theta}$, $-m_{\theta}$, $-z_{\dot{\theta}}$ and $-m_{\dot{\theta}}$. The effect of Mach number is shown in Table 20b, and from $M = 0$ to $M = 0{\cdot}866$ compressibility has caused the lift derivatives to increase by about 14 per cent and those of pitching moment by roughly 60 per cent. The hinge-moment derivatives in Table 20c introduce the control-span parameter η_a, and it is found that the trend of $-h_{\theta}$ against η_a reverses as M increases from 0 to 0·866. For $\eta_a \leqslant 0{\cdot}5$ this derivative varies by less than 14 per cent, while $-h_{\dot{\theta}}$ shows a large dependence on Mach number similar to that of $-m_{\dot{\theta}}$. The calculations from equations (28) present no special difficulty. The chief uncertainty arises from lack of experimental data on $-h_{\dot{\theta}}$, especially in view of the expected large effects of boundary layers on the stiffness derivative.

The wing forces due to control oscillation are presented in Figs. 25 and 26 as functions of M and η_a; these results for $m = 15$, $N = 3$, $q = 6$ and the planform rounding of equation (6) are taken from Tables 21b and 22b respectively. The stiffness derivatives $-z_{\xi}$ and $-m_{\xi}$ are plotted against Mach number in Fig. 25 for the particular values $\eta_a = 0$, 0·25, 0·50 and 0·75. Both derivatives show a steady decrease as the control span $s(1-\eta_a)$ decreases, and the greatest effect of M occurs in the full-span case. The damping derivatives in Fig. 26 are plotted against η_a for the four Mach numbers $M = 0$, 0·553, 0·745 and 0·866. There is again a progressively larger effect of compressibility as control span increases, until for $\eta_a = 0$ the value of $-z_{\dot{\xi}}$ decreases from 0·12 to $-0{\cdot}21$ as M increases from 0 to 0·866; the smaller effect on $-m_{\dot{\xi}}$ is limited to an increase of at most 22 per cent. The further results for the four derivatives in Tables 21a and 22a show quite small dependence on the spanwise integration parameter q and satisfactory convergence with respect to the number of chordwise terms.

Before discussing the integrated hinge-moment stiffness and damping, we consider their spanwise distributions in Figs. 27 and 28. The case of greatest theoretical interest is the steady distribution of $-h_{\xi_L}$ in Fig. 27a over the half-span outboard control, for which E varies from 0·25 to 1 and passes through the special value $E = 0{\cdot}58\dot{3}$ at $\eta = 0{\cdot}881$. Although this position is nearly midway between the collcation sections $\eta = \sin(\nu\pi/16)$ with $\nu = 5$ and 6, the implied singularity in τ_{lp}, discussed in Sections 3.2 and 6.1, clearly disrupts the standard solution with $N = 4$. The effective remedy is to reduce by one the order of the polynomial representing the chordwise equivalent slopes; the designation $N' = 3$ implies a quadratic variation in $\alpha_e(X)$ at all sections, and the combination $N = 4$, $N' = 3$ means that the four chordwise terms and collocation positions are retained. The dot-dash curve in Fig. 27a is preferable to the standard solution $N = N' = 4$ in the peculiar circumstances and should also be more accurate than the result with $N = N' = 3$. In the case of the inboard control $\eta_f = 0{\cdot}5$ in Fig. 27b, $E \leqslant 0{\cdot}25$ and the same difficulty

does not arise; the standard $N = 4$ solution is then the best available and gives some idea of the deficiencies of the solution with $N = 4, N' = 3$. The general impression from Fig. 27 is the inadequacy of the standard $N = 2$ solutions for hinge moment and accuracy of the order ± 10 per cent in the solutions with $N' = 3$. The distributions of hinge-moment damping for the four Mach numbers in Fig. 28 are given for $\eta_a = 0{\cdot}5$ by standard $N = 3$ solutions that present no difficulty. The quantity $-h_{\dot{\xi}L}$ from equation (91) or (96) is more sensitive to Mach number away from the wing tip, and this results in a more peaky maximum near $\eta = 0{\cdot}75$ as M increases. Since $-h_{\dot{\xi}}$ is the average value of $-h_{\dot{\xi}L}$, the large compressibility effect on this damping derivative in Table 22b can be associated with the inner part of the control span. The values of $-h_{\xi}$ and $-h_{\dot{\xi}}$ in the last two columns of Tables 21a and 22a show rather less dependence on N' than might be expected. Changes of sign in the discrepancies between the full and dot-dash curves in Fig. 27a lead to considerable cancellation of errors in the integrated derivative $-h_{\xi}$, and the resulting difference is no more than 5 per cent, and in the case of $-h_{\dot{\xi}}$ it is only 3 per cent. This smaller discrepancy could be anticipated from the direct-flow results ($N = 4$) for the rectangular wing at $M = 0$ in Fig. 13, where the divergence of $-h_{\dot{\xi}}$ near $E = 0{\cdot}583$ reflects the localized effect of the weak singularity in α_{2f} in contrast to the wider influence of the discontinuity in α_{1f} on the divergence of $-h_{\xi}$. Of course, for compressible flow the step discontinuities in α_{1f} and α_{4f} influence $-h_{\dot{\xi}}$ through the coefficients $-I^*_{h1f}$ and $-I_{h4f}$ of equation (36), and there is reason to prefer the results from the last column of Table 22a.

In Fig. 29, the two hinge-moment derivatives in the full-span case are plotted against M and compared with the experimental results of Ref. 10 for an amplitude of oscillation $\zeta_o = 1^\circ$ and frequencies of 27 and 104 cycles per second. The present theoretical results in the limiting case $\bar{\nu} \to 0$ are used for the lower frequency; but, since $\bar{\nu}$ is shown to range from 0·6 to 0·25 for the higher frequency, $-h_{\dot{\xi}}$ has been corrected for frequency effect by equation (17) of Ref. 20, whence for sufficiently small $\bar{\nu}$

$$-h_{\dot{\xi}} = (-h_{\dot{\xi}})_{\bar{\nu}\to 0} + (A\bar{\nu}/16)(z_{\xi} h_{\theta})_{\bar{\nu}\to 0} . \tag{121}$$

With the aid of the derivatives in Tables 20c and 21b and the graph of $\bar{\nu}$ in Fig. 29, the small correction to $-h_{\dot{\xi}}$ is indicated by the curve of long dashes, which is somewhat closer in shape to the experimental points ($\times$) for the higher frequency. The greatest differences occur in $-h_{\xi}$, whose ratio of experimental to theoretical value varies from 0·72 at $M = 0{\cdot}553$ to 0·58 at $M = 0{\cdot}866$. At the lower Mach number the Reynolds number based on $\bar{c}$ is about $1{\cdot}5 \times 10^6$, and the chord ratio at mid-semi-span is $E = 0{\cdot}25$; when the charts of Ref. 19 are applied to this particular 10 per cent RAE 102 aerofoil section at $M = 0$ with boundary-layer transition $x_{tr} = 0{\cdot}35c$, the two-dimensional quantity $-h_{\xi} = -\frac{1}{2} b_2 = 0{\cdot}330$ is estimated to be 0·70 times its theoretical value 0·474 for a thin hinged plate. It is not known how much Mach number affects this ratio 0·70, but it is of the correct order to explain the low experimental values of $-h_{\xi}$ in Fig. 29. The measured damping derivative shows relatively small discrepancies due to the combined effects of thickness and viscosity until the Mach number exceeds 0·8. However, a curve through the preferred theoretical value (+) at $M = 0{\cdot}745$ would give somewhat larger differences, which are rather similar to that for the rectangular wing in Fig. 11.

7. *Empirical Correction to Damping Derivatives.*

The predictions of the present linear theory and the available measurements of oscillatory hinge moment on the rectangular and cropped delta wings have shown a consistent tendency towards better agreement for damping than for stiffness. Whilst experience from steady flow gives some indication of non-linear effects on stiffness derivatives at low frequencies, there is no such direct approach to the damping. The available two-dimensional experiments are of little help, because the theoretical damping derivatives at low frequency usually contain a dominant term in log $\bar{\nu}$ that does not arise for wings of finite aspect ratio. A greater barrier to the understanding of the three-dimensional problem is the unpredictable behaviour of unsteady boundary layers and their possible influence on the damping derivatives, especially those that involve control surfaces. The greatest uncertainty and the greatest need are felt in the upper subsonic speed range; the saving grace is that predictions within ± 10 per cent will suffice in practice and, therefore, a much simpler empirical approach to the problem can be adopted.

Damping forces due to control oscillation are split into the quasi-steady contribution from $\alpha = \alpha_{2f}$ and the residual part with the application of respective correction factors k_1 and k_2. Thus we write the corrected hinge-moment damping in the form

$$(-h_{\dot{\xi}})_c = \frac{k_1}{2\beta}(-I_{h2f}) + k_2\left[-h_{\dot{\xi}} - \frac{1}{2\beta}(-I_{h2f})\right] \tag{122}$$

with some prospect of determining k_1 and the possibility that k_2 will not be very different from unity. In the absence of further information we approximate to k_1 by putting

$$(-h_{\dot{\xi}})_c = k_1(-h_{\dot{\xi}}) \tag{123}$$

and identifying $(-h_{\dot{\xi}})_c$ with the measured stiffness derivative. From the following table it emerges that $(-h_{\dot{\xi}})_c$ is a fair approximation to the measured damping derivative when $k_2 = 1$, that is, when the residual part of the damping is taken to be insensitive to aerofoil thickness and boundary layers.

Wing	N, N'	M	k_1	$-h_{\dot{\xi}}$	$\frac{1}{2\beta}(-I_{h2f})$	$(-h_{\dot{\xi}})_c$	$(-h_{\dot{\xi}})_{\exp}$
Rectangular	4, 4	0	0·56	0·167	0·106	0·121	0·114
Cropped delta	3, 3	0·553	0·72	0·236	0·133	0·199	0·226
		0·745	0·66	0·302	0·156	0·250	0·264
		0·866	0·58	0·433	0·187	0·354	0·333
Cropped delta	4, 3	0·745	0·68	0·340	0·164	0·288	0·264

Although this is probably an oversimplification, it succeeds to an accuracy of at worst ± 10 per cent in all the present examples. The resulting formula from equations (122) and (123) with $k_2 = 1$,

$$(-h_{\dot{\xi}})_c = -h_{\dot{\xi}} - \left[1 - \frac{(h_{\dot{\xi}})_c}{h_{\dot{\xi}}}\right]\frac{1}{2\beta}(-I_{h2f}) \tag{124}$$

where $(h_{\dot{\xi}})_c$ is taken from experiment, gives a significant improvement in all cases except the cropped delta wing at $M = 0{\cdot}553$. Even so, for this Mach number the preferred solution $N = 4$, $N' = 3$ would probably give a larger value of $-h_{\dot{\xi}}$ in Fig. 29, and correction by equation (124) should then give a satisfactory improvement. Thus the preferred result with empirical correction for $M = 0{\cdot}745$ is illustrated by the point (*) in Fig. 30. At lower Mach numbers excellent comparison with experiment would be obtained, while at higher Mach numbers under transonic conditions the empirical correction would fail through being too small.

The principle of equation (124) may be applied just as easily to estimate the order of magnitude of corrections to theoretical values of other damping derivatives. It is necessary to evaluate the stiffness derivative either from steady-flow measurements or from some semi-empirical procedure. It remains to be seen how successfully the procedure will fit the measurements of $-z_{\dot{\xi}}$, $-m_{\dot{\xi}}$, $-b_{\dot{\xi}}$ and $-h_{\dot{\xi}}$ to be made on the half-model of the tapered swept planform (Section 6.3).

As a further illustration, the cross derivative $-h_{\dot{\theta}}$ in equation (28) would be corrected by the formula

$$(-h_{\dot\theta})_c = -h_{\dot\theta} - \left[1 - \frac{(h_\theta)_c}{h_\theta}\right]\frac{1}{2\beta}\left[(-I_{h2}) - \frac{x_o}{\bar c}(-I_{h1})\right]. \tag{125}$$

A rough estimate of the importance of the correction term can be deduced from a two-dimensional value of $(h_\theta)_c/h_\theta$; in the following table $(h_\theta)_c$ is obtained as $\frac{1}{2}b_1 = \frac{1}{2}\partial C_h/\partial\alpha$ from the charts of Ref. 19 and h_θ is the corresponding quantity from thin aerofoil theory, while the Reynolds numbers (R.N.) and positions of boundary-layer transition x_{tr} are those already used in Sections 6.1 and 6.4.

Aerofoil	E	R.N.	$\frac{x_{tr}}{c}$	$(-h_\theta)_c$	$-h_\theta$	$\frac{(h_\theta)_c}{h_\theta}$
10% RAE 101	0·20	$1{\cdot}0\times10^6$	0·10	0·102	0·250	0·41
			0·60	0·120	0·250	0·48
10% RAE 102	0·25	$1{\cdot}5\times10^6$	0·35	0·144	0·283	0·51

Thus, for the respective rectangular and cropped delta wings with mid-root-chord pitching axis, we apply equation (125) and calculate the following results.

Wing	M	$\frac{x_0}{\bar c}$	$\frac{-I_{h1}}{2\beta}$	$\frac{-I_{h2}}{2\beta}$	$\frac{(h_\theta)_c}{h_\theta}$	$-h_{\dot\theta}$	$(-h_{\dot\theta})_c$
Rectangular	0	0·500	0·124	0·249	0·41	0·329	0·219
					0·48	0·329	0·232
Cropped delta	0·553	0·875	0·106	0·340	0·51	0·537	0·416

The indications are that the cross derivative $-h_{\dot\theta}$ from linear theory may require larger corrections than $-h_{\dot\xi}$, with the corollary that measured values of $-h_{\dot\theta}$ may be more dependent on Reynolds number.

8. *Concluding Remarks.*

(1) A linear theoretical method is presented for the treatment of arbitrary configurations of wing planform and trailing-edge control surface in low-frequency oscillatory motion in a uniform subsonic stream. Calculations of wing forces and control hinge moments and the associated spanwise distributions are illustrated and discussed for rectangular, untapered swept, tapered swept and cropped delta wings.

(2) The present method uses combinations of chordwise and spanwise equivalent slopes to determine smooth equivalent incidences without discontinuities at the hinge-line and part-span boundaries. The equivalent incidences vary according to the aerodynamic quantity being evaluated and include allowance for wing and control taper. The example of the tapered swept wing introduces the full complication of a swept hinge line, spanwise variation of control-chord ratio E and additional terms due to compressibility.

(3) Particular attention is given to h_ξ and $h_{\dot\xi}$, the direct control derivatives, and to the corresponding distributions over the control span. Several refinements in technique have been investigated numerically,

especially those associated with the choice of chordwise equivalent slopes τ_{rp}, the incidence α_{3e}, the spanwise integration parameter q, and the central rounding of swept edges. An important consideration is the degree of convergence as the number of chordwise terms N is increased up to 4, a process greatly accelerated by the use of equivalent slopes.

(4) The reverse-flow theorem yields wing forces due to control rotation without recourse to equivalent slopes. Results so calculated confirm that the present method is highly satisfactory for wing forces, and the special equivalent slopes for hinge moment are therefore applied with some confidence. The reverse-flow approach to hinge moment requires different equivalent slopes, as discussed in the Appendix; in application this alternative has proved less successful.

(5) Derivatives of lift and pitching moment are calculated to a theoretical accuracy of 2 or 3 significant figures or decimal places. Theoretical errors in the hinge-moment derivative h_ξ are usually reduced by an order of magnitude to within 2 per cent as a result of the special equivalent slopes. The damping derivative $-h_{\dot{\xi}}$ converges less well with respect to N, but with $N = 4$ it is thought to lie within ± 10 per cent of the true linear solution. Smooth variations with flap chord, control span and Mach number are predicted for all derivatives.

(6) The present method has limitations in addition to those of inviscid flow, thin wing, sub-critical Mach number and others associated with linear lifting-surface theory. The analysis is restricted to first order in frequency and to $N \leqslant 4$, and it covers spanwise loading but not the complete load distribution; attempts to remove these limitations are envisaged in the final remarks below. Rigorous treatment of discontinuities at corners of a control surface is becoming possible on the principles of Ref. 21, but this cannot be incorporated in the present method.

(7) The practical problem of a wing with fuselage remains unsolved. With a central body, it is probably best to extend the leading and trailing edges through the body side to define a gross wing. The present method can then be applied to the gross wing, suitably rounded, in combination with an oscillating control surface of given geometry. It should be noted that the expedient of rounding the central kink of a swept wing is a purely numerical artifice, the spanwise extent of the rounding being unrelated to body diameter.

(8) The untapered swept wing is of special interest in relation to available comparisons with an electrical analogue of the steady flow. It is shown that the calculated spanwise lift distribution due to control deflection is in close agreement with the analogue results, especially when the artificial central rounding is increased so as to reduce collocation error.

(9) The tapered swept wing is later to be tested as a half-model with aileron. Consideration of symmetrical and antisymmetrical spanwise loading shows that reflection-plane symmetry has an important effect on rolling-moment stiffness and damping, while that on hinge moment is practically negligible.

(10) Experimental hinge moments are available for the rectangular and cropped delta wings. In each case the large discrepancies between the measured and calculated h_ξ are closely related to predictions from charts based on two-dimensional static tests. The damping derivative from the present method fits the experimental data much better, but the calculated values are larger in magnitude and the differences often exceed the 10 per cent accuracy that is claimed from a theoretical standpoint.

(11) A simple empirical correction to $-h_{\dot{\xi}}$ is suggested in Section 7. The theoretical result is split into the quasi-steady damping and a residual contribution, the former being corrected by the factor required to reconcile the calculated and measured values of $h_{\dot{\xi}}$. At low speed and over a range of Mach number the available measurements of $-h_{\dot{\xi}}$ are thus reproduced within ± 10 per cent. The procedure suggests a method of estimating the likely order of magnitude of scale effect on other damping derivatives in the absence of experimental data.

(12) While available measurements of oscillatory hinge moment are all too scarce, there is even less information on wing forces due to control rotation. The urgent need for relevant experiments is widely recognized; in view of the greater difficulties of measuring cross derivatives, the use of pressure plotting

may well play an important part in future developments.

(13) An extension of the present method to include chordwise load distributions is in course of investigation. Whether the approach is through new chordwise equivalent slopes or through results already known at the collocation sections, there are basic difficulties to be overcome. For the rectangular wing with full-span control consistent results have already been obtained by the two approaches.

(14) Just as there is a singularity in each of the chordwise equivalent slopes τ_{rp} when $N = 4$ and $E = 0{\cdot}58\dot{3}$ and more numerous singularities in reverse flow, so similar difficulties would occur for more values of E as N increases. The extension of the present method to $N > 4$ would certainly improve the solution associated with α_{3e} without the above difficulties, because the equivalent slopes τ_{rp} are not involved. The other incidences α_{re} for hinge moment could probably be treated, if necessary, with $N' < N$, as became expedient in the present calculations for the cropped delta wing when $N = 4$; the contributions from α_{re} $(r \neq 3)$ seem less sensitive to the number of terms in the chordwise equivalent slopes.

(15) Previous investigations in Refs. 1 and 2 have shown on the basis of reverse flow, that equivalent incidences are virtually linear in frequency. It may be possible to use the equivalent incidences from the present low-frequency method to formulate the equations and obtain satisfactory solutions for an arbitrary frequency, when a suitable computer program is available.

Acknowledgements.

The authors wish to acknowledge the assistance of Mrs. S. Lucas and Mrs. S. Inch of the Aerodynamics Division, N.P.L. Mrs. Lucas was responsible for most of the extensive desk calculations of equivalent incidences and hinge moments. Mrs. Inch was responsible for the data tapes used on the KDF 9 computer in the Central Computer Unit, and also helped to prepare the tables and figures of the report.

A	Aspect ratio of wing; $2s/\bar{c}$
$A_\gamma, A_\mu, A_\kappa, A_\lambda$	Chordwise integration functions for hinge moment in equations (55)
$\mathbf{A}, \mathbf{B}$	Real square matrices of order mN represented in equation (19)
$\bar{\mathbf{A}}, \bar{\mathbf{B}}$	Corresponding matrices for reversed-wing planform
$b_{\nu\nu}$	Quantity defined in equation (17)
$b_{\bar{\xi}}, b_{\dot{\xi}}$	Bending-moment derivatives due to control rotation in equations (120)
$B_\gamma, B_\mu, B_\kappa, B_\lambda$	Chordwise integration functions for hinge moment in equations (95)
$c(y)$	Local chord of wing
$c_f(y)$	Local chord of control surface
c_n, c_ν	$c(y_n), c(y_\nu)$, including any planform rounding where $\lvert y\rvert < y_i$
c_r, c_t	Root chord, tip chord of wing
$\bar{c}$	Geometric mean chord of wing
$\bar{c}_f$	Geometric mean chord of control surface
$(C_h)_r$	Two-dimensional hinge-moment coefficient in equation (53)
$(C_L)_r$	Two-dimensional lift coefficient in equation (46)
$(C_m)_r$	Two-dimensional pitching-moment coefficient about quarter-chord axis in equation (46)
$(C_{mm})_r$	Second pitching-moment coefficient in equation (46)
$(C_{mmm})_r$	Third pitching-moment coefficient in equation (46)
$C_\gamma, C_\mu, C_\kappa, C_\lambda$	Functions of ϕ_h in equations (50)
$D_\gamma, D_\mu, D_\kappa, D_\lambda$	Functions of ϕ_h in equations (52)
E	Local control-chord ratio; c_f/c
E_a	Value of E at section $y = y_a$
E_{tk}	Coefficient in equation (61) for $\alpha_e(\eta)$
$f(\lambda)$	Function in equation (5) or (6) defining central rounding
$f_r(\eta)$	Planform geometry in equations (80)
$F_r(\eta)$	Functions in equation (93) defining local hinge moment ($r = 1, 2, 3, 4$)
$F_1^*(\eta)$	Spanwise function in equation (97)
h_r	Column matrices for equation (22) and pitching motion
h_{rf}	Column matrices for equation (24) and control rotation
$h_\theta, h_{\dot{\theta}}$	Hinge-moment derivatives in equations (27) and (28) due to pitching
$h_\xi, h_{\dot{\xi}}$	Hinge-moment derivatives in equations (32) and (36) due to control rotation
$h_{\xi L}, h_{\dot{\xi} L}$	Local hinge moments in equations (90) and (92), (91) and (96)

H_T	True hinge moment (*see* table of conversion factors)
I_{brf}, I^*_{brf}	Coefficients for bending moment in equations (37) due to control rotation
I_{hr}, I^*_{hr}	Coefficients for hinge moment in equations (26) due to pitching
I_{hrf}, I^*_{hrf}	Coefficients for hinge moment in equations (31) due to control rotation
$I_{Lrf}, \ldots I^*_{mrf}$	Coefficients for lift, rolling moment and pitching moment in equations (30) due to control rotation
k_1, k_2	Empirical correction factors in equation (122)
$l(X)$	Two-dimensional smooth load distribution; equation (43) when $N' = N = 4$
$l_r(X)$	Two-dimensional loading due to $\alpha_r(X)$; $l_1(X)$, $l_2(X)$ in equations (41), (42)
$l(x, y)$	Non-dimensional load distribution in equations (7) and (8)
l_r, l_{re}, l_{rf}	Loading $l(x, y)$ due to incidence $\alpha_r, \alpha_{re}, \alpha_{rf}$
$\bar{l}(\bar{x}, \bar{y})$	Loading on reversed wing; equation (8) with a bar over each symbol in square brackets
$\bar{l}_r, \bar{l}_{re}$	Loading $\bar{l}(\bar{x}, \bar{y})$ on reversed wing due to $\bar{\alpha}_r, \bar{\alpha}_{re}$
$l_\xi, l_{\dot{\xi}}$	Rolling-moment derivatives in equations (32) and (35) due to control rotation
ln	Natural logarithm
L, L_r, L_{rf}	Column matrix of unknowns from equation (11) in equations (19), (22), 24)
m	Number of collocation sections; $m = 15$ in examples
$\bar{m}$	Spanwise integration parameter in equation (15)
$m_\theta, m_{\dot{\theta}}$	Direct pitching derivatives from equation (32) with ξ replaced by θ; derivatives in equations (39) of Ref. 5
$m_\xi, m_{\dot{\xi}}$	Pitching-moment derivatives in equations (32) and (34) due to control rotation
M	Mach number of free stream
N	Number of chordwise terms to be used in equation (8)
N'	Number of terms ($\leqslant N$) in polynomial for $\alpha_e(X)$
p	Integer denoting chordwise position of collocation point in equation (13)
q	Unity or even integer; $(\bar{m}+1)/(m+1)$
Q_r, Q_{re}	Functions used in reverse-flow calculation of wing forces, hinge moment; equation (110) corresponding to $\bar{\alpha}_r, \bar{\alpha}_{re}$
R_1, R_2, R_{2e}	Function in equation (111) corresponding to $\bar{\alpha}_1, \bar{\alpha}_2, \bar{\alpha}_{2e}$
$\mathscr{R}$	Real part of
s	Semi-span of wing
s_f	$s(1-\eta_a)$ for outboard control; $s\eta_f$ for inboard control
S	Area of wing planform; $2s\bar{c}$
S_f	Plan area of starboard (or port) control; $s_f \bar{c}_f$

t	time
$u, \bar{u}$	integers $\frac{1}{2}(m-1), \frac{1}{2}(\bar{m}-1)$
U	Uniform velocity of free stream
$w(x, y)$	Upwash velocity over planform
x, y, z	Rectangular co-ordinates with origin at root leading edge (Fig. 1a)
x_0	Pitching axis (Fig. 1a); $x_0 = \frac{1}{2}c_r$ in examples
$x_h(y)$	Hinge line of control surface
$x_l(y)$	Leading edge of wing
x_{ln}, x_{lv}	$x_l(y_n), x_l(y_v)$ including any planform rounding where $\lvert y\rvert < y_i$
x_{pv}	Streamwise position of collocation point in equation (13)
$x_t(y)$	Trailing edge of wing
x_{tr}	Chordwise position of boundary-layer transition
$\bar{x}, \bar{y}$	Rectangular co-ordinates for reversed wing in equations (103) and (107)
$\bar{x}_h(\bar{y})$	Hinge line on reversed wing; $c_r - x_h(y)$
$\bar{x}_l(\bar{y})$	Leading edge of reversed wing; $c_r - x_l(y)$
X, X_h	Non-dimensional chordwise parameter in equation (39), (53)
X_{cp}	Local centre of pressure in equation (116)
y_a	Spanwise ordinate defining span of outboard control in Fig. 1a
y_f	Spanwise limit of inboard control
y_i	Spanwise extent of central rounding in equations (4) and (117)
y_n, y_v	$s \sin [n\pi/(m+1)], s \sin [v\pi/(m+1)]$ (n or $v = 0, \pm 1, \ldots \pm u$)
z	Upward displacement; mode of oscillation
$-z_\theta, -z_{\dot{\theta}}$	Lift derivatives due to pitching in equation (32) with ξ replaced by θ; derivatives in equations (39) of Ref. 5
$-z_\xi, -z_{\dot{\xi}}$	Lift derivatives in equations (32) and (33) due to control rotation
α	Local incidence
$\alpha_e(X)$	Chordwise equivalent slopes to represent $\alpha_r(X)$; equation (44) when $N' = N = 4$
$\alpha_e(\eta)$	Spanwise equivalent slopes in equation (61) or (76) to represent $\alpha_t(\eta)$
α_r	Steady incidences in equations (21) and (22) for pitching mode ($r = 1, 2, 3$)
$\alpha_r(X)$	Singular distributions of incidence in equations (39) ($r = 1, 2$)
α_{re}	Smooth equivalent incidences to represent α_{rf}
$(\alpha_{re})_{pv}$	α_{re} at collocation point in equation (84) or (85)
α_{rf}	Steady incidences in equations (23) and (24) for control-rotation mode ($r = 1, 2, 3, 4$)
$\alpha_{rp}(\eta)$	Singular distributions of incidence in equation (79)
$\alpha_t(\eta)$	Singular distributions of incidence in equations (60) ($t = 1, 2$)

$\alpha_I, \alpha_{II}, \alpha_{III}$	Three contributions to $\alpha_{rp}(\eta)$ in equations (81) and (82)
$\alpha'(\eta_a)$	Spanwise gradient of $\alpha(\eta)$ at $\eta = \eta_a$
$\bar{\alpha}_r$	Steady incidences for reversed wing in equation (104) ($r = 1, 2, \ldots 5$)
$\bar{\alpha}_{re}$	Smooth equivalent incidences for hinge moment by reverse flow ($r = 2, 5, 6, 7, 8$) as in Appendix
β	Compressibility factor; $(1-M^2)^{\frac{1}{2}}$
$\gamma(y), \gamma_n$	First term in $l(x, y)$, its value at $y = y_n$
$\gamma(\eta)$	Non-dimensional spanwise loading; circulation/$(2sU)$
$\gamma_e, \mu_e, \kappa_e, \lambda_e$	Arbitrary coefficients in $l(X)$ and $\alpha_e(X)$
$\gamma_{rf}(y), \mu_{rf}(y), \ldots$	Particular distributions of $\gamma(y), \mu(y), \ldots$ for loading l_{rf}
$\gamma_{rfn}, \mu_{rfn}, \ldots$	Values of $\gamma_{rf}(y_n), \mu_{rf}(y_n), \ldots$
$\gamma_t(\eta)$	Non-dimensional circulation for incidences $\alpha_t(\eta)$; $\gamma_1(\eta), \gamma_2(\eta)$ in equations (73), (74)
$\bar{\gamma}_r(\bar{y}), \bar{\mu}_r(\bar{y}), \ldots$	Distributions for reversed wing at incidence $\bar{\alpha}_r$
$\bar{\gamma}_{re}(\bar{y}), \bar{\mu}_{re}(\bar{y}), \ldots$	Distributions for reversed wing at incidence $\bar{\alpha}_{re}$
$\delta, \varepsilon, \zeta, \psi$	Chordwise equivalent slopes used in reverse flow (Appendix)
ε	± 1 according as control rotation is symmetrical or antisymmetrical
η, η_n, η_ν	Non-dimensional spanwise ordinates; $y/s, y_n/s, y_\nu/s$
η_a	Parameter for outboard control; y_a/s
η_f	Parameter for inboard control; y_f/s
$\bar{\eta}$	Non-dimensional spanwise ordinate for reversed wing; $\bar{y}/s$
$\theta, \theta_a, \theta_n$	Angular spanwise positions; $\cos^{-1}\eta, \cos^{-1}\eta_a, \cos^{-1}\eta_n$
θ_0	Amplitude of oscillation in pitching mode (radians)
$\kappa(y), \kappa_n$	Third term in $l(x, y)$, its value at $y = y_n$
λ	$\lvert y\rvert/y_t (\leqslant 1)$
$\lambda(y), \lambda_n$	Fourth term in $l(x, y)$, its value at $y = y_n$
Λ	Angle of sweepback
$\Lambda_L, \Lambda_T, \Lambda_h$	Sweepback of leading edge, trailing edge, hinge line
$\mu(y), \mu_n$	Second term in $l(x, y)$, its value at $y = y_n$
ν	Integer denoting collocation section $y = y_\nu$
$\bar{\nu}$	Frequency parameter; $\omega\bar{c}/U$
ξ	Angle of control deflection relative to stream direction (radians)
ξ_0	Amplitude of oscillation in control-rotation mode (radians or specified in degrees)
ξ_T	True angle of control deflection in plane normal to hinge line; $\xi\sec\Lambda_h$
ξ_{0T}	True amplitude in control-rotation mode (*see* table of conversion factors)

ρ	Density of free stream
σ_r	$\alpha_e(X)$ to satisfy wing forces in Section 3.1 ($r = 1, 2$)
$\sigma_{rp}(E)$	Chordwise equivalent slopes at positions $\phi = \phi_p$ ($r = 1, 2$)
τ_r	$\alpha_e(X)$ to satisfy hinge moment in Section 3.2 ($r = 1, 2$)
$\tau_{rp}(E)$	Chordwise equivalent slopes at positions $\phi = \phi_p$ ($r = 1, 2$)
ϕ	Angular chordwise position in equation (9)
ϕ_h	ϕ on hinge line; $\cos^{-1}(2E-1)$
ϕ_p	$2\pi p/(2N+1)$ ($p = 1, 2, \ldots N$)
$\bar{\phi}$	Angular chordwise position on reversed wing in equation (107)
$\bar{\phi}_h$	Hinge-line parameter on reversed wing; $(\pi - \phi_h)$
$\Psi_t(\eta, \eta_a)$	Representation of $\alpha_t(\eta)$ to satisfy sectional loads in Section 4.2
$\Psi_{tv}(\eta_a)$	Spanwise equivalent slopes at positions $\eta = \eta_v$ ($t = 1, 2$)
ω	Circular frequency of oscillation
$\Omega_t(\eta, \eta_a)$	Representation of $\alpha_t(\eta)$ to satisfy wing forces in Section 4.1
$\Omega_{tv}(\eta_a)$	Spanwise equivalent slopes at positions $\eta = \eta_v$ ($t = 1, 2$)
c	Subscript denoting empirical correction in Section 7
e	Subscript indicating use of equivalent incidences
f	Subscript denoting control-rotation mode, inboard flap or control-surface geometry
n	Subscript numerating loading station $y = y_n$
p	Subscript numerating chordwise position of collocation point
r	Subscript relating to steady incidence α_r, α_{rf}, $\alpha_r(X)$, $\bar{\alpha}_r$, $\bar{\alpha}_{re}$
v	Subscript numerating collocation section $y = y_v$

Conversion factors when hinge line is swept

Quantities	Conversion factor
ξ, ξ_0	$\sec \Lambda_h$
Hinge moment	$\cos \Lambda_h$
$b_\xi, b_{\dot{\xi}}, l_\xi, l_{\dot{\xi}}$	$\cos \Lambda_h$
$m_\xi, m_{\dot{\xi}}, z_\xi, z_{\dot{\xi}}$	$\cos \Lambda_h$
$h_\theta, h_{\dot{\theta}}$	$\cos \Lambda_h$
$h_\xi, h_{\dot{\xi}}, h_{\xi L}, h_{\dot{\xi} L}$	$\cos^2 \Lambda_h$

REFERENCES

No.	Author(s)	Title, etc.
1	D. E. Davies	Calculation of unsteady generalised airforces on a thin wing oscillating harmonically in subsonic flow. A.R.C. R. & M. 3409. August, 1963.
2	D. E. Lehrian	Calculation of subsonic flutter derivatives for an arrowhead wing with control surfaces. A.R.C. R. & M. 3561. March, 1967.
3	H. Multhopp	Methods of calculating the lift distribution of wings (Subsonic lifting-surface theory). A.R.C. R. & M. 2884. January, 1950.
4	H. C. Garner	Multhopp's subsonic lifting-surface theory of wings in slow pitching oscillations. A.R.C. R. & M. 2885. July, 1952.
5	H. C. Garner and D. A. Fox ..	Algol 60 programme for Multhopp's low-frequency subsonic lifting-surface theory. A.R.C. R. & M. 3517. April, 1966.
6	D. E. Lehrian and H. C. Garner	Comparative numerical applications of the reverse-flow theorem to oscillating wings and control surfaces. A.R.C. R. & M. 3488. August, 1965.
7	M. Enselme	Deux méthodes de calcul rhéoélectrique appliquées aux surfaces portantes. La Recherche Aéronautique, No. 64, pp. 35-40. May-June, 1958.
8	D. L. Woodcock	On the accuracy of collocation solutions of the integral equation of linearised subsonic flow past an oscillating aerofoil. Proceedings of the International Symposium on Analogue and Digital Techniques applied to Aeronautics, Liège, 1963. pp. 173-202, 1964.
9	W. G. Molyneux and F. Ruddlesden	Derivative measurements and flutter tests on a rectangular wing with a full-span control surface, oscillating in modes of wing roll and aileron rotation. A.R.C. R. & M. 3010. February, 1955.
10	J. B. Bratt, C. J. W. Miles and R. F. Johnson	Measurements of the direct hinge-moment derivatives at subsonic and transonic speeds for a cropped delta wing with oscillating flap. A.R.C. R. & M. 3163. May, 1957.
11	H. C. Garner	Numerical appraisal of Multhopp's low-frequency subsonic lifting-surface theory. A.R.C. R. & M. 3634. October, 1968.
12	P. J. Zandbergen, T. E. Labrujere and J. G. Wouters	A new approach to the numerical solution of the equation of subsonic lifting surface theory. N.L.R. Report TR G.49. November, 1967.
13	H. Glauert	Theoretical relationships for an aerofoil with hinged flap. A.R.C. R. & M. 1095. April, 1927.

14 V. M. Falkner . . . . . The use of equivalent slopes in vortex lattice theory.
A.R.C. R. & M. 2293. March, 1946.

15 D. E. Lehrian . . . . Vortex-lattice treatment of rectangular wings with oscillating control surfaces.
A.R.C. R. & M. 3182. December, 1957.

16 H. Multhopp . . . . . Die Berechnung der Auftriebsverteilung von Tragflügeln.
Luftfahrtforschung, pp. 153-169. 1938.
Translation in A.R.C. Report 8516.

17 J. De Young . . . . . Spanwise loading for wings and control surfaces of low aspect ratio.
N.A.C.A. TN 2011. January, 1950.

18 E. J. Watson . . . . . Calculation of the circulation from the downwash.
Appendix to A.R.C. R. & M. 2593. February, 1948.

19 H. C. Garner . . . . . Charts for low-speed characteristics of two-dimensional trailing-edge flaps.
A.R.C. R. & M. 3174. August, 1957.

20 H. C. Garner and R. D. Milne Asymptotic expansion for transient forces from quasi-steady subsonic wing theory.
Aeronaut. Quart., Vol. XVII, pp. 343-350. November, 1966.

21 H. Ashley . . . . . Subsonic oscillatory or steady airloads on wings with control surfaces and other discontinuities.
Stanford University Report SUDAAR No. 336, AFOSR-68-0419. December, 1967.

APPENDIX

Hinge Moments by Reverse Flow.

The reverse-flow theorem is applied in Section 5.2 of Ref. 6 to an oscillating control surface when the frequency parameter $\bar{\nu} \to 0$, expressions for the lift and pitching-moment derivatives being obtained in terms of integrated steady loads on the reversed wing. Now, a similar formulation of the direct control derivatives is considered for the symmetrical control-rotation mode. Relative to the stream direction

$$\text{Hinge moment} = \int_S \int \bar{c} f_1(x, y) \Delta p(x, y) \, dx \, dy \,, \tag{A.1}$$

where

$$\left.\begin{aligned} f_i(x, y) &= -(x - x_h)/\bar{c} \qquad \text{on the control surface} \\ &= 0 \qquad\qquad\quad \text{elsewhere on the planform} \end{aligned}\right\} \tag{A.2}$$

and $\Delta p(x, y)$ is the loading on the wing due to the control-deflection mode $z(x, y)$ of equation (3) with $\varepsilon = +1$. If equation (A.1) is identified with equation (5) of Ref. 6, it follows from the reverse-flow relation in equations (11) and (12) of Ref. 6 that

$$\text{Hinge moment} = \int_S \int \bar{c} \left[\frac{\partial z}{\partial x} + i\bar{\nu} \frac{z}{\bar{c}} \right] \Delta \bar{p}_i \, dx \, dy \,, \tag{A.3}$$

where $\Delta \bar{p}_i$ is the load distribution over the wing in reverse flow due to an upwash

$$\bar{w}_i = \mathscr{R} \left[U f_i(x, y) \, e^{i\omega t} \right] ; \tag{A.4}$$

the direction of the free stream is reversed, but its magnitude and the frequency of oscillation remain unchanged. Inspection of the above equations shows that the gradients $\partial z/\partial x$ and $\partial w_i/\partial x$ are both discontinuous at $x = x_h$. Therefore, the reverse-flow formulation of hinge moment in equation (A.3) retains singularities in force and upwash modes with the associated difficulties encountered in the direct-flow problem. The singularities in $\bar{w}_i$ have to be removed by the use of smooth equivalent incidences in the collocation solution.

To express equation (A.3) in terms of solutions for the reversed wing, we take a new origin at its root leading-edge and co-ordinates

$$\bar{x} = (c_r - x) \text{ and } \bar{y} = -y \,. \tag{A.5}$$

Then, equations (A.2) and (A.4) transform to give the upwash distribution on the reversed wing as

$$\left.\begin{aligned} \frac{\bar{w}_i(\bar{x}, \bar{y})}{U} &= \mathscr{R} \left[\left(\frac{\bar{x} - \bar{x}_h(\bar{y})}{\bar{c}} \right) e^{i\omega t} \right] \quad \text{on the control surface} \\ &= 0 \qquad\qquad\qquad\qquad\quad \text{elsewhere on the planform} \end{aligned}\right\} \tag{A.6}$$

where $\bar{x}_h(\bar{y}) = [c_r - x_h(y)]$ by planform symmetry. With $z(x, y)$ from equation (3) and $\Delta \bar{p}_i(\bar{x}, \bar{y})$ denoting the load distribution in the new co-ordinates, equation (A.3) becomes

$$\frac{\text{Hinge moment}}{\rho U^2 S\bar{c}} = -\xi_o \int\int_{S_f} \left[1 - i\bar{\nu}\left(\frac{\bar{x}-\bar{x}_h}{\bar{c}}\right)\right] \frac{\Delta\bar{p}_i(\bar{x},\bar{y})}{\frac{1}{2}\rho U^2} \frac{d\bar{x}\,d\bar{y}}{S} \tag{A.7}$$

where $S_f = s_f \bar{c}_f$ is the starboard half of the control area, which for an outboard control is bounded by

$$\bar{x}_l(\bar{y}) \leqslant \bar{x} \leqslant \bar{x}_h(\bar{y}) \text{ and } y_a \leqslant \bar{y} \leqslant 1 .$$

The solution for the loading $\Delta\bar{p}_i(\bar{x},\bar{y})$ to first order in frequency is formulated by applying the theory of Section 2 to the reversed-wing planform; a bar inserted over any variable parameter will refer it to the co-ordinate system $(\bar{x},\bar{y})$. In particular, the boundary condition in the notation of equation (23) is determined from equation (A.6) as the column matrix

$$\bar{h} = \frac{1}{b_{vv}}\left[\bar{\alpha}_{2f} - i\bar{\nu}\frac{M^2}{\beta^2}(\bar{\alpha}_{7f}+\bar{\alpha}_{8f})\right]_{pv}, \tag{A.8}$$

where

$$\left.\begin{aligned} \bar{\alpha}_{2f} &= -\left[\frac{\bar{x}-\bar{x}_h(\bar{y})}{\bar{c}}\right] \\ \bar{\alpha}_{7f} &= -\left[\frac{\bar{x}-\bar{x}_h(\bar{y})}{\bar{c}}\right]^2 \\ \bar{\alpha}_{8f} &= \frac{\bar{x}_h(\bar{y})}{\bar{c}}\bar{\alpha}_{2f} \end{aligned}\right\} \text{ on the control surface} \tag{A.9}$$

and $\bar{\alpha}_{2f} = \bar{\alpha}_{7f} = \bar{\alpha}_{8f} = 0$ elsewhere on the planform. If $\bar{l}_{rf}(\bar{x},\bar{y})$ denotes the steady load distribution corresponding to the column matrix $\bar{h}_{rf} = (\bar{\alpha}_{rf}/b_{vv})$, then to first order in $\bar{\nu}$

$$\Delta\bar{p}_i(\bar{x},\bar{y}) = \tfrac{1}{2}\rho\, U^2\, \mathscr{R}\left[\left\{\bar{l}_{2f} + i\bar{\nu}\left(\frac{M^2\bar{x}}{\beta^2\bar{c}}\bar{l}_{2f} + \frac{1}{\beta^2}\bar{l}_{5f} - \frac{M^2}{\beta^2}\bar{l}_{7f} - \frac{M^2}{\beta^2}\bar{l}_{8f}\right)\right\} e^{i\omega t}\right], \tag{A.10}$$

where the loading $\bar{l}_{5f}$ corresponds to the incidence $\bar{\alpha}_{5f}$ determined by

$$(\bar{\alpha}_{5f}/b_{vv}) = \bar{h}_{5f} = \bar{\mathbf{B}}\,\bar{\mathbf{A}}^{-1}(\bar{\alpha}_{2f}/b_{vv})_{pv} \tag{A.11}$$

with matrices $\bar{\mathbf{A}}$ and $\bar{\mathbf{B}}$ for the reversed-wing analogous to those in equations (19) to (22). Formulae for the hinge-moment derivatives defined in equation (32) follow from equations (A.7) and (A.10), whence to first order in $\bar{\nu}$

$$\left.\begin{aligned} -h_\xi &= \frac{\bar{c}}{2\,S_f\,\bar{c}_f}\int\int_{S_f} \bar{l}_{2f}\,d\bar{x}\,d\bar{y} \\ \text{and} \\ -h_{\dot{\xi}} &= \frac{\bar{c}}{2\,S_f\,\bar{c}_f}\int\int_{S_f}\left[-\left(\frac{\beta^2-M^2}{\beta^2}\right)\left(\frac{\bar{x}-\bar{x}_h}{\bar{c}}\right)\bar{l}_{2f} + \frac{1}{\beta^2}\bar{l}_{5f} + \frac{M^2}{\beta^2}\left(\frac{\bar{x}_h}{\bar{c}}\bar{l}_{2f} - \bar{l}_{7f} - \bar{l}_{8f}\right)\right] d\bar{x}\,d\bar{y} \end{aligned}\right\} . \tag{A.12}$$

In order to apply the collocation method of Section 2, each $\bar{l}_{rf}(\bar{x}, \bar{y})$ must be replaced by a smooth load distribution $\bar{l}_{re}(\bar{x}, \bar{y})$. The remaining problem is, therefore, the choice of smooth equivalent incidences $\bar{\alpha}_{re}$, at the collocation positions $(\bar{x}_{pv}, \bar{y}_v)$, to represent the incidences $\bar{\alpha}_{rf}$ of equations (A.9) and (A.11). By inspection of equations (A.12), we see that the first term in the integral for $-h_{\bar{\xi}}$ is a hinge moment on S_f due to the loading l_{2f}, but that the other four terms in $-h_{\bar{\xi}}$ and the one term in $-h_{\bar{\zeta}}$ can each be interpreted as a 'hinge reaction' proportional to the integral of $\bar{l}_{rf}$ over S_f. The following table summarizes the five sets of equivalent incidences $(\bar{\alpha}_{re})_{pv}$, $r = 2, 5, 6, 7, 8$, used in the calculation of $-h_{\bar{\zeta}}$ and $-h_{\bar{\xi}}$.

Eqn. (A.12)	Term	Incidence eqn. (A.9)	Chordwise slopes	Spanwise slopes	Equivalent incidences
$-h_{\bar{\zeta}}$	—	$\bar{\alpha}_{2f}$	ζ_p	Ψ_{tv}	$(\bar{\alpha}_{6e})_{pv}$
$-h_{\bar{\xi}}$	1st.	$\bar{\alpha}_{2f}$	ε_p	Ψ_{tv}	$(\bar{\alpha}_{2e})_{pv}$
	2nd.	$\bar{\alpha}_{5f}$	δ_p	Ω_{tv}	$(\bar{\alpha}_{5e})_{pv}$
	3rd.	$\bar{\alpha}_{2f}$	ζ_p	Ψ_{tv}	$(\bar{\alpha}_{6e})_{pv}$
	4th	$\bar{\alpha}_{7f}$	ψ_p	Ψ_{tv}	$(\bar{\alpha}_{7e})_{pv}$
	5th.	$\bar{\alpha}_{8f}$	ζ_p	Ψ_{tv}	$(\bar{\alpha}_{8e})_{pv}$

Thus, the terms in $-h_{\bar{\xi}}$ involve four different chordwise equivalent slopes that require special formulation; as regards $\bar{\alpha}_{5f}$, the chordwise slopes δ_p relate to the smooth incidence to replace $\bar{\alpha}_{2f}$ in equation (A.11). In the case of a part-span control, the symmetrical spanwise slopes Ψ_{1v} and Ψ_{2v} of Section 4.2 apply, except as regards $\bar{\alpha}_{5f}$ when Ω_{1v} and Ω_{2v} are more appropriate. The equivalent slopes are combined by the numerical procedure of Section 5.1.

It remains to formulate the four sets of chordwise equivalent slopes, $\varepsilon, \delta, \zeta$ and ψ, by analogy with the two-dimensional principles of Section 3. At any section within the control span, we write the incidences of equation (A.9) as

$$\left.\begin{aligned} \bar{\alpha}_{2f} &= \left(\frac{c}{\bar{c}}\right)\bar{\alpha}_1(\bar{X}) \\ \bar{\alpha}_{7f} &= \left(\frac{c}{\bar{c}}\right)^2\bar{\alpha}_2(\bar{X}) \\ \bar{\alpha}_{8f} &= \left(\frac{\bar{x}_h}{\bar{c}}\right)\left(\frac{c}{\bar{c}}\right)\bar{\alpha}_1(\bar{X}) \end{aligned}\right\}, \tag{A.13}$$

where

$$\left.\begin{aligned} \bar{\alpha}_s(\bar{X}) &= -(\bar{X}-E)^s \quad \text{when } 0 \leqslant \bar{X} < E \\ &= 0 \quad \text{when } E < \bar{X} \leqslant 1 \end{aligned}\right\}, \tag{A.14}$$

with

$$\bar{X} = \left[\frac{\bar{x}-\bar{x}_l(\bar{y})}{c(\bar{y})}\right] \text{and } E = \left[\frac{\bar{x}_h(\bar{y})-\bar{x}_l(\bar{y})}{c(\bar{y})}\right]$$

By analogy with equation (44) with $N = 4$ terms, we write

$$\bar{\alpha}_e(\bar{X}) = \frac{1}{\pi}\left[\bar{\gamma}_e + 4\,\bar{\mu}_e(1+2\cos\bar{\phi}) + \kappa_e\,(1+2\cos\bar{\phi}+2\cos 2\bar{\phi}) + \bar{\lambda}_e(1+2\cos\bar{\phi}+2\cos 2\bar{\phi}+2\cos 3\bar{\phi})\right], \quad \text{(A.15)}$$

where $\bar{\phi} = \cos^{-1}(1-2\bar{X})$. The unknown coefficients $\bar{\gamma}_e$, $\bar{\mu}_e$, ... are chosen to satisfy the conditions for the first $(N-1)$ wing forces together with one special condition; when $N = 4$,

$$\left.\begin{aligned} &\text{each } \bar{\alpha}_e(\bar{X}) \text{ gives } (\bar{C}_L)_s,\ (\bar{C}_m)_s,\ (\bar{C}_{mm})_s\ (s = 1 \text{ or } 2),\\ &\bar{\alpha}_e(\bar{X}) = \varepsilon \text{ gives the correct } (\bar{C}_H)_1,\\ &\bar{\alpha}_e(\bar{X}) = \delta \text{ gives the correct } (\bar{C}_{mmm})_1,\\ &\bar{\alpha}_e(\bar{X}) = \zeta \text{ gives the correct } (\bar{C}_R)_1,\\ &\bar{\alpha}_e(\bar{X}) = \psi \text{ gives the correct } (\bar{C}_R)_2. \end{aligned}\right\} \quad \text{(A.16)}$$

The coefficients $(\bar{C}_L)_s$, $(\bar{C}_m)_s$, $(\bar{C}_{mm})_s$ and $(\bar{C}_{mmm})_1$ have analogous definitions to the coefficients in equations (46); on the other hand, we note that

$$(-\bar{C}_H)_1 = \frac{1}{E^2}\int_0^E (\bar{X}-E)\,\bar{l}_1(\bar{X})\,d\bar{X} \quad \text{(A.17)}$$

is the hinge moment on a leading-edge control, in contrast to $(-C_h)_r$ in equation (53), and that $(\bar{C}_R)_s$ for $s = 1$ or 2 is defined as the hinge-reaction coefficient

$$(\bar{C}_R)_s = \int_0^E \bar{l}_s(\bar{X})\,d\bar{X}, \quad \text{(A.18)}$$

where $\bar{l}_s(\bar{X})$ is the two-dimensional loading corresponding to $\bar{\alpha}_s(\bar{X})$ of equation (A.14).

It can be shown that the slopes $\bar{\alpha}_e(\bar{X}) = \varepsilon(\bar{X}, E)$ are determined by equation (A.15) with the matrix equation

$$\begin{bmatrix} 2 & 0 & 0 & 0 \\ 0 & 2 & 0 & 0 \\ 1 & -4 & 1 & 0 \\ D_\gamma & D_\mu & D_\kappa & D_\lambda \end{bmatrix} \begin{bmatrix} \bar{\gamma}_e \\ \bar{\mu}_e \\ \bar{\kappa}_e \\ \bar{\lambda}_e \end{bmatrix} = \begin{bmatrix} (\bar{C}_L)_1 \\ (\bar{C}_m)_1 \\ 8(\bar{C}_{mm})_1 \\ \pi E^2(\bar{C}_H)_1 \end{bmatrix}, \quad \text{(A.19)}$$

where D_γ, D_μ, ... are defined in equations (52) and

$$\left.\begin{aligned} 2(\bar{C}_L)_1 &= (\pi E^2)\,A_\gamma \quad \text{of equation (55)}\\ 32(\bar{C}_m)_1 &= -(\pi E^2)\,A_\mu\\ 32(\bar{C}_{mm})_1 &= (\pi E^2)(A_\gamma + \tfrac{1}{4}A_\mu + A_\kappa)\\ (\bar{C}_H)_1 &= (-C_h)_2 \quad \text{of equation (57)} \end{aligned}\right\} \quad \text{(A.20)}$$

If equivalent slopes ε are required for $N < 4$, then $\bar{\alpha}_e(\overline{X})$ is represented by the first N terms of equation (A.15) and only the conditions for the first $(N-1)$ wing forces and for $(\bar{C}_H)_1$ are retained in equation (A.19). Bearing in mind that the equivalent slopes ε represent $\bar{\alpha}_1\ (\overline{X})$ from equation (A.14), we can manipulate the equations when $N \geqslant 3$ to express ε in terms of τ_2; at the collocation positions

$$\varepsilon_p(E) = [E - \overline{X}_p + \tau_{2p}(1-E)], p = 1(1)N,$$

where $\overline{X}_p = \frac{1}{2}\left(1 - \cos\frac{2\pi p}{2N+1}\right)$ and $\tau_{2p}(1-E)$ are the chordwise equivalent slopes in Table 4 with argument $(1-E)$ instead of E.

The slopes $\bar{\alpha}_e(\overline{X}) = \delta(\overline{X}, E)$ are obtained, when $N = 4$, by equations (A.15) and (A.16), so that the last row in the matrix equation (A.19) is replaced by

$$-\bar{\gamma}_e + 12\,\bar{\mu}_e - 2\,\bar{\kappa}_e + \bar{\lambda}_e = 32(\bar{C}_{mmm})_1 = -\tfrac{1}{4}(\pi E^2)(A_\gamma + \tfrac{3}{4}A_\mu + 2A_\kappa + A_\lambda). \tag{A.21}$$

The slopes $\delta(\overline{X}, E)$ can be determined for $N < 4$ by reducing $\bar{\alpha}_e(\overline{X})$ and the matrix equation to the first N terms and force conditions respectively. By manipulation of the formulae it can be shown that when $N \geqslant 3$

$$\delta_p(E) = [E - \overline{X}_p + \sigma_{2p}(1-E)],$$

where $\overline{X}_p = \frac{1}{2}\left(1 - \cos\frac{2\pi p}{2N+1}\right)$ and σ_{2p} with argument $(1-E)$ instead of E may be obtained from Table 2.

The hinge-reaction coefficient $(\bar{C}_R)_s$ of equation (A.18) and the first $(N-1)$ wing forces are given correctly by the incidence $\bar{\alpha}_e(\overline{X})$ of equation (A.15), if the $N = 4$ unknown coefficients $(\bar{\gamma}_e, \bar{\mu}_e, \ldots$ satisfy the matrix equation

$$\begin{bmatrix} 2 & 0 & 0 & 0 \\ 0 & 2 & 0 & 0 \\ 1 & -4 & 1 & 0 \\ C_\gamma & C_\mu & C_\kappa & C_\lambda \end{bmatrix} \begin{bmatrix} \bar{\gamma}_e \\ \bar{\mu}_e \\ \bar{\kappa}_e \\ \bar{\lambda}_e \end{bmatrix} = \begin{bmatrix} (\bar{C}_L)_s \\ (\bar{C}_m)_s \\ 8(\bar{C}_{mm})_s \\ \frac{1}{2}\pi(\bar{C}_R)_s \end{bmatrix} \tag{A.22}$$

where C_γ, C_μ, ... are defined in equations (50) and the aerodynamic coefficients on the right-hand side correspond to the incidence $\bar{\alpha}_s(\overline{X})$ of equation (A.14). When $s = 1$, the equivalent slopes ζ are determined by equations (A.15) and (A.22) with $(\bar{C}_L)_1$, $(\bar{C}_m)_1$ and $(\bar{C}_{mm})_1$ from equations (A.20) and with

$$(\bar{C}_R)_1 \equiv E^2(-C_h)_1 \qquad \text{of equation (57).} \tag{A.23}$$

Likewise, when $s = 2$, to obtain the remaining chordwise equivalent slopes ψ defined in equations (A.16), the right-hand side of equation (A.22) requires the coefficients

$$\left.\begin{aligned} 2(\bar{C}_L)_2 &= -(\pi E^2)\,B_\gamma \\ 32(\bar{C}_m)_2 &= (\pi E^2)\,B_\mu \\ 32(\bar{C}_{mm})_2 &= -(\pi E^2)(B_\gamma + \tfrac{1}{4}B_\mu + B_\kappa) \\ 4\pi(\bar{C}_R)_2 &= [(\pi - \phi_h)^2(-1 + 2\cos\phi_h - 2\cos^2\phi_h) + (\pi - \phi_h)\sin\phi_h(1 - 3\cos\phi_h) - \sin^2\phi_h\cos\phi_h] \end{aligned}\right\}, \tag{A.24}$$

where B_ν, B_μ and B_κ are defined as functions of $\phi_h = \cos^{-1}(2E-1)$ in equations (95). To determine the slopes ζ and ψ for $N < 4$, the matrix equation (A.22) is reduced to the conditions for the first $(N-1)$ wing forces and the hinge reaction $(\bar{C}_R)_s$, together with $\bar{\lambda}_e = 0$ when $N = 3$ and $\bar{\kappa}_e = \bar{\lambda}_e = 0$ when $N = 2$.

The slopes ε and ζ or ψ are determined by equations (A.19) and (A.22) respectively, provided that the matrices are non-singular. Conversely, when $N = 4$, the slopes ε are indeterminate if $D_\lambda = 0$, whilst the slopes ζ and ψ are indeterminate if $C_\lambda = 0$. Likewise, there are singularities in the corresponding matrices for $N = 3$ if $D_\kappa = 0$ or $C_\kappa = 0$, but only the latter is possible for $0 < E < 1$; no singularities occur when $N = 2$. Hence, by means of equations (50) and (52), indeterminate slopes are found to occur in the following cases:

$$\left.\begin{array}{c} \text{for } \varepsilon, \text{ when } N = 4 \text{ and } E = 0{\cdot}41\dot{6} \\ \text{for } \zeta \text{ and } \psi, \text{ when } N = 4 \text{ and } E = \dfrac{5 \pm \sqrt{7}}{12} \\ \text{or when } N = 3 \text{ and } E = 0{\cdot}375 \end{array}\right\} \tag{A.25}$$

From equations (A.19) and (A.21) for $N = 4$ it follows that δ can always be determined because the matrix is non-singular, and this remains true for all N.

In conclusion, it follows from the above equivalent-incidence procedure that the hinge-moment derivatives of equations (A.12) are evaluated from

$$\left.\begin{aligned} -h_\xi &= \frac{\bar{c}}{2 S_f \bar{c}_f} \int_{S_f}\int \bar{l}_{6e}\, d\bar{x}\, d\bar{y} \\ \text{and} \qquad -h_{\dot{\xi}} &= \frac{\bar{c}}{2 S_f \bar{c}_f} \int_{S_f}\int \left[-\left(\frac{\beta^2 - M^2}{\beta^2}\right)\left(\frac{\bar{x} - \bar{x}_h}{\bar{c}}\right)\bar{l}_{2e} + \frac{1}{\beta^2}\bar{l}_{5e} + \frac{M^2}{\beta^2}\left(\frac{\bar{x}_h}{\bar{c}}\bar{l}_{6e} - \bar{l}_{7e} - \bar{l}_{8e}\right)\right] d\bar{x}\, d\bar{y} \end{aligned}\right\}, \tag{A.26}$$

where the load distributions $\bar{l}_{re}(\bar{x}, \bar{y})$ are obtained from collocation solutions for the equivalent incidences $(\bar{\alpha}_{re})_{pv}$ on the reversed wing in steady flow. For incompressible flow the calculation of $-h_{\dot{\xi}}$ involves just the two loadings $\bar{l}_{2e}$ and $\bar{l}_{5e}$, with indeterminate chordwise slopes ε only when $N = 4$ and $E = 0{\cdot}41\dot{6}$; singularities in the slopes ζ would still affect $-h_\xi$ through $\bar{l}_{6e}$, if the particular conditions in equation (A.25) were approached.

TABLE 1

Chordwise Equivalent Slopes σ_{1p} for $N = 2, 3, 4$ and $E = 0{\cdot}05(0{\cdot}05)0{\cdot}75$.

E	σ_{1p} for N = 4			
	p = 1	p = 2	p = 3	p = 4
0·05	−0·067546	0·082910	−0·127177	0·726131
0·10	−0·015801	0·016212	0·001624	0·912025
0·15	0·038897	−0·056951	0·179077	0·995830
0·20	0·075837	−0·108616	0·365110	1·030325
0·25	0·088379	−0·127029	0·540082	1·038650
0·30	0·076697	−0·108205	0·693420	1·033513
0·35	0·045041	−0·052866	0·819821	1·022530
0·40	0·000266	0·035117	0·917446	1·010355
0·45	−0·049136	0·149698	0·986894	0·999739
0·50	−0·093782	0·283349	1·030516	0·992124
0·55	−0·124031	0·427618	1·051929	0·988020
0·60	−0·130570	0·573602	1·055615	0·987273
0·65	−0·105030	0·712397	1·046589	0·989258
0·70	−0·040644	0·835551	1·030084	0·993038
0·75	+0·066936	0·935555	1·011247	0·997510

E	σ_{1p} for N = 2		σ_{1p} for N = 3		
	p = 1	p = 2	p = 1	p = 2	p = 3
0·05	−0·144234	0·445241	0·101655	−0·148884	0·595402
0·10	−0·160420	0·608283	0·077635	−0·109327	0·783700
0·15	−0·144774	0·719336	0·029982	−0·023088	0·893594
0·20	−0·109431	0·801625	−0·023072	0·086608	0·961173
0·25	−0·060054	0·864553	−0·071756	0·207650	1·001938
0·30	−0·000108	0·913170	−0·109795	0·332224	1·024635
0·35	0·067954	0·950626	−0·132897	0·454780	1·034932
0·40	0·142228	0·979086	−0·138116	0·571201	1·036809
0·45	0·221130	1·000144	−0·123540	0·678376	1·033204
0·50	0·303274	1·015036	−0·088118	0·773970	1·026354
0·55	0·387390	1·024765	−0·031581	0·856285	1·017986
0·60	0·472269	1·030174	0·045592	0·924184	1·009435
0·65	0·556716	1·032000	0·142158	0·977047	1·001720
0·70	0·639503	1·030907	0·256052	1·014755	0·995584
0·75	0·719314	1·027516	0·384260	1·037714	0·991523

TABLE 2

Chordwise Equivalent Slopes σ_{2p} for $N = 2, 3, 4$ and $E = 0{\cdot}05(0{\cdot}05)0{\cdot}75$

E	σ_{2p} for N = 2		σ_{2p} for N = 3		
	p = 1	p = 2	p = 1	p = 2	p = 3
0·05	−0·005228	0·015046	0·004112	−0·005999	0·020429
0·10	−0·013023	0·041694	0·008754	−0·012730	0·055374
0·15	−0·020752	0·075035	0·011495	−0·016173	0·097532
0·20	−0·027175	0·113154	0·011667	−0·014653	0·144037
0·25	−0·031462	0·154877	0·009263	−0·007325	0·193205
0·30	−0·033004	0·199372	0·004670	0·006170	0·243931
0·35	−0·031338	0·246008	−0·001467	0·025863	0·295463
0·40	−0·026106	0·294285	−0·008322	0·051545	0·347285
0·45	−0·017038	0·343794	−0·014948	0·082828	0·399053
0·50	−0·003939	0·394197	−0·020328	0·119189	0·450552
0·55	0·013322	0·445212	−0·023408	0·160004	0·501663
0·60	0·034813	0·496601	−0·023141	0·204577	0·552347
0·65	0·060542	0·548169	−0·018525	0·252171	0·602621
0·70	0·090457	0·599753	−0·008636	0·302029	0·652546
0·75	0·124443	0·651222	+0·007320	0·353401	0·702214

E	σ_{2p} for N = 4			
	p = 1	p = 2	p = 3	p = 4
0·05	−0·003285	0·004040	−0·006252	0·025416
0·10	−0·005460	0·006644	−0·009732	0·066997
0·15	−0·004836	0·005576	−0·005310	0·114971
0·20	−0·001873	0·001315	0·008309	0·165771
0·25	0·002338	−0·004727	0·031012	0·217573
0·30	0·006559	−0·010764	0·061954	0·269414
0·35	0·009673	−0·014937	0·099903	0·320828
0·40	0·010844	−0·015506	0·143455	0·371648
0·45	0·009622	−0·010981	0·191178	0·421891
0·50	0·006009	−0·000218	0·241714	0·471673
0·55	0·000484	0·017531	0·293858	0·521162
0·60	−0·005998	0·042573	0·346611	0·570531
0·65	−0·012037	0·074771	0·399208	0·619935
0·70	−0·015852	0·113551	0·451145	0·669487
0·75	−0·015380	0·157939	0·502178	0·719250

TABLE 3

Chordwise Equivalent Slopes τ_{1p} *for* $N = 2, 3, 4$ *and* $E = 0{\cdot}05(0{\cdot}05)0{\cdot}75$.

E	τ_{1p} for N = 2		τ_{1p} for N = 3		
	p = 1	p = 2	p = 1	p = 2	p = 3
0·05	-1·555513	0·984302	0·690024	-0·556048	0·740717
0·10	-0·844983	0·869763	0·139581	-0·152195	0·798999
0·15	-0·483765	0·848819	-0·114748	0·077068	0·857849
0·20	-0·242158	0·852322	-0·250972	0·244320	0·904886
0·25	-0·060054	0·864553	-0·320121	0·379524	0·940597
0·30	0·086596	0·880052	-0·344603	0·494716	0·966642
0·35	0·209696	0·896485	-0·336647	0·595779	0·984610
0·40	0·315965	0·912725	-0·303902	0·685929	0·995864
0·45	0·409544	0·928177	-0·251630	0·767018	1·001569
0·50	0·493157	0·942507	-0·183714	0·840124	1·002744
0·55	0·568678	0·955519	-0·103178	0·905832	1·000303
0·60	0·637444	0·967083	-0·012482	0·964372	0·995092
0·65	0·700415	0·977112	0·086319	1·015688	0·987929
0·70	0·758286	0·985536	0·191467	1·059449	0·979633
0·75	0·811531	0·992292	0·301473	1·095004	0·971076

E	τ_{1p} for N = 4			
	p = 1	p = 2	p = 3	p = 4
0·05	-0·206760	+0·196398	-0·201251	0·751857
0·10	0·195550	-0·156083	0·114082	0·872969
0·15	0·314771	-0·281845	0·325867	0·944850
0·20	0·323992	-0·310914	0·497151	0·984468
0·25	0·282659	-0·285407	0·643456	1·002748
0·30	0·221916	-0·226589	0·770689	1·006678
0·35	0·162390	-0·148530	0·882261	1·000845
0·40	0·121278	-0·063533	0·981835	0·987993
0·45	0·119545	0·012188	1·076647	0·968568
0·50	0·205331	0·039510	1·189671	0·936850
0·55	0·677253	-0·225595	1·478283	0·839949
0·60	-1·701061	1·853878	0·219974	1·277488
0·65	-0·450383	0·993931	0·862831	1·053077
0·70	-0·197880	0·963731	0·946420	1·022094
0·75	-0·019408	1·005943	0·965304	1·013466

TABLE 4

Chordwise Equivalent Slopes τ_{2p} *for* $N = 2, 3, 4$ *and* $E = 0{\cdot}05(0{\cdot}05)0{\cdot}75$.

E	τ_{2p} for N = 2		τ_{2p} for N = 3		
	p = 1	p = 2	p = 1	p = 2	p = 3
0·05	−0·116954	0·057722	0·068241	−0·050378	0·036268
0·10	−0·149936	0·093990	0·074830	−0·058456	0·071693
0·15	−0·164823	0·130065	0·068363	−0·055527	0·111577
0·20	−0·168750	0·167231	0·055717	−0·045137	0·154916
0·25	−0·164718	0·205776	0·040309	−0·028809	0·200873
0·30	−0·154390	0·245737	0·024295	−0·007412	0·248779
0·35	−0·138826	0·287065	0·009203	0·018479	0·298098
0·40	−0·118765	0·329678	−0·003826	0·048434	0·348395
0·45	−0·094759	0·373481	−0·013902	0·082104	0·399311
0·50	−0·067233	0·418373	−0·020328	0·119189	0·450552
0·55	−0·036532	0·464254	−0·022552	0·159411	0·501875
0·60	−0·002941	0·511022	−0·020144	0·202503	0·553087
0·65	0·033299	0·558575	−0·012782	0·248196	0·604040
0·70	0·071980	0·606811	−0·000225	0·296209	0·654623
0·75	0·112916	0·655625	+0·017668	0·346239	0·704770

E	τ_{2p} for N = 4			
	p = 1	p = 2	p = 3	p = 4
0·05	−0·041733	0·035383	−0·026710	0·032521
0·10	−0·035409	0·031059	−0·025668	0·072531
0·15	−0·022358	0·019860	−0·014633	0·118209
0·20	−0·009339	0·007401	0·004336	0·167151
0·25	0·000719	−0·003407	0·030151	0·217872
0·30	0·006547	−0·010754	0·061948	0·269416
0·35	0·007804	−0·013413	0·098909	0·321173
0·40	0·004688	−0·010488	0·140180	0·372785
0·45	−0·002431	−0·001155	0·184765	0·424118
0·50	−0·013932	0·016038	0·231104	0·475358
0·55	−0·038962	0·049688	0·272869	0·528451
0·60	+0·039143	0·005774	0·370630	0·562189
0·65	−0·008515	0·071900	0·401082	0·619284
0·70	−0·015840	0·113541	0·451152	0·669485
0·75	−0·014301	0·157059	0·502752	0·719051

TABLE 5

Symmetrical Spanwise Factors in Equivalent Slopes for Outboard Controls ($m = 15$).

	ν \ η_a	0	0·15	0·25	0·35	0·40	0·45
$\Omega_{1\nu}$	0	1	−0·11524	−0·11265	0·07610	0·08775	0·03923
	1	1	0·75876	0·25531	−0·09492	−0·11176	−0·05049
	2	1	1·04506	1·02223	0·69217	0·42338	0·15953
	3	1	0·97957	0·98698	1·06346	1·07080	0·99821
	4	1	1·01243	1·00834	0·96778	0·96409	0·99242
	5	1	0·99107	0·99389	1·02150	1·02396	1·00634
	6	1	1·00721	1·00498	0·98325	0·98132	0·99467
	7	1	0·99361	0·99557	1·01460	1·01627	1·00479
$\Omega_{2\nu}$	0	0·03994	−0·01183	0·00367	0·00456	0·00016	−0·00319
	1	0·19032	0·05007	−0·00150	−0·00635	−0·00076	0·00351
	2	0·38443	0·23235	0·12731	0·03860	0·01059	−0·00381
	3	0·55465	0·40561	0·30791	0·20555	0·15195	0·09981
	4	0·70770	0·55711	0·45571	0·35686	0·30868	0·25990
	5	0·83103	0·68145	0·58246	0·48171	0·43050	0·37966
	6	0·92424	0·77390	0·67308	0·57366	0·52460	0·47527
	7	0·98046	0·83077	0·73149	0·63099	0·58017	0·52959
$\Psi_{1\nu}$	0	1	−0·15004	0·02514	0·02114	0·00649	−0·00677
	1	1	0·83587	0·12804	−0·08475	−0·00627	0·01789
	2	1	0·97943	1·07563	0·77143	0·31890	0·06608
	3	1	1·00394	0·98266	0·99045	1·08600	1·05196
	4	1	0·99155	1·01376	1·00011	0·98889	0·97933
	5	1	1·00280	0·99436	0·99367	1·01178	1·01358
	6	1	0·99475	1·00698	1·00139	0·99662	0·99242
	7	1	1·00202	0·99616	0·99529	1·00615	1·00776
$\Psi_{2\nu}$	0	0·02772	−0·00425	0·00274	−0·00015	−0·00085	−0·00083
	1	0·19769	0·04470	−0·00218	−0·00117	0·00166	0·00116
	2	0·38171	0·23443	0·13009	0·03410	0·00582	−0·00303
	3	0·55649	0·40482	0·30550	0·20748	0·15590	0·10191
	4	0·70667	0·55760	0·45720	0·35634	0·30662	0·25743
	5	0·83196	0·68115	0·58130	0·48205	0·43198	0·38129
	6	0·92359	0·77415	0·67400	0·57351	0·52356	0·47384
	7	0·98105	0·83048	0·73058	0·63110	0·58111	0·53072

TABLE 5 (contd.)

Symmetrical Spanwise Factors in Equivalent Slopes for Outboard Controls ($m = 15$).

	η_a / ν	0·50	0·55	0·60	0·65	0·75	0·85
$\Omega_{1\nu}$	0	-0·02545	-0·05786	-0·03855	0·00925	0·02227	-0·02260
	1	0·02741	0·06517	0·04345	-0·00952	-0·02403	0·02386
	2	-0·02913	-0·10067	-0·06690	0·00962	0·03089	-0·02836
	3	0·81708	0·54214	0·23972	0·00482	-0·05254	0·03942
	4	1·04570	1·08372	1·04137	0·86281	0·19865	-0·07181
	5	0·97502	0·95431	0·97332	1·03611	1·03067	0·32165
	6	1·01789	1·03284	1·01987	0·97925	0·97522	1·08266
	7	0·98499	0·97239	0·98308	1·01596	1·02048	0·94499
$\Omega_{2\nu}$	0	-0·00349	-0·00120	0·00141	0·00216	-0·00091	0·00014
	1	0·00402	0·00146	-0·00148	-0·00235	0·00095	-0·00014
	2	-0·00664	-0·00288	0·00165	0·00309	-0·00110	0·00014
	3	0·05397	0·01970	0·00023	-0·00541	0·00138	-0·00012
	4	0·20900	0·15557	0·10197	0·05374	-0·00064	-0·00011
	5	0·33011	0·28198	0·23400	0·18389	0·07672	0·00364
	6	0·42496	0·37361	0·32216	0·27211	0·17640	0·07089
	7	0·47983	0·43097	0·38220	0·33227	0·22891	0·13240
$\Psi_{1\nu}$	0	-0·01461	-0·00933	0·00565	0·00543	-0·00130	0·00083
	1	0·01597	0·00746	-0·00165	-0·00785	0·00330	0·00008
	2	-0·05427	-0·05943	0·01124	0·01390	-0·00168	0·00125
	3	0·90204	0·57173	0·13425	-0·03315	0·01058	0·00145
	4	0·97950	1·02688	1·08112	0·94336	0·10309	0·00101
	5	1·00564	0·99322	0·98054	0·97630	1·07582	0·21732
	6	0·99114	1·00079	1·01664	1·00866	0·97609	1·11062
	7	1·00405	0·99811	0·99200	0·98895	1·02071	0·97639
$\Psi_{2\nu}$	0	-0·00026	0·00043	0·00038	0·00008	-0·00014	0·00006
	1	0·00027	-0·00033	-0·00047	-0·00021	0·00016	-0·00006
	2	-0·00290	0·00059	0·00107	0·00036	-0·00028	0·00011
	3	0·05257	0·01446	-0·00088	-0·00283	0·00072	-0·00016
	4	0·20853	0·15881	0·10480	0·05357	-0·00116	0·00053
	5	0·33078	0·28080	0·23146	0·18261	0·07903	0·00164
	6	0·42427	0·37456	0·32392	0·27324	0·17399	0·07336
	7	0·48042	0·43036	0·38061	0·33111	0·23069	0·13048

TABLE 6

Antisymmetrical Spanwise Factors in Equivalent Slopes for Outboard Controls ($m = 15$).

	ν \ η_a	0	0·15	0·25	0·35	0·40	0·45
$\Omega_{1\nu}$	1	1·18028	0·69084	0·19392	−0·04292	−0·05228	−0·02435
	2	0·90018	1·09287	1·06448	0·65241	0·37807	0·13985
	3	1·07024	0·94215	0·95427	1·09609	1·10793	1·01422
	4	0·94435	1·04382	1·03561	0·93959	0·93204	0·97868
	5	1·04751	0·96336	0·96990	1·04686	1·05277	1·01865
	6	0·95715	1·03270	1·02700	0·95965	0·95453	0·98325
	7	1·04040	0·96952	0·97462	1·03722	1·04196	1·01572
$\Omega_{2\nu}$	1	0·19509	0·04440	0·00133	−0·00350	−0·00089	0·00111
	2	0·38268	0·23600	0·12507	0·03654	0·01079	−0·00188
	3	0·55557	0·40289	0·30977	0·20719	0·15173	0·09818
	4	0·70711	0·55932	0·45410	0·35547	0·30890	0·26134
	5	0·83147	0·67954	0·58392	0·48294	0·43029	0·37835
	6	0·92388	0·77563	0·67173	0·57252	0·52481	0·47649
	7	0·98078	0·82912	0·73279	0·63207	0·57996	0·52841
$\Psi_{1\nu}$	1	1·09007	0·81037	0·13158	−0·06830	−0·00842	0·01054
	2	0·98684	0·99829	1·06765	0·76663	0·31818	0·06903
	3	1·00731	0·99754	0·98501	0·99629	1·08457	1·04859
	4	0·99724	0·99889	1·00972	0·99790	0·98873	0·98104
	5	1·00242	0·99955	0·99590	0·99703	1·01076	1·01142
	6	0·99866	0·99939	1·00416	0·99990	0·99657	0·99368
	7	1·00145	0·99970	0·99750	0·99798	1·00534	1·00606
$\Psi_{2\nu}$	1	0·19509	0·04468	−0·00110	−0·00137	0·00102	0·00080
	2	0·38268	0·23436	0·12951	0·03427	0·00613	−0·00278
	3	0·55558	0·40498	0·30587	0·20734	0·15562	0·10177
	4	0·70712	0·55748	0·45695	0·35645	0·30678	0·25756
	5	0·83148	0·68126	0·58149	0·48195	0·43180	0·38120
	6	0·92387	0·77405	0·67383	0·57359	0·52368	0·47392
	7	0·98074	0·83061	0·73075	0·63104	0·58098	0·53067

TABLE 6 (contd.)

Antisymmetrical Spanwise Factors in Equivalent Slopes for Outboard Controls ($m = 15$).

	ν \ η_a	0·50	0·55	0·60	0·65	0·75	0·85
$\Omega_{1\nu}$	1	0·00773	0·02195	0·01470	−0·00183	−0·00653	0·00550
	2	−0·01303	−0·06593	−0·04382	0·00304	0·01639	−0·01281
	3	0·80330	0·51272	0·22020	0·01061	−0·04001	0·02579
	4	1·05793	1·10966	1·05856	0·85756	0·18747	−0·05951
	5	0·96384	0·93068	0·95767	1·04097	1·04095	0·31026
	6	1·02840	1·05500	1·03455	0·97463	0·96552	1·09346
	7	0·97485	0·95103	0·96894	1·02043	1·02985	0·93453
$\Omega_{2\nu}$	1	0·00148	0·00064	−0·00034	−0·00067	0·00021	−0·00002
	2	−0·00463	−0·00227	0·00069	0·00170	−0·00047	0·00003
	3	0·05229	0·01920	0·00106	−0·00422	0·00082	−0·00002
	4	0·21046	0·15600	0·10123	0·05268	−0·00013	−0·00020
	5	0·32878	0·28161	0·23469	0·18486	0·07626	0·00372
	6	0·42620	0·37396	0·32151	0·27120	0·17685	0·07081
	7	0·47864	0·43064	0·38282	0·33316	0·22848	0·13248
$\Psi_{1\nu}$	1	0·01010	0·00511	−0·00028	−0·00398	0·00143	0·00009
	2	−0·04923	−0·05658	0·00878	0·01166	−0·00100	0·00081
	3	0·89945	0·57079	0·13505	−0·03119	0·00954	0·00147
	4	0·98223	1·02834	1·07964	0·94205	0·10352	0·00072
	5	1·00400	0·99266	0·98110	0·97761	1·07510	0·21734
	6	0·99311	1·00182	1·01553	1·00768	0·97643	1·11039
	7	1·00277	0·99771	0·99251	0·99007	1·02012	0·97642
$\Psi_{2\nu}$	1	0·00025	−0·00013	−0·00025	−0·00013	0·00008	−0·00002
	2	−0·00285	0·00040	0·00092	0·00034	−0·00022	0·00008
	3	0·05258	0·01456	−0·00078	−0·00280	0·00067	−0·00014
	4	0·20854	0·15870	0·10472	0·05357	−0·00113	0·00051
	5	0·33079	0·28086	0·23153	0·18263	0·07900	0·00165
	6	0·42427	0·37448	0·32386	0·27324	0·17402	0·07334
	7	0·48044	0·43042	0·38067	0·33113	0·23067	0·13050

TABLE 7

Chordwise Integration Functions for Local Hinge Moments with E = 0·05(0·05)0·75.

E	A_γ	A_μ	A_κ	A_λ
0·05	0·153509	−1·789249	0·702990	−0·899827
0·10	0·219543	−2·482957	0·916732	−1·063410
0·15	0·272027	−2·981658	1·030511	−1·071732
0·20	0·317916	−3·372871	1·086498	−0·999578
0·25	0·359911	−3·690810	1·102658	−0·882126
0·30	0·399419	−3·953055	1·089147	−0·740620
0·35	0·437304	−4·169977	1·052647	−0·589482
0·40	0·474157	−4·348191	0·998012	−0·439125
0·45	0·510426	−4·492105	0·929029	−0·297289
0·50	0·546479	−4·604695	0·848826	−0·169765
0·55	0·582644	−4·687924	0·760114	−0·060809
0·60	0·619237	−4·742973	0·665341	0·026614
0·65	0·656586	−4·770347	0·566810	0·090690
0·70	0·695060	−4·769895	0·466777	0·130698
0·75	0·735105	−4·740741	0·367553	0·147021

E	B_γ	B_μ	B_κ	B_λ
0·05	0·004369	−0·051354	0·020439	−0·026713
0·10	0·012483	−0·143090	0·054344	−0·066005
0·15	0·023137	−0·258956	0·093608	−0·105112
0·20	0·035950	−0·392554	0·134750	−0·139072
0·25	0·050720	−0·539866	0·175543	−0·165399
0·30	0·067327	−0·697955	0·214392	−0·182977
0·35	0·085702	−0·864455	0·250097	−0·191582
0·40	0·105807	−1·037350	0·281742	−0·191618
0·45	0·127629	−1·214849	0·308627	−0·183948
0·50	0·151174	−1·395305	0·330235	−0·169765
0·55	0·176466	−1·577155	0·346203	−0·150503
0·60	0·203550	−1·758875	0·356316	−0·127746
0·65	0·232488	−1·938948	0·360496	−0·103159
0·70	0·263365	−2·115816	0·358799	−0·078419
0·75	0·296296	−2·287843	0·351429	−0·055133

TABLE 8

Chordwise Integration Functions in Evaluating Control Derivatives by Reverse Flow.

E	C_γ	C_μ	C_K	C_λ
0·05	0·886917	3·312763	0·717765	0·568691
0·10	1·243501	4·320000	0·792000	0·446400
0·15	1·509542	4·856171	0·728426	0·218528
0·20	1·727295	5·120000	0·597333	-0·017067
0·25	1·913223	5·196152	0·433013	-0·216506
0·30	2·075795	5·132485	0·256624	-0·359274
0·35	2·220043	4·960484	0·082675	-0·438176
0·40	2·349234	4·703020	-0·078384	-0·454625
0·45	2·465616	4·377945	-0·218897	-0·415905
0·50	2·570796	4·000000	-0·333333	-0·333333
0·55	2·665951	3·581955	-0·417895	-0·220887
0·60	2·751950	3·135347	-0·470302	-0·094060
0·65	2·829428	2·671030	-0·489689	0·031162
0·70	2·898828	2·199636	-0·476588	0·139310
0·75	2·960420	1·732051	-0·433013	0·216506

E	D_γ	D_μ	D_K	D_λ
0·05	0·059329	0·227877	0·052452	0·046158
0·10	0·166950	0·615002	0·129600	0·098496
0·15	0·305113	1·076615	0·206387	0·132088
0·20	0·467270	1·577257	0·273067	0·141995
0·25	0·649519	2·094395	0·324760	0·129904
0·30	0·849140	2·611844	0·359274	0·100597
0·35	1·064069	3·117290	0·376170	0·060187
0·40	1·292648	3·601097	0·376242	0·015050
0·45	1·533490	4·055644	0·361180	-0·028894
0·50	1·785398	4·474926	0·333333	-0·066667
0·55	2·047315	4·854308	0·295511	-0·094564
0·60	2·318283	5·190366	0·250828	-0·110364
0·65	2·597421	5·480788	0·202553	-0·113430
0·70	2·883900	5·724335	0·153974	-0·104703
0·75	3·176927	5·920841	0·108253	-0·086602

TABLE 9

Lift and Pitching-Moment Derivatives for Rectangular Wing ($A = 4, M = 0$) with Oscillating Full-Span Controls.

(a) Stiffness derivatives

	E	By direct flow (m = 15)			By reverse flow (m = 15)		
		N = 2	N = 3	N = 4	N = 2	N = 3	N = 4
$-z_\xi$	0·05	0·5442	0·5528	0·5573	0·5435	0·5505	0·5526
	0·10	0·7596	0·7694	0·7734	0·7587	0·7667	0·7687
	0·15	0·9180	0·9274	0·9300	0·9170	0·9246	0·9264
	0·20	1·0459	1·0540	1·0552	1·0449	1·0515	1·0527
	0·25	1·1536	1·1600	1·1598	1·1525	1·1578	1·1586
	0·35	1·3275	1·3302	1·3284	1·3265	1·3287	1·3288
	0·50	1·5192	1·5173	1·5156	1·5183	1·5169	1·5168
$-m_\xi$	0·05	0·0476	0·0488	0·0502	0·0476	0·0487	0·0498
	0·10	0·0488	0·0503	0·0514	0·0487	0·0501	0·0510
	0·15	0·0376	0·0392	0·0398	0·0376	0·0390	0·0396
	0·20	0·0188	0·0204	0·0205	0·0187	0·0202	0·0203
	0·25	-0·0056	-0·0040	-0·0044	-0·0057	-0·0042	-0·0045
	0·35	-0·0659	-0·0646	-0·0655	-0·0661	-0·0648	-0·0655
	0·50	-0·1732	-0·1724	-0·1732	-0·1736	-0·1728	-0·1734

(b) Damping derivatives

	E	By direct flow (m = 15)			By reverse flow (m = 15)		
		N = 2	N = 3	N = 4	N = 2	N = 3	N = 4
$-z'_\xi$	0·05	-0·2214	-0·2238	-0·2264	-0·2220	-0·2231	-0·2244
	0·10	-0·2658	-0·2680	-0·2698	-0·2665	-0·2673	-0·2683
	0·15	-0·2687	-0·2702	-0·2708	-0·2696	-0·2697	-0·2702
	0·20	-0·2460	-0·2466	-0·2460	-0·2470	-0·2464	-0·2463
	0·25	-0·2048	-0·2045	-0·2030	-0·2059	-0·2046	-0·2039
	0·35	-0·0820	-0·0800	-0·0775	-0·0831	-0·0806	-0·0794
	0·50	+0·1711	+0·1749	+0·1766	+0·1700	+0·1736	+0·1748
$-m'_\xi$	0·05	0·0933	0·0735	0·0743	0·0933	0·0731	0·0736
	0·10	0·1299	0·1082	0·1089	0·1299	0·1078	0·1083
	0·15	0·1557	0·1359	0·1366	0·1556	0·1356	0·1361
	0·20	0·1749	0·1591	0·1595	0·1749	0·1588	0·1592
	0·25	0·1892	0·1782	0·1784	0·1891	0·1779	0·1783
	0·35	0·2058	0·2048	0·2047	0·2056	0·2047	0·2049
	0·50	0·2050	0·2158	0·2157	0·2047	0·2159	0·2160

TABLE 10

Lift and Pitching-Moment Derivatives for Rectangular Wing ($A = 4, M = 0$) with Oscillating Part-Span Controls.

(a) Constant control span $\eta_a = 0{\cdot}45$

	E	N = 2	N = 3	N = 4
$-z_\xi$	0·15	0·4384	0·4453	0·4468
	0·25	0·5488	0·5534	0·5533
	0·35	0·6291	0·6309	0·6299
	0·35+	0·6278	0·6296	0·6286
$-m_\xi$	0·15	0·0260	0·0276	0·0282
	0·25	0·0059	0·0074	0·0071
	0·35	-0·0234	-0·0221	-0·0229
	0·35+	-0·0233	-0·0220	-0·0228
$-z_\xi^\bullet$	0·15	-0·1118	-0·1126	-0·1129
	0·25	-0·0756	-0·0751	-0·0742
	0·35	-0·0120	-0·0104	-0·0090
	0·35+	-0·0118	-0·0102	-0·0088
$-m_\xi^\bullet$	0·15	0·0729	0·0630	0·0634
	0·25	0·0887	0·0834	0·0836
	0·35	0·0964	0·0965	0·0965
	0·35+	0·0962	0·0963	0·0963

+ With spanwise factors $\Psi_{1\nu}$ in place of $\Omega_{1\nu}$

(b) Constant control chord E = 0·25

	$\eta_a = 0$	$\eta_a = 0{\cdot}25$	$\eta_a = 0{\cdot}45$	$\eta_a = 0{\cdot}65$	$\eta_a = 0{\cdot}85$
$-z_\xi$	1·1600	0·8181	0·5534	0·3066	0·0963
$-m_\xi$	-0·0040	0·0032	0·0074	0·0086	0·0049
$-z_\xi^\bullet$	-0·2045	-0·1289	-0·0751	-0·0328	-0·0067
$-m_\xi^\bullet$	0·1782	0·1244	0·0834	0·0460	0·0146

TABLE 11

Hinge-Moment Derivatives for Rectangular Wing ($A = 4, M = 0$) with Various Oscillating Controls.

(a) Stiffness derivative

η_a	E	$-h_\xi$ by direct flow			$-h_\xi$ by reverse flow		
		N = 2	N = 3	N = 4	N = 2	N = 3	N = 4
0	0·05	0·3926	0·4014	0·4067	0·3745	0·3992	0·4044
	0·10	0·3848	0·3918	0·3954	0·3717	0·3908	0·3941
	0·15	0·3776	0·3830	0·3853	0·3691	0·3826	0·3833
	0·20	0·3709	0·3752	0·3763	0·3666	0·3748	0·4080
	0·25	0·3647	0·3681	0·3681	0·3643	0·3673	0·3713
	0·35	0·3544	0·3566	0·3547	0·3604	0·3468	0·3570
	0·50	0·3445	0·3455	0·3405	0·3572	0·3479	0·3451
0·45	0·15	0·3031	0·3174	0·3223	0·2895	0·3186	0·3176
	0·25	0·2762	0·2812	0·2813	0·2755	0·2836	0·2904
	0·35	0·2519	0·2515	0·2481	0·2616	0·2442	0·2522
0	0·25		0·3681				
0·25	0·25		0·3133				
0·45	0·25		0·2812				
0·65	0·25		0·2268				
0·85	0·25		0·1343				

(b) Damping derivative

η_a	E	$-h_\xi^\bullet$ by direct flow			$-h_\xi^\bullet$ by reverse flow		
		N = 2	N = 3	N = 4	N = 2	N = 3	N = 4
0	0·05	0·0314	0·0348	0·0379	0·0299	0·0342	0·0378
	0·10	0·0638	0·0724	0·0801	0·0612	0·0715	0·0799
	0·15	0·0970	0·1119	0·1237	0·0935	0·1108	0·1235
	0·20	0·1309	0·1524	0·1670	0·1268	0·1511	0·1667
	0·25	0·1655	0·1932	0·2088	0·1610	0·1918	0·2085
	0·35	0·2357	0·2731	0·2868	0·2311	0·2718	0·2862
	0·50	0·3422	0·3840	0·3902	0·3383	0·3828	0·3891
0	0·15	0·0742	0·1200	0·1359	α_{3e} solution with slopes		
	0·25	0·1655	0·2097	0·2176			
	0·35	0·2500	0·2878	0·2916	τ_{1p} in place of σ_{1p}		
0·45	0·15	0·0929	0·1124	0·1252	0·0870	0·1104	0·1244
	0·25	0·1540	0·1864	0·2030	0·1465	0·1844	0·2023
	0·35	0·2140	0·2550	0·2696	0·2060	0·2535	0·2690
0·45	0·15	0·0773	0·1201	0·1376	α_{3e} solution with slopes		
	0·25	0·1546	0·2018	0·2125			
	0·35	0·2247	0·2691	0·2757	$\tau_{1p}\,\Psi_{1\nu}$ in place of $\sigma_{1p}\,\Omega_{1\nu}$		

TABLE 12

Convergence of $-h_\xi$ and $-h_\xi$ with Respect to Chordwise Parameters for Rectangular Wing ($A = 4, M = 0$) with Full-Span Control.

E	N'†	$-h_\xi$			$-h_\xi^\circ$		
		N = 2	N = 3	N = 4	N = 2	N = 3	N = 4
0.05	2	0.3926	0.3914	0.3990	0.0314	0.0340	0.0372
	3		0.4014	0.4041		0.0348	0.0376
	4			0.4067			0.0379
0.10	2	0.3848	0.3851	0.3911	0.0638	0.0711	0.0789
	3		0.3918	0.3951		0.0724	0.0797
	4			0.3954			0.0801
0.15	2	0.3776	0.3791	0.3838	0.0970	0.1103	0.1222
	3		0.3830	0.3864		0.1119	0.1233
	4			0.3853			0.1237
0.20	2	0.3709	0.3735	0.3770	0.1309	0.1506	0.1652
	3		0.3752	0.3783		0.1524	0.1666
	4			0.3763			0.1670
0.25	2	0.3647	0.3681	0.3708	0.1655	0.1913	0.2069
	3		0.3681	0.3708		0.1932	0.2085
	4			0.3681			0.2088
0.35	2	0.3544	0.3588	0.3602	0.2357	0.2714	0.2849
	3		0.3566	0.3581		0.2731	0.2866
	4			0.3547			0.2868
0.50	2	0.3445	0.3490	0.3496	0.3422	0.3828	0.3888
	3		0.3455	0.3456		0.3840	0.3902
	4			0.3405			0.3902

† $N' \leq N$ is the number of chordwise terms in the equivalent slopes.

TABLE 13

Steady Forces and Local Centres of Pressure on Untapered Swept Wing ($A = 4, M = 0$) with Deflected Controls ($m = 15, q = 2N$).

(a) Lift and pitching moment

E	η_a	$-z_\xi$			$-m_\xi$		
		N = 2	N = 3	N = 4	N = 2	N = 3	N = 4
0·15	0	0·7063	0·7066	0·7085	0·7192	0·7214	0·7241
0·25	0	0·8961	0·8974	0·8986	0·8649	0·8675	0·8691
0·35	0	1·0409	1·0430	1·0436	0·9518	0·9543	0·9550
0·15	0·45	0·2914	0·2929	0·2937	0·4280	0·4295	0·4306
0·25	0·45	0·3720	0·3730	0·3736	0·5186	0·5200	0·5207
0·35	0·45	0·4348	0·4352	0·4355	0·5751	0·5763	0·5766
0·25	0			0·8986			0·8691
	0·25			0·5792			0·6944
	0·45			0·3736			0·5207
	0·65			0·1966			0·3157
	0·85			0·0578			0·1065
0·25*	0			0·9330			0·8862
	0·25			0·5844			0·6965
	0·45			0·3758			0·5217
	0·65			0·1973			0·3160
	0·85			0·0578			0·1064

*Rounding from equation (6) is used in place of equation (5).

(b) Values of X_{cp}

	E = 0·15, η_a = 0				E = 0·35, η_a = 0·45		
Rounding	Equation (5)			Eqn.(6)	Equation (5)		
η	N = 2	N = 3	N = 4	N = 4	N = 2	N = 3	N = 4
0+	0·7156	0·6640	0·6723	0·6351	0·4701	0·4593	0·4620
0·1951	0·5789	0·5796	0·5792	0·5654	0·4300	0·4127	0·4076
0·3827	0·5278	0·5268	0·5277	0·5206	0·5226	0·5086	0·5104
0·5556	0·5138	0·5160	0·5158	0·5098	0·5436	0·5482	0·5485
0·7071	0·5035	0·5054	0·5055	0·5013	0·4913	0·4941	0·4947
0·8315	0·4968	0·5069	0·5060	0·5020	0·4679	0·4708	0·4715
0·9239	0·4874	0·5099	0·5110	0·5074	0·4458	0·4495	0·4469
0·9808	0·4802	0·5217	0·5233	0·5196	0·4343	0·4381	0·4254

+ Referred to rounded leading edge. Referred to apex, X_{cp} at $\eta = 0$ would be respectively 0·0650 and 0·1301 larger with rounding from equations (5) and (6).

TABLE 14

Hinge Moment on Untapered Swept Wing ($A = 4$, $M = 0$) with Deflected Controls.

(a) Effect of N on $-h_{\xi}$ ($m = 15$, $q = 2N$)

E	Outboard Controls				Inboard Controls			
	η_a	N = 2	N = 3	N = 4	η_f	N = 2	N = 3	N = 4
0·15	0	0·2851	0·2884	0·2911	0·25	0·2813	0·2932	0·3032
	0·25	0·2517	0·2550	0·2558	0·45	0·2850	0·2895	0·2950
	0·45	0·2393	0·2456	0·2490	0·65	0·2951	0·2988	0·3024
	0·65	0·2061	0·2128	0·2133	0·85	0·2942	0·2974	0·3010
	0·85	0·1377	0·1538	0·1583	1·00	0·2851	0·2884	0·2911
0·25	0	0·2817	0·2841	0·2857	0·25	0·2700	0·2807	0·2884
	0·25	0·2397	0·2401	0·2399	0·45	0·2820	0·2880	0·2920
	0·45	0·2219	0·2245	0·2262	0·65	0·2934	0·2962	0·2986
	0·65	0·1848	0·1851	0·1841	0·85	0·2930	0·2954	0·2978
	0·85	0·1177	0·1201	0·1187	1·00	0·2817	0·2841	0·2857
0·35	0	0·2799	0·2816	0·2823	0·25	0·2597	0·2692	0·2741
	0·25	0·2296	0·2283	0·2275	0·45	0·2799	0·2863	0·2890
	0·45	0·2064	0·2069	0·2072	0·65	0·2929	0·2950	0·2964
	0·65	0·1654	0·1623	0·1604	0·85	0·2931	0·2949	0·2962
	0·85	0·0993	0·0940	0·0892	1·00	0·2799	0·2816	0·2823
0·25*	0			0·2855	0·45			0·2914
	0·45			0·2263	1·00			0·2855

* Rounding from equation (6) is used in place of equation (5).

(b) Effect of rounding on spanwise distribution ($m = 15$, $N = 4$, $q = 8$)

	Values of $-h_{\xi L}$ ($E = 0·25$)					
Rounding	Equation (5)			Equation (6)		
η	$\eta_a = 0$	$\eta_a = 0·45$	$\eta_f = 0·45$	$\eta_a = 0$	$\eta_a = 0·45$	$\eta_f = 0·45$
0	0·4663		0·4483	0·4392		0·4224
0·1951	0·3204		0·3036	0·3241		0·3069
0·3827	0·2999		0·2103	0·3048		0·2150
0·4500		0·1778	0·1228		0·1779	0·1251
0·5556	0·2984	0·2743		0·2983	0·2744	
0·7071	0·2750	0·2507		0·2772	0·2508	
0·8315	0·2399	0·2360		0·2393	0·2360	
0·9239	0·1603	0·1538		0·1613	0·1538	
0·9808	0·0639	0·0644		0·0634	0·0644	

TABLE 15

Spanwise Loading on Untapered Swept Wing ($A = 4$, $M = 0$) with Deflected Controls ($m = 15$, $N = 4$, $q = 8$).

(a) Values of y with rounding from equation (5)

η	E = 0·25	E = 0·25	E = 0·25	E = 0·25	E = 0·25
	η_a = 0	η_a = 0·25	η_a = 0·45	η_a = 0·65	η_a = 0·85
0	0·1950	0·0319	0·0124	0·0039	0·0010
0·1951	0·2296	0·0608	0·0179	0·0052	0·0013
0·3827	0·2481	0·1693	0·0422	0·0096	0·0019
0·5556	0·2535	0·2040	0·1464	0·0227	0·0034
0·7071	0·2459	0·2097	0·1767	0·1121	0·0084
0·8315	0·2214	0·1963	0·1727	0·1381	0·0353
0·9239	0·1723	0·1557	0·1418	0·1204	0·0798
0·9808	0·0957	0·0877	0·0805	0·0708	0·0531
η	E = 0·15*	E = 0·15	E = 0·15	E = 0·35	E = 0·35
	η_a = 0	η_a = 0	η_a = 0·45	η_a = 0	η_a = 0·45
0	0·1506	0·1486	0·0090	0·2331	0·0156
0·1951	0·1788	0·1788	0·0131	0·2695	0·0225
0·3827	0·1946	0·1950	0·0289	0·2891	0·0550
0·5556	0·1993	0·1998	0·1142	0·2945	0·1714
0·7071	0·1947	0·1947	0·1404	0·2842	0·2037
0·8315	0·1762	0·1770	0·1383	0·2533	0·1971
0·9239	0·1376	0·1414	0·1176	0·1930	0·1574
0·9808	0·0764	0·0819	0·0697	0·1042	0·0866

*This solution for N = 2 shows small effect of N over most of the span.

(b) Values of y with rounding from equation (6)

η	E = 0·15	E = 0·15	E = 0·25	E = 0·25	E = 0·35	E = 0·35
	η_a = 0	η_a = 0·45	η_a = 0	η_a = 0·45	η_a = 0	η_a = 0·45
0	0·1762	0·0105	0·2265	0·0143	0·2663	0·0180
0·1951	0·1901	0·0137	0·2425	0·0187	0·2832	0·0236
0·3827	0·2008	0·0292	0·2550	0·0427	0·2966	0·0555
0·5556	0·2042	0·1145	0·2586	0·1467	0·2998	0·1718
0·7071	0·1977	0·1406	0·2495	0·1770	0·2881	0·2040
0·8315	0·1793	0·1384	0·2240	0·1728	0·2561	0·1973
0·9239	0·1429	0·1176	0·1740	0·1419	0·1948	0·1575
0·9808	0·0826	0·0698	0·0966	0·0805	0·1051	0·0867

TABLE 16

Pitching Derivatives ($x_0 = 0{\cdot}5c_r$) *for Tapered Swept Wing* ($A = 2$, $M = 0{\cdot}7806$).

(a) Lift and pitching moment (m = 15, q = 6)

	By direct flow			By reverse flow		
	N = 2	N = 3	N = 4	N = 2	N = 3	N = 4
$-z_\theta$	1·2734	1·2750	1·2760	1·2726	1·2744	1·2746
$-m_\theta$	0·3488	0·3487	0·3486	0·3504	0·3498	0·3502
$-z_{\dot\theta}$	1·2705	1·2831	1·2854	1·2618	1·2800	1·2821
$-m_{\dot\theta}$	0·7435	0·7676	0·7695	0·7507	0·7670	0·7686

(b) Hinge moment by direct flow (m = 15)

	Rounding	Equation (5)		Equation (6)		
	η_a	N = 3	N = 3	N = 2	N = 3	N = 4
		q = 1	q = 6	q = 6	q = 6	q = 6
$-h_\theta$	0*	0·1577	0·1719	0·1847	0·1679	0·1666
	0	-	-	0·1746	0·1579	0·1564
	0·25	0·1224	0·1295	0·1511	0·1284	0·1248
	0·50	0·0869	0·0883	0·1161	0·0885	0·0869
	0·75	0·0337	0·0286	0·0451	0·0289	0·0363
$-h_{\dot\theta}$	0*	0·6973	0·7256	0·6401	0·7103	0·7209
	0	-	-	0·6075	0·6721	0·6814
	0·25	0·5548	0·5620	0·5268	0·5526	0·5503
	0·50	0·4163	0·4161	0·4119	0·4120	0·4104
	0·75	0·2552	0·2497	0·2540	0·2488	0·2530

* Calculations with actual straight hinge line.

TABLE 17

Stiffness Derivatives for Tapered Swept Wing ($A = 2$, $M = 0{\cdot}7806$) with Symmetrical Oscillating Controls of Different Span.

(a) Direct-flow solutions (m = 15)

	Rounding	Equation (5)		Equation (6)			Ref. 8
	η_a	N = 3	N = 3	N = 2	N = 3	N = 4	m = 20
		q = 1	q = 6	q = 6	q = 6	q = 6	N = 4
$-z_\xi$	0 *	0·9455	0·9184	-	0·9420	-	-
	0	-	-	-	0·9373	-	-
	0·25	0·5844	0·5709	-	0·5818	-	-
	0·50	0·3031	0·2971	0·3013	0·2990	0·2984	0·3017
	0·75	0·1001	0·0983	-	0·0991	-	-
$-m_\xi$	0*	0·5951	0·5868	-	0·5919	-	-
	0	-	-	-	0·5936	-	-
	0·25	0·4223	0·4140	-	0·4178	-	-
	0·50	0·2502	0·2447	0·2410	0·2447	0·2438	0·2459
	0·75	0·0936	0·0916	-	0·0923	-	-
$-h_\xi$	0*	0·4764	0·4831	-	0·4807	-	-
	0	-	-	-	0·4648	-	-
	0·25	0·3593	0·3549	-	0·3553	-	-
	0·50	0·3007	0·2964	0·2531	0·2965	0·3034	0·3627
	0·75	0·2116	0·2089	-	0·2091	-	-

(b) Reverse-flow solutions (m = 15)

	Rounding	Equation (5)	Equation (6)		
	η_a	N = 3	N = 2	N = 3	N = 4
		q = 1	q = 6	q = 6	q = 6
$-z_\xi$	0*	0·9269	-	-	-
	0	-	0·9140	0·9346	0·9372
	0·25	0·5740	0·5757	0·5807	0·5815
	0·50	0·2950	0·2981	0·2985	0·2984
	0·75	0·0977	0·0988	0·0990	0·0988
$-m_\xi$	0*	0·5805	-	-	-
	0	-	0·5570	0·5929	0·5948
	0·25	0·4102	0·3988	0·4166	0·4173
	0·50	0·2408	0·2370	0·2440	0·2441
	0·75	0·0910	0·0903	0·0922	0·0921
$-h_\xi$	0		-	0·4257	-
	0·25		-	0·3268	-
	0·50		0·2524	0·2742	0·3318
	0·75		-	0·1960	-

*Calculations with actual straight hinge line.

TABLE 18

Damping Derivatives for Tapered Swept Wing ($A = 2$, $M = 0{\cdot}7806$) with Symmetrical Oscillating Controls of Different Span.

(a) Direct-flow solutions (m = 15)

	Rounding	Equation (5)		Equation (6)			Ref. 8
	η_a	N = 3	N = 3	N = 2	N = 3	N = 4	m = 20
		q = 1	q = 6	q = 6	q = 6	q = 6	N = 4
$-z'_\xi$	0*	-0·0830	-0·0519	-	-0·0794	-	-
	0	-	-	-	-0·0921	-	-
	0·25	-0·0912	-0·0767	-	-0·0906	-	-
	0·50	-0·0580	-0·0520	-0·0544	-0·0568	-0·0565	-0·0551
	0·75	-0·0205	-0·0188	-	-0·0195	-	-
$-m'_\xi$	0*	0·1096	0·1114	-	0·1087	-	-
	0	-	-	-	0·1017	-	-
	0·25	0·0491	0·0480	-	0·0464	-	-
	0·50	0·0171	0·0166	0·0183	0·0162	0·0162	0·0192
	0·75	0·0032	0·0032	-	0·0035	-	-
$-h'_\xi$	0*	0·3890	0·3945	-	0·3444	-	-
	0	-	-	-	0·3246	-	-
	0·25	0·2602	0·2543	-	0·2222	-	-
	0·50	0·2113	0·2058	0·1216	0·1769	0·1987	0·1973
	0·75	0·1399	0·1362	-	0·1214	-	-

(b) Reverse-flow solutions (m = 15)

	Rounding	Equation (5)	Equation (6)		
	η_a	N = 3	N = 2	N = 3	N = 4
		q = 1	q = 6	q = 6	q = 6
$-z'_\xi$	0*	-0·0878	-	-	-
	0	-	-0·0969	-0·0952	-0·0949
	0·25	-0·0882	-0·0875	-0·0894	-0·0911
	0·50	-0·0551	-0·0561	-0·0560	-0·0564
	0·75	-0·0191	-0·0202	-0·0194	-0·0193
$-m'_\xi$	0*	0·1071	-	-	-
	0	-	0·0564	0·0990	0·0995
	0·25	0·0493	0·0249	0·0461	0·0452
	0·50	0·0178	0·0072	0·0162	0·0160
	0·75	0·0038	0·0007	0·0034	0·0034
$-h'_\xi$	0		-	0·3146	-
	0·25		-	0·2156	-
	0·50		0·1043	0·1695	0·2045
	0·75		-	0·1154	-

*Calculations with actual straight hinge line.

TABLE 19

Rolling and Hinge Moments for Tapered Swept Wing ($A = 2$, $M = 0{\cdot}7806$) with Antisymmetrical and Symmetrical Controls.

(a) Rolling-moment derivatives ($m = 15$, $q = 6$)

	η_a	Antisymmetrical			Symmetrical*	Ratio
		N = 2	N = 3	N = 4	N = 3	N = 3
$-\ell_\xi$	0	-	-	-	0·2070	-
	0·25	-	0·1181	-	0·1505	0·785
or	0·50	0·0786	0·0805	0·0805	0·0921	0·874
$-b_\xi$	0·75	-	0·0335	-	0·0362	0·926
$-\ell^\bullet_\xi$	0	-	-	-	-0·0262	
	0·25	-	0·0243	-	-0·0145	
or	0·50	0·0132	0·0132	0·0131	-0·0061	
$-b^\bullet_\xi$	0·75	-	0·0042	-	-0·0016	

*See equations (37) and (120); the rolling moment on a half-model with reflection-plane symmetry is termed 'bending' moment and the derivatives $-\ell_\xi$ and $-\ell^\bullet_\xi$ are replaced by $-b_\xi$ and $-b^\bullet_\xi$.

(b) Hinge-moment derivatives ($m = 15$, $q = 6$)

	η_a	Anti-symmetrical	Symmetrical	Ratio
		N = 3	N = 3	N = 3
$-h_\xi$	0	-	0·4648	-
	0·25	0·3043	0·3553	0·857
	0·50	0·2864	0·2965	0·966
	0·75	0·2079	0·2091	0·994
$-h^\bullet_\xi$	0	-	0·3246	-
	0·25	0·2181	0·2222	0·982
	0·50	0·1786	0·1769	1·010
	0·75	0·1219	0·1214	1·004

TABLE 20

Pitching Derivatives ($x_0 = 0{\cdot}5c_r$) for Cropped Delta Wing ($A = 1{\cdot}8$).

(a) Lift and pitching moment (M = 0·7454)

m,N,q	15,3,1	15,2,6	15,3,6	15,4,6
$-z_\theta$	1·2192	1·2172	1·2168	1·2173
$-m_\theta$	0·1180	0·1170	0·1137	0·1140
$-z_{\dot\theta}$	1·2252	1·2136	1·2246	1·2247
$-m_{\dot\theta}$	0·5722	0·5534	0·5696	0·5698

(b) Lift and pitching moment (m = 15, N = 3, q = 6)

	M = 0	M = 0·5528	M = 0·7454	M = 0·8660
$-z_\theta$	1·1055	1·1595	1·2168	1·2767
$-m_\theta$	0·0859	0·0985	0·1137	0·1316
$-z_{\dot\theta}$	1·1313	1·1764	1·2246	1·2776
$-m_{\dot\theta}$	0·4104	0·4793	0·5696	0·6936

(c) Hinge moments (m = 15, N = 3, q = 6)

	η_a	M = 0	M = 0·5528	M = 0·7454	M = 0·8660
$-h_\theta$	0	0·1032	0·1057	0·1078	0·1092
	0·25	0·1100	0·1107	0·1101	0·1077
	0·50	0·1174	0·1152	0·1106	0·1026
	0·75	0·1186	0·1122	0·1025	0·0886
$-h_{\dot\theta}$	0	0·3822	0·4445	0·5309	0·6557
	0·25	0·3605	0·4189	0·5003	0·6182
	0·50	0·3272	0·3785	0·4500	0·5536
	0·75	0·2690	0·3070	0·3600	0·4367

TABLE 21

Stiffness Derivatives for Cropped Delta Wing ($A = 1{\cdot}8$) with Oscillating Controls of Different Span.

(a) Constant Mach number M = 0·7454

	η_a	N = 3	N = 2	N = 3	N = 4	N = 4*
		q = 1	q = 6	q = 6	q = 6	q = 6
$-z_\xi$	0	0·9286	0·9083	0·9242	0·9237	0·9244
	0·25	-	-	0·6418	-	-
	0·50	0·3763	0·3758	0·3732	0·3719	0·3727
	0·75	-	-	0·1409	-	-
$-m_\xi$	0	0·4677	0·4319	0·4643	0·4633	0·4639
	0·25	-	-	0·3272	-	-
	0·50	0·1947	0·1947	0·1934	0·1914	0·1922
	0·75	-	-	0·0743	-	-
$-h_\xi$	0	0·4056	0·3696	0·4066	0·4052	0·3982
	0·25	-	-	0·3129	-	-
	0·50	0·2259	0·2346	0·2291	0·2099	0·2196
	0·75	-	-	0·1111	-	-

* In this solution N' = 3 in place of the standard N' = N.

(b) Solutions N = 3, q = 6

	η_a	M = 0	M = 0·5528	M = 0·7454	M = 0·8660
$-z_\xi$	0	0·7824	0·8462	0·9242	1·0221
	0·25	0·5447	0·5884	0·6418	0·7091
	0·50	0·3186	0·3433	0·3732	0·4107
	0·75	0·1219	0·1305	0·1409	0·1538
$-m_\xi$	0	0·3560	0·4034	0·4643	0·5444
	0·25	0·2532	0·2856	0·3272	0·3825
	0·50	0·1524	0·1703	0·1934	0·2242
	0·75	0·0603	0·0664	0·0743	0·0847
$-h_\xi$	0	0·3120	0·3528	0·4066	0·4803
	0·25	0·2499	0·2773	0·3129	0·3615
	0·50	0·1962	0·2109	0·2291	0·2531
	0·75	0·1100	0·1107	0·1111	0·1114

TABLE 22

Damping Derivatives for Cropped Delta Wing ($A = 1{\cdot}8$) with Oscillating Controls of Different Span.

(a) Constant Mach number $M = 0{\cdot}7454$

	η_a	N = 3	N = 2	N = 3	N = 4	N = 4*
		q = 1	q = 6	q = 6	q = 6	q = 6
$-z'_\xi$	0	-0·0470	-0·0312	-0·0463	-0·0459	-0·0455
	0·25	-	-	-0·0266	-	-
	0·50	-0·0085	-0·0087	-0·0093	-0·0081	-0·0078
	0·75	-	-	+0·0005	-	-
$-m'_\xi$	0	0·1356	0·1255	0·1329	0·1330	0·1321
	0·25	-	-	0·0946	-	-
	0·50	0·0594	0·0616	0·0574	0·0575	0·0581
	0·75	-	-	0·0234	-	-
$-h'_\xi$	0	0·3058	0·2145	0·3024	0·3383	0·3405
	0·25	-	-	0·2579	-	-
	0·50	0·2267	0·1653	0·2236	0·2353	0·2426
	0·75	-	-	0·1599	-	-

*In this solution $N' = 3$ in place of the standard $N' = N$.

(b) Solutions $N = 3$, $q = 6$

	η_a	M = 0	M = 0·5528	M = 0·7454	M = 0·8660
$-z'_\xi$	0	0·1191	0·0549	-0·0463	-0·2115
	0·25	0·0844	0·0414	-0·0266	-0·1380
	0·50	0·0516	0·0282	-0·0093	-0·0711
	0·75	0·0215	0·0135	+0·0005	-0·0214
$-m'_\xi$	0	0·1139	0·1245	0·1329	0·1346
	0·25	0·0806	0·0880	0·0946	0·0984
	0·50	0·0493	0·0536	0·0574	0·0600
	0·75	0·0204	0·0220	0·0234	0·0243
$-h'_\xi$	0	0·1957	0·2362	0·3024	0·4328
	0·25	0·1733	0·2059	0·2579	0·3576
	0·50	0·1597	0·1854	0·2236	0·2903
	0·75	0·1275	0·1417	0·1599	0·1840

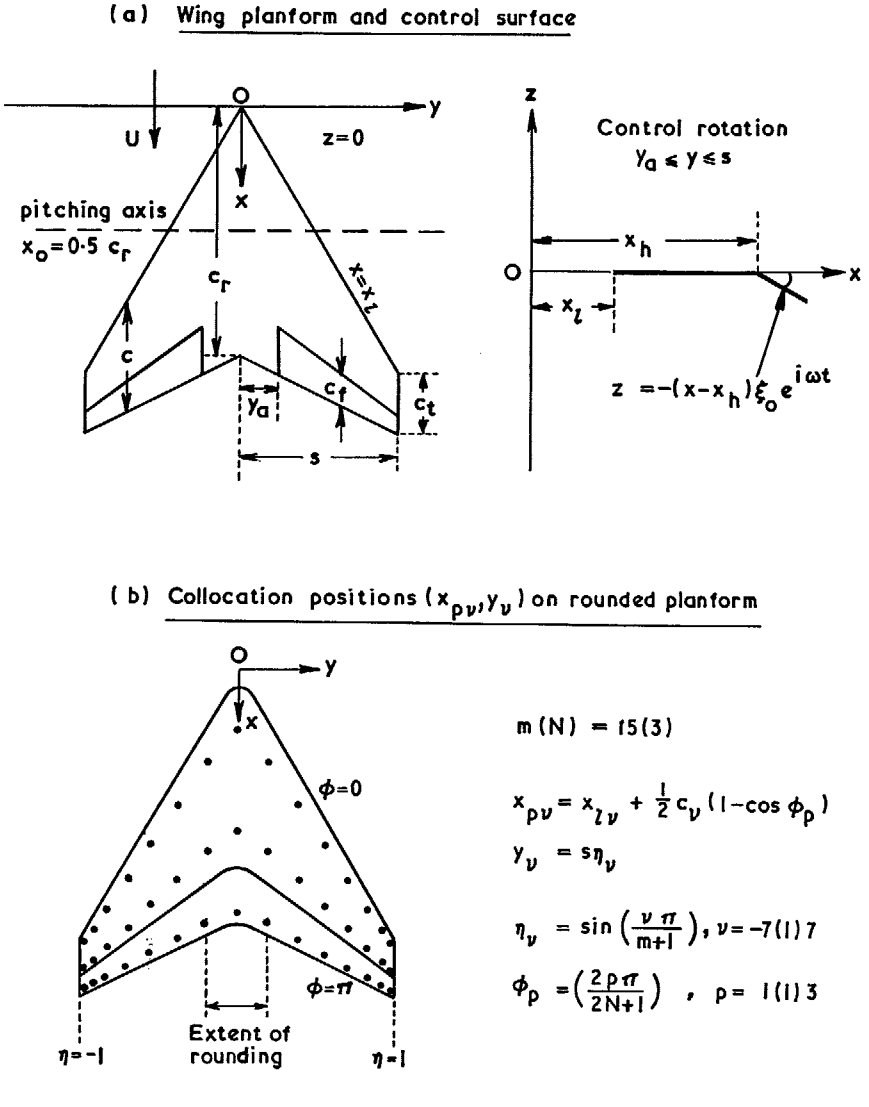

FIG. 1. Definition of symbols relating to wing geometry.

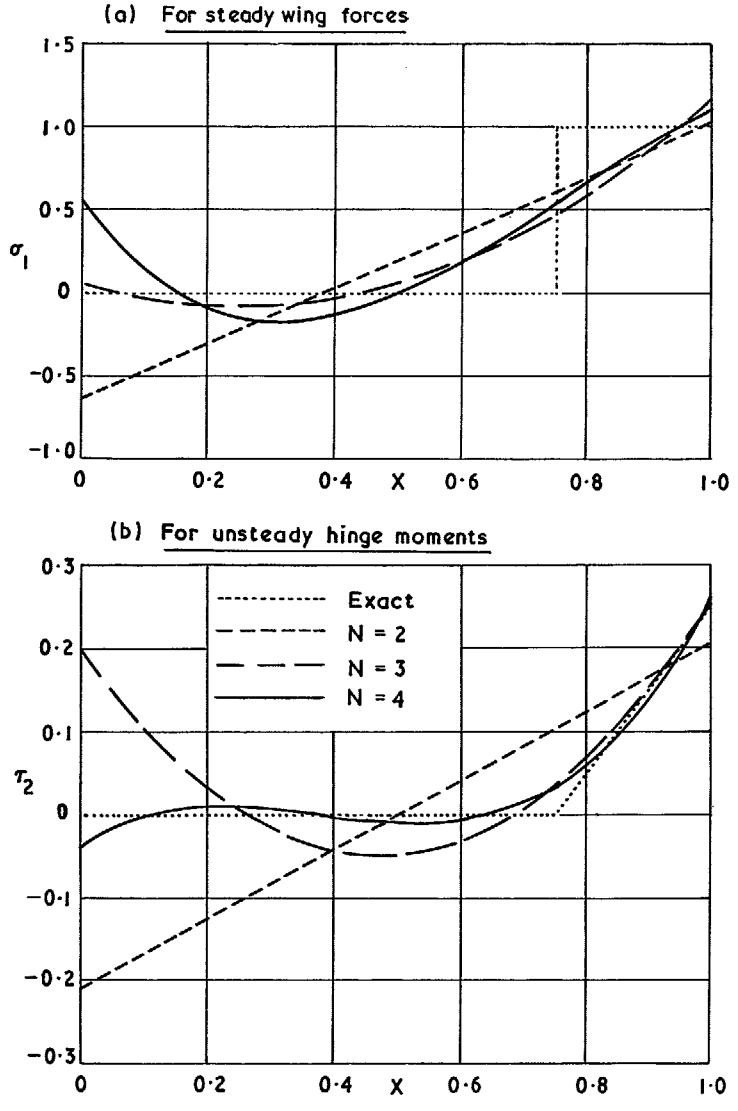

FIG. 2. Smooth chordwise equivalent slopes to represent two-dimensional control deflection ($E = 0{\cdot}25$).

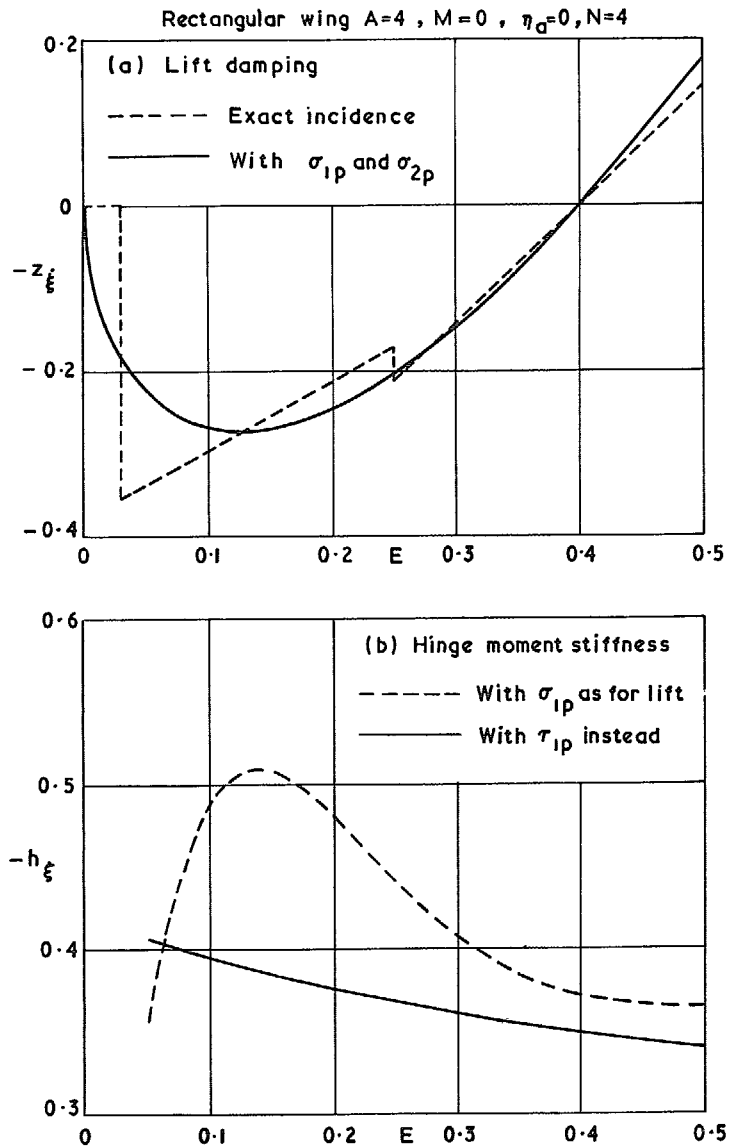

FIG. 3. Importance of chordwise equivalent slopes over a range of control size.

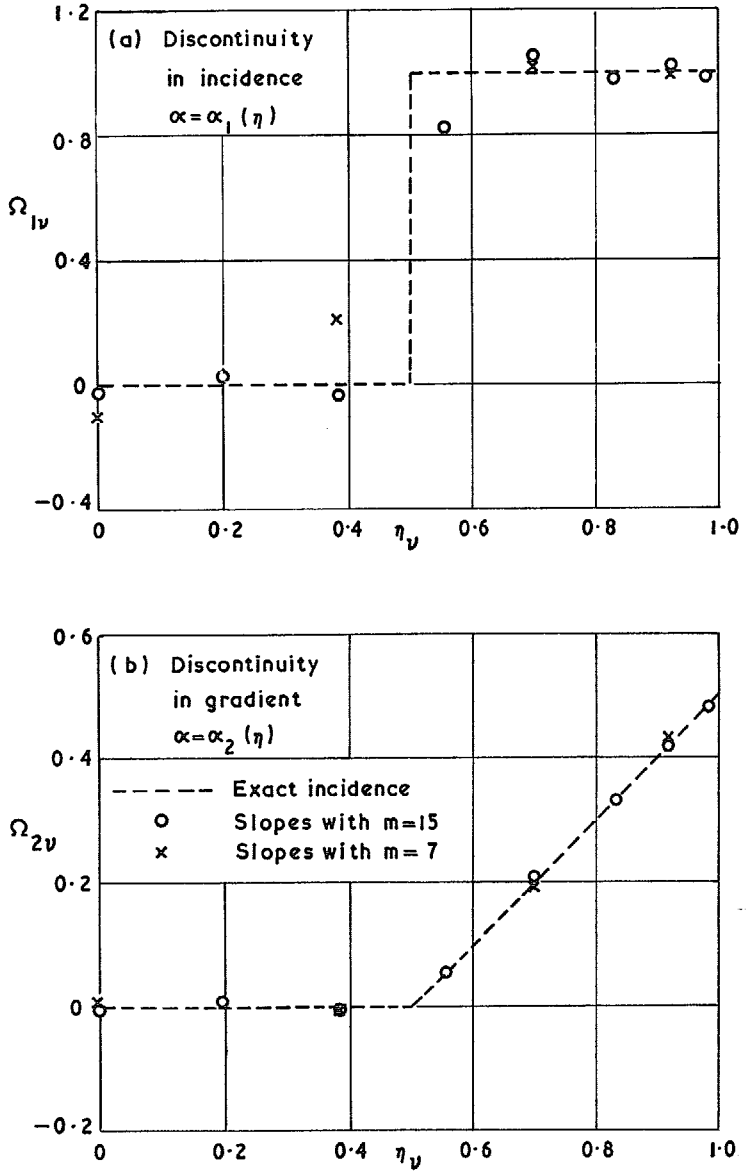

FIG. 4. Smooth spanwise equivalent slopes to represent symmetrical part-span control deflection ($\eta_a = 0{\cdot}5$).

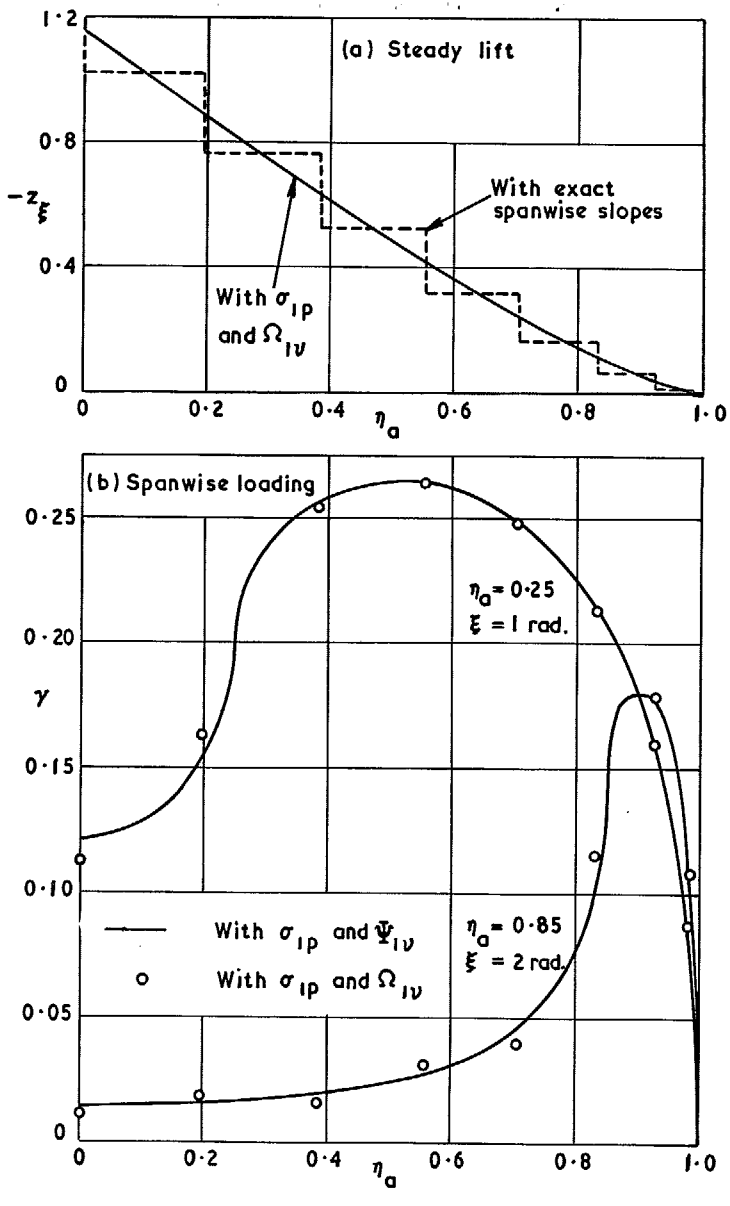

FIG. 5. Importance of spanwise equivalent slopes for part-span controls.

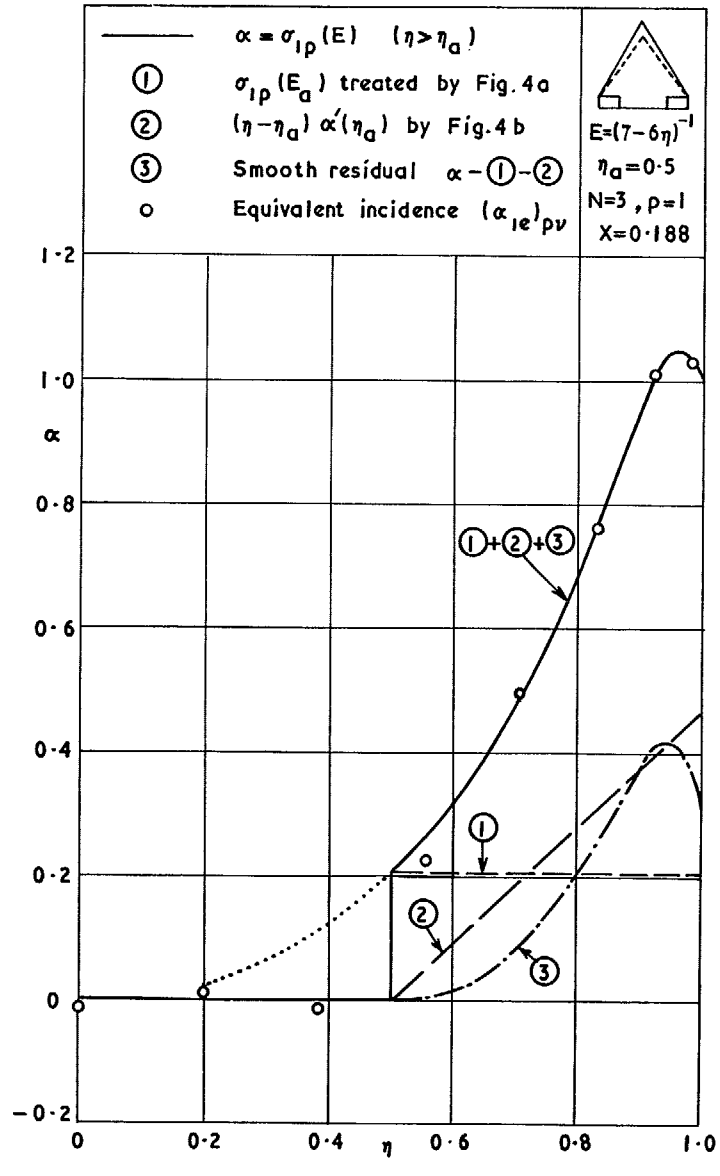

FIG. 6. Procedure for obtaining the spanwise distribution of smooth equivalent incidence.

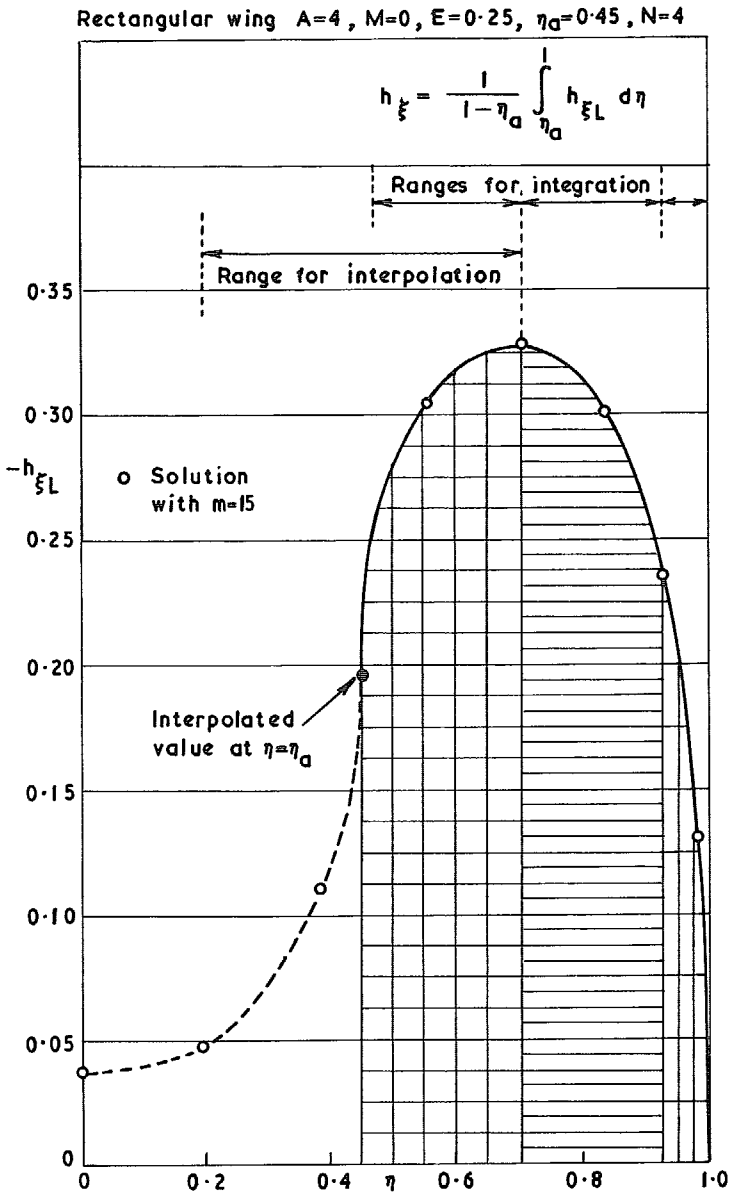

FIG. 7. Procedure for spanwise integration of hinge moment.

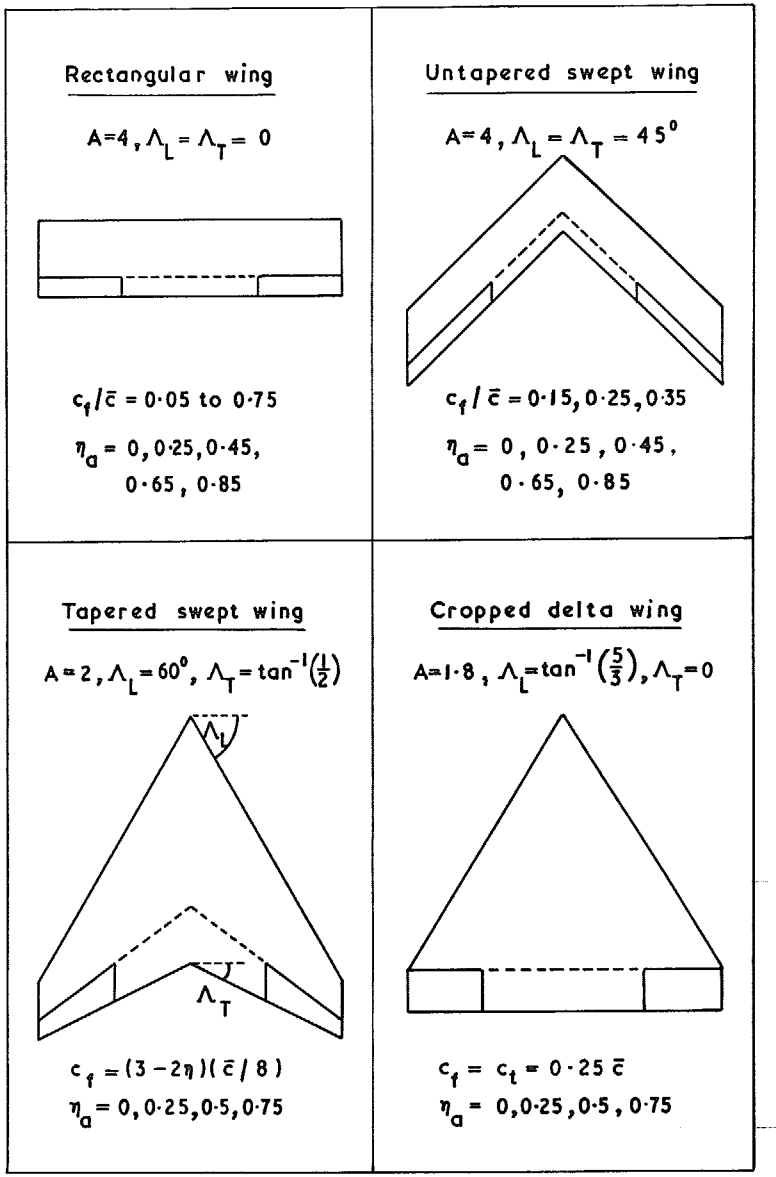

FIG. 8. Four planforms with various part-span controls.

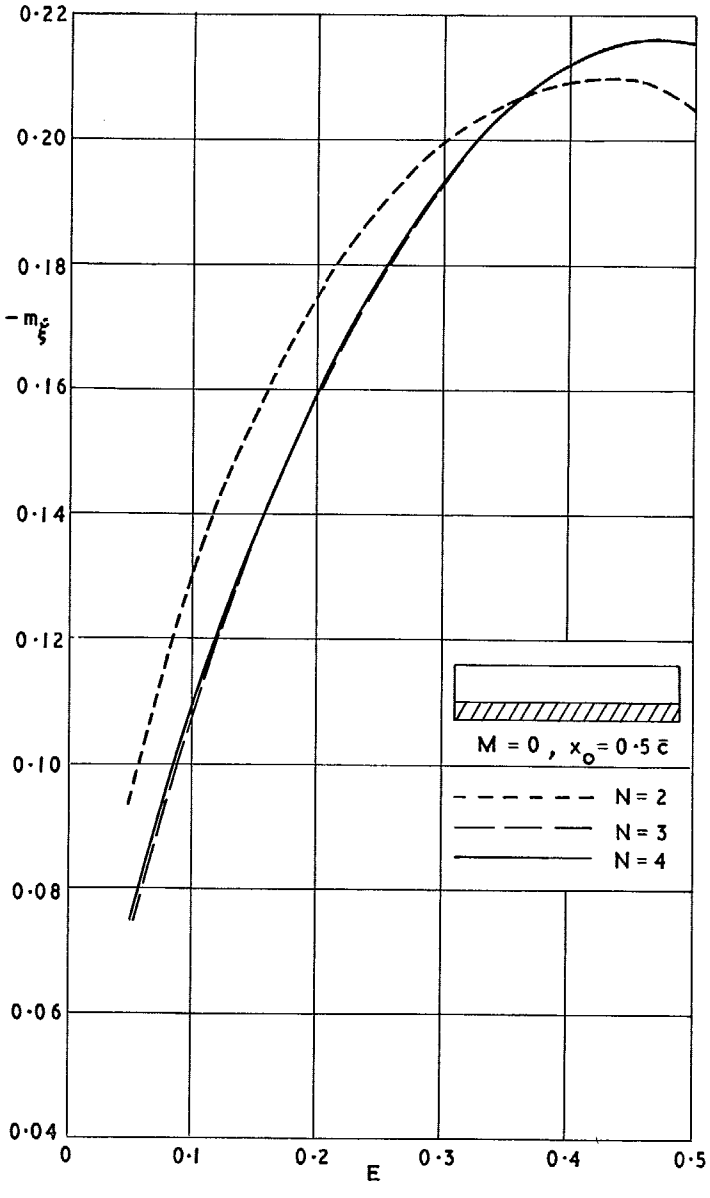

FIG. 9. $-m_\xi$ against E for rectangular wing with full-span controls, showing convergence with respect to N.

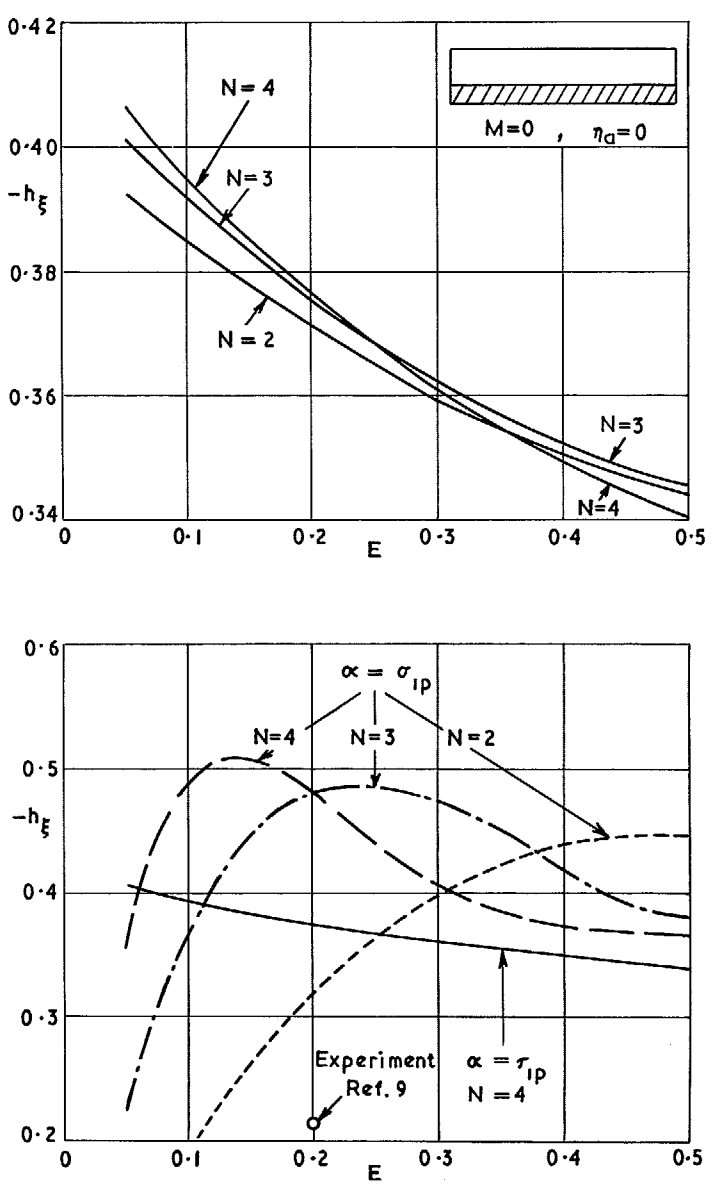

FIG. 10. $-h_\xi$ against E for rectangular wing with full-span controls, showing improved convergence with respect to N.

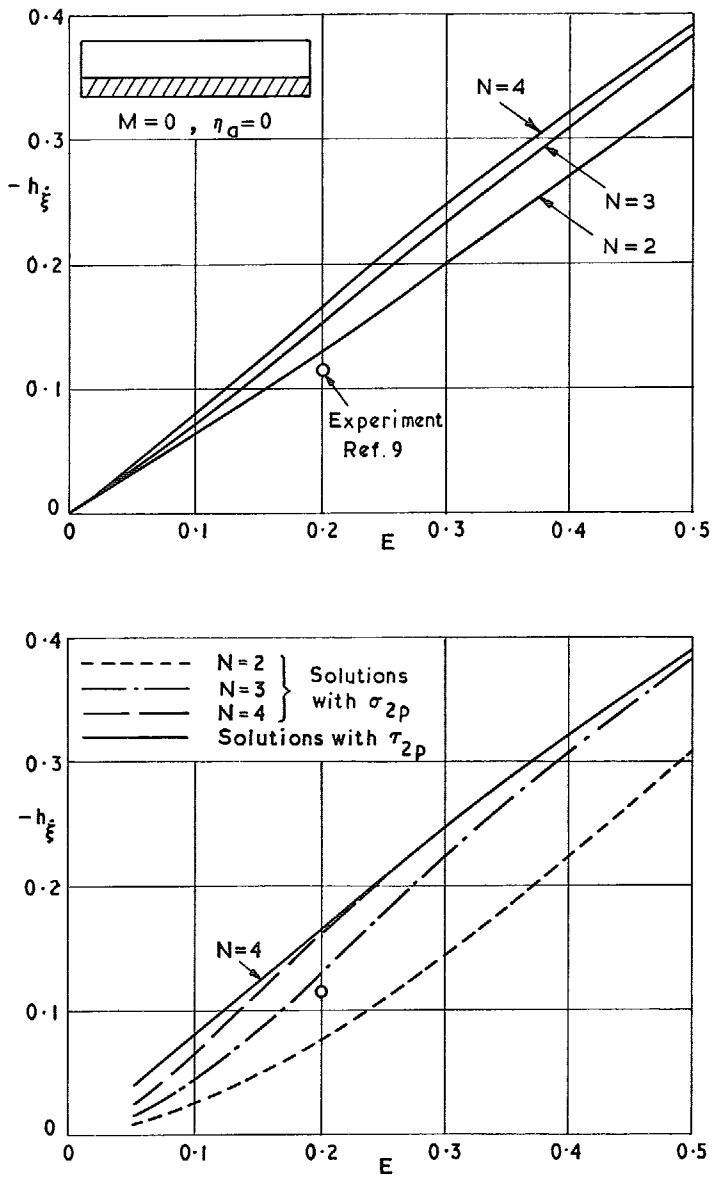

FIG. 11. $-h_\xi$ against E for rectangular wing with full-span controls, showing convergence with respect to N.

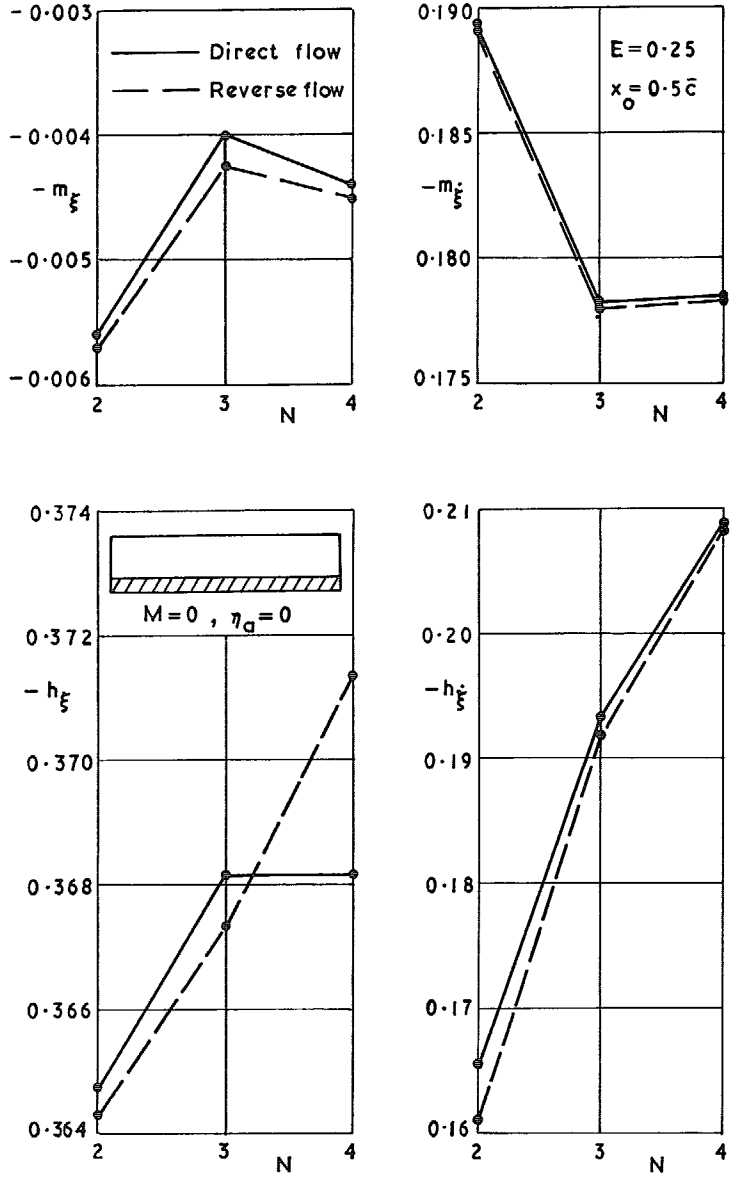

FIG. 12. Convergence with respect to N of pitching and hinge moments for rectangular wing with full-span control.

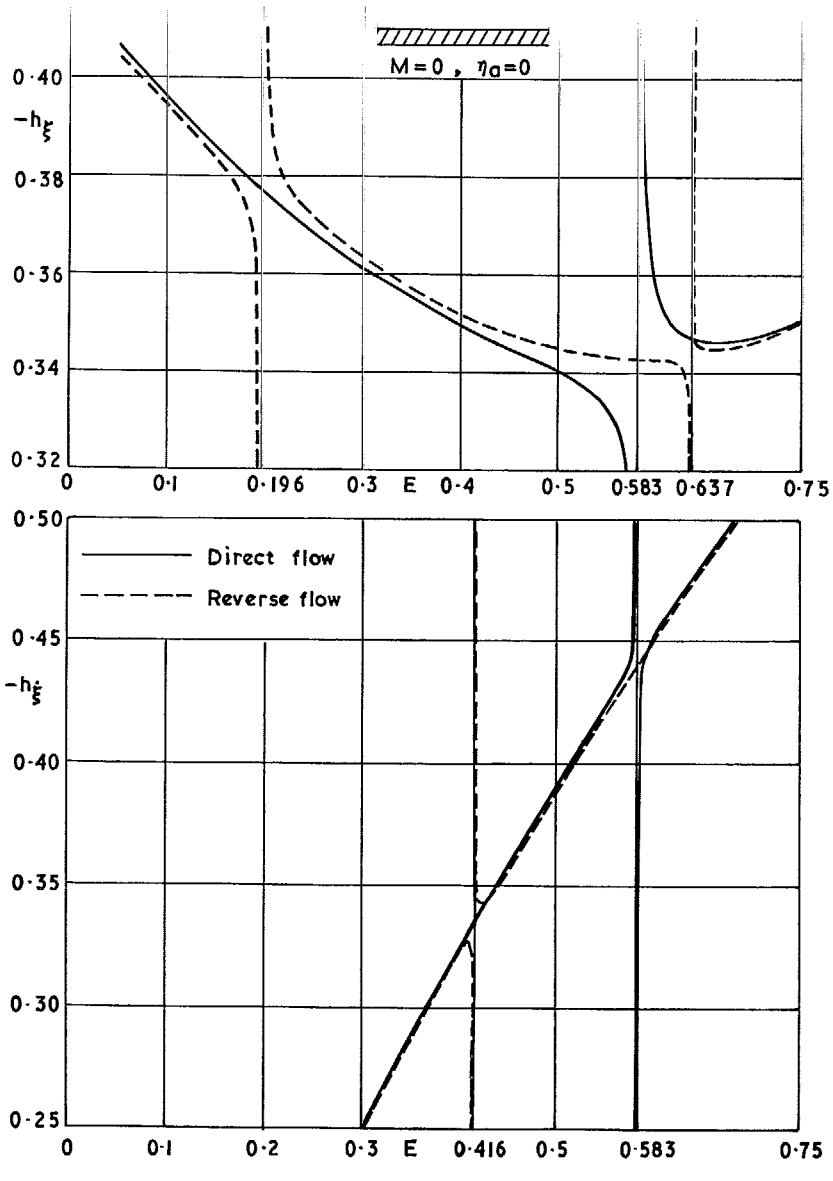

FIG. 13. Singularities in hinge moment from solutions ($N = 4$) in direct and reverse incompressible flow over a range of E.

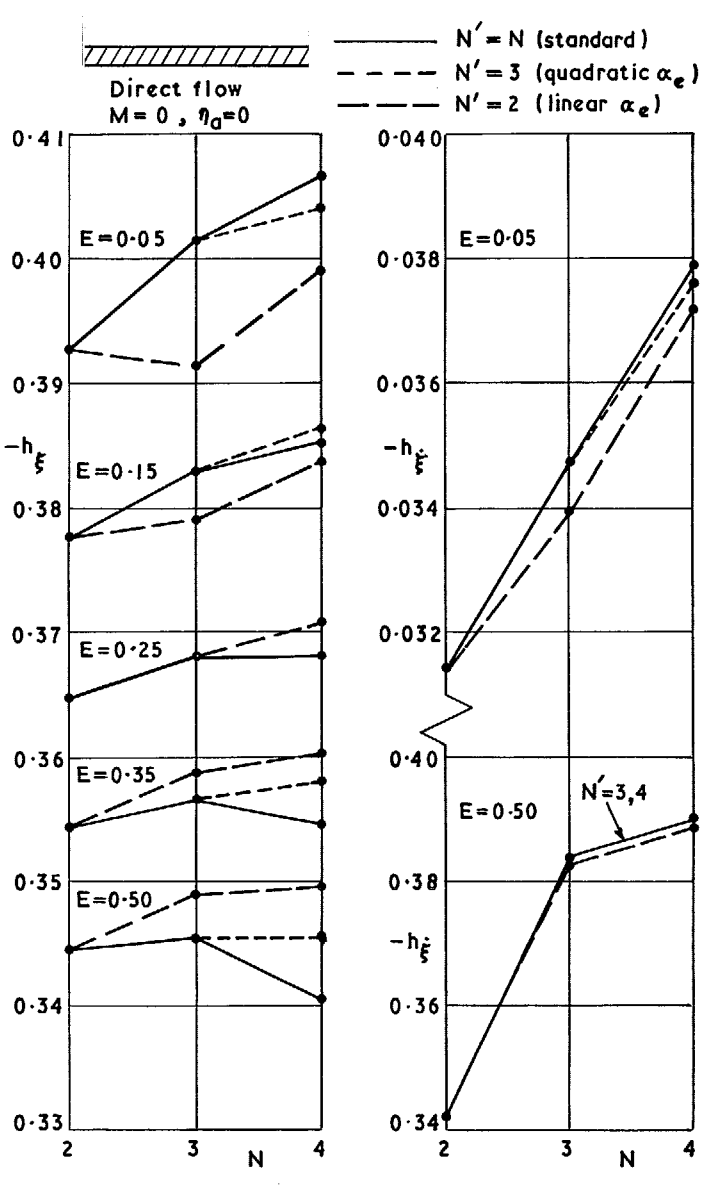

FIG. 14. Influence of N' on convergence of hinge moments with respect to N.

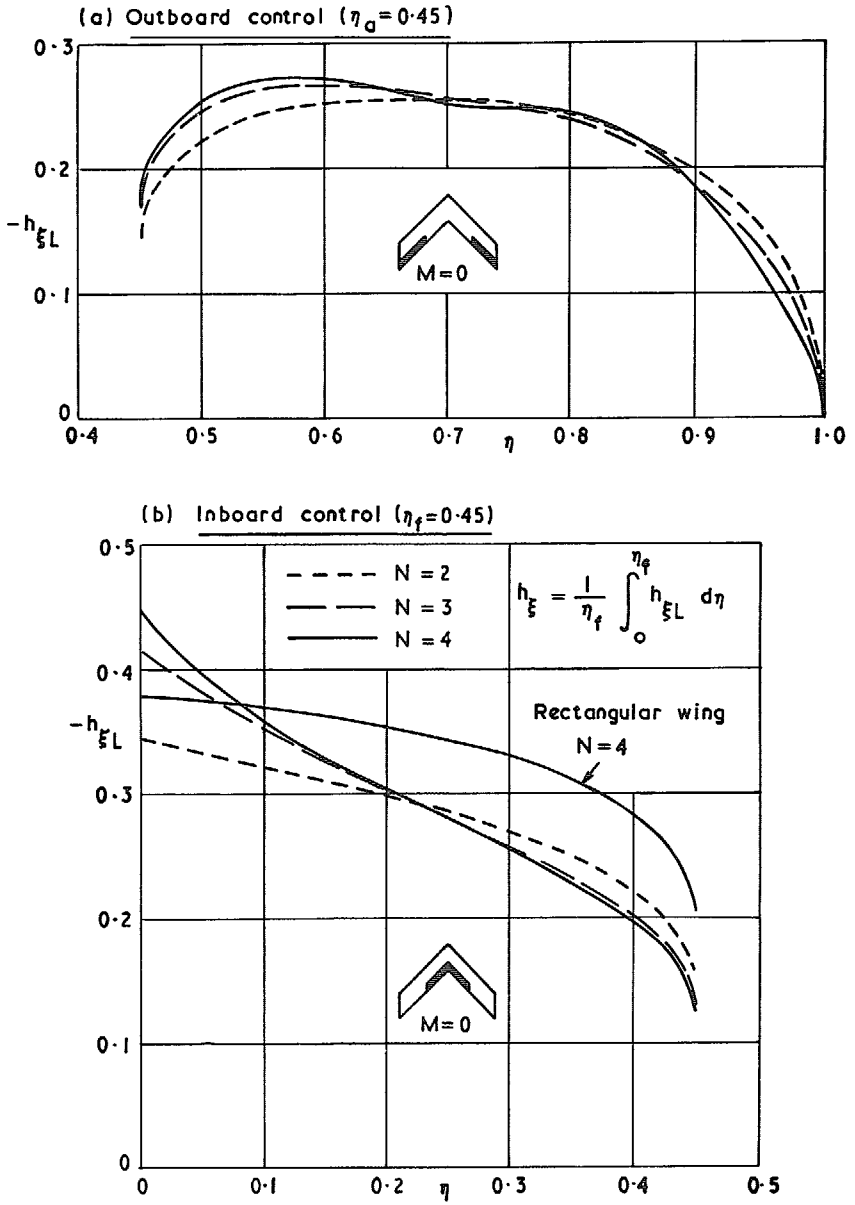

FIG. 15. Spanwise distributions of hinge moment on untapered swept wing with part-span controls (E = 0·25).

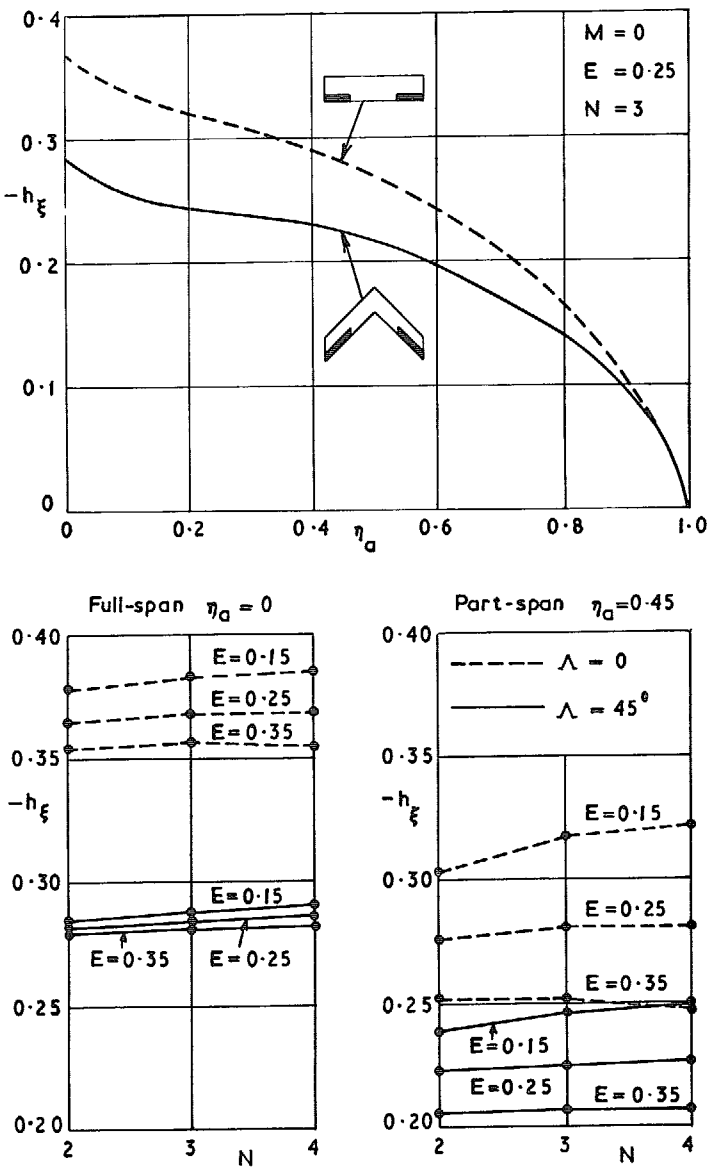

FIG. 16. Steady hinge moment on unswept and swept wings of constant chord.

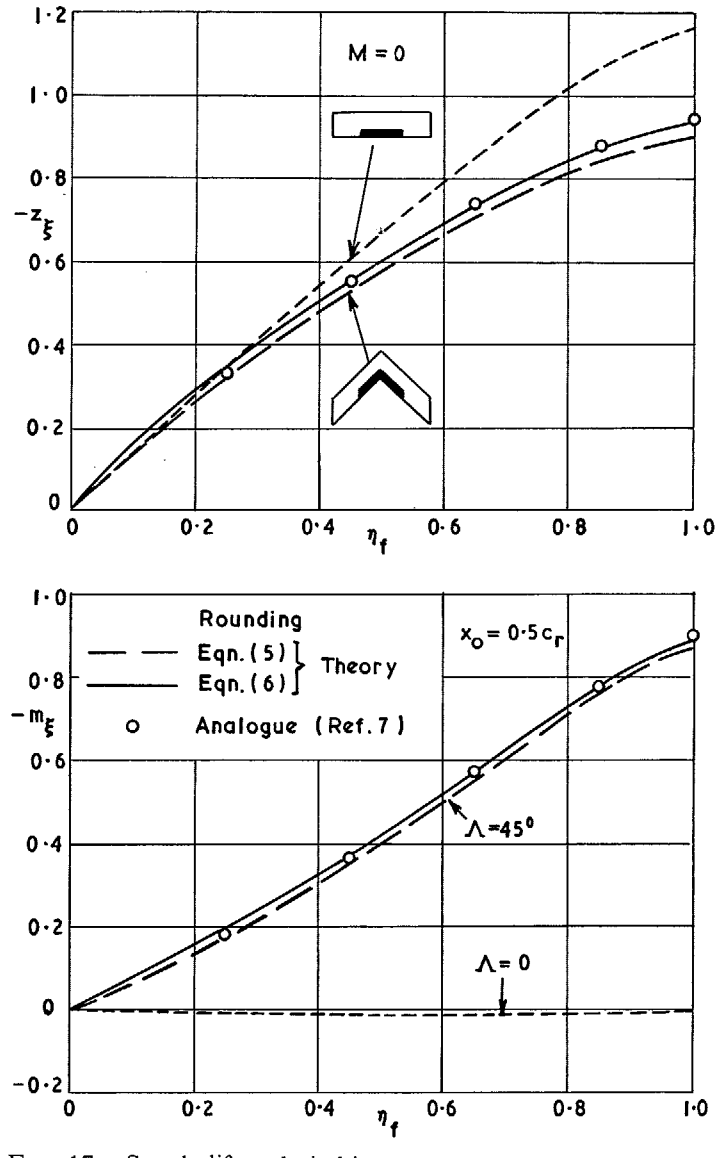

FIG. 17. Steady lift and pitching moment on unswept and swept wings of constant chord with inboard flaps ($E = 0{\cdot}25$).

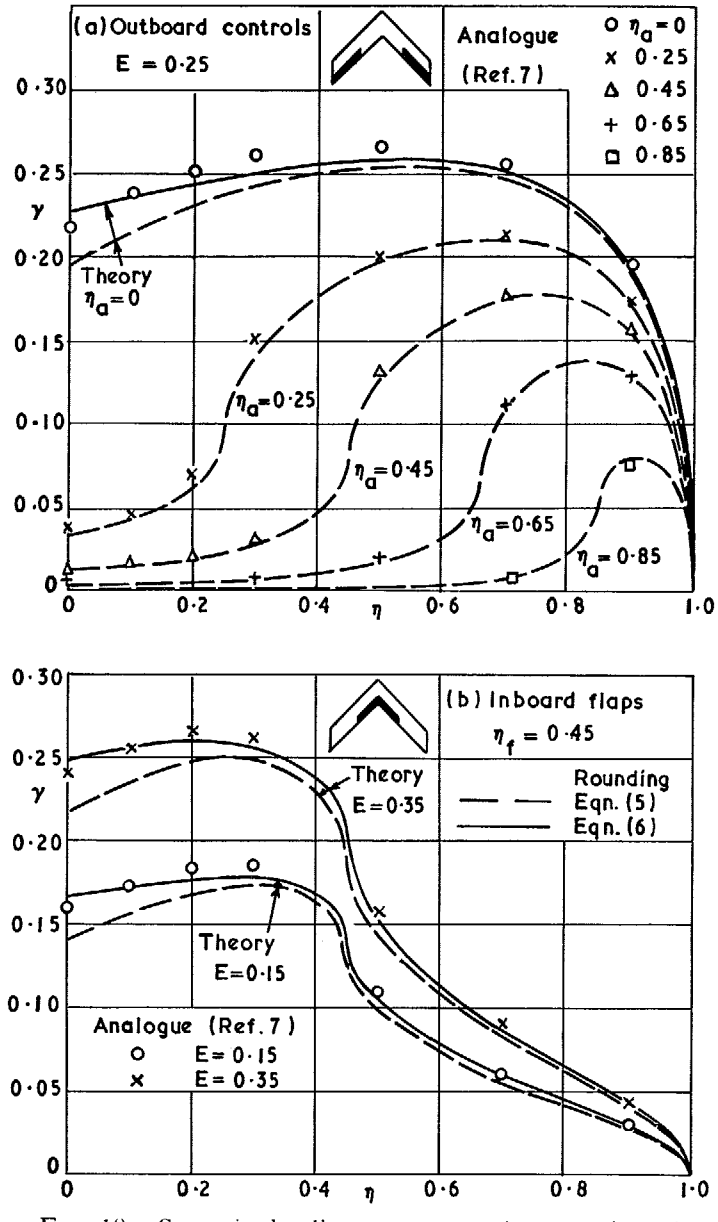

FIG. 18. Spanwise loading on untapered swept wing with part-span controls from theory and analogue ($M = 0$).

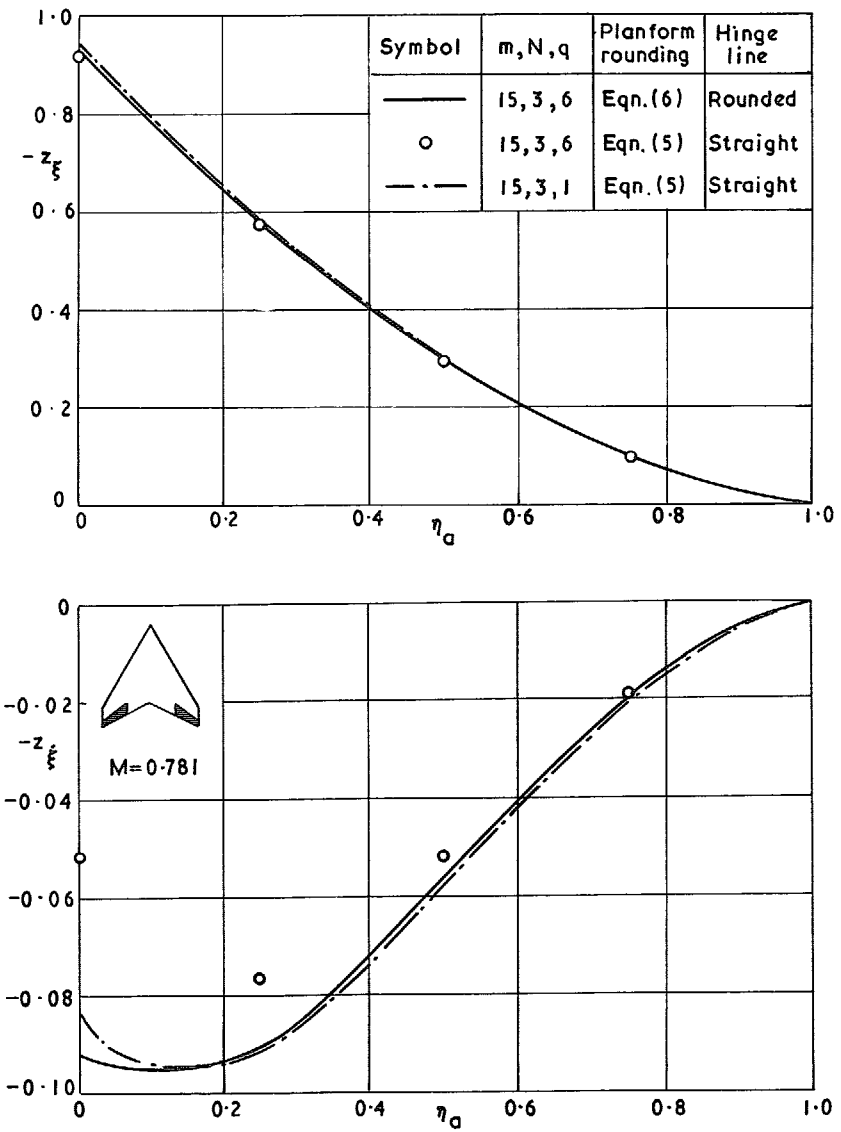

FIG. 19. Lift derivatives against control span for tapered swept wing.

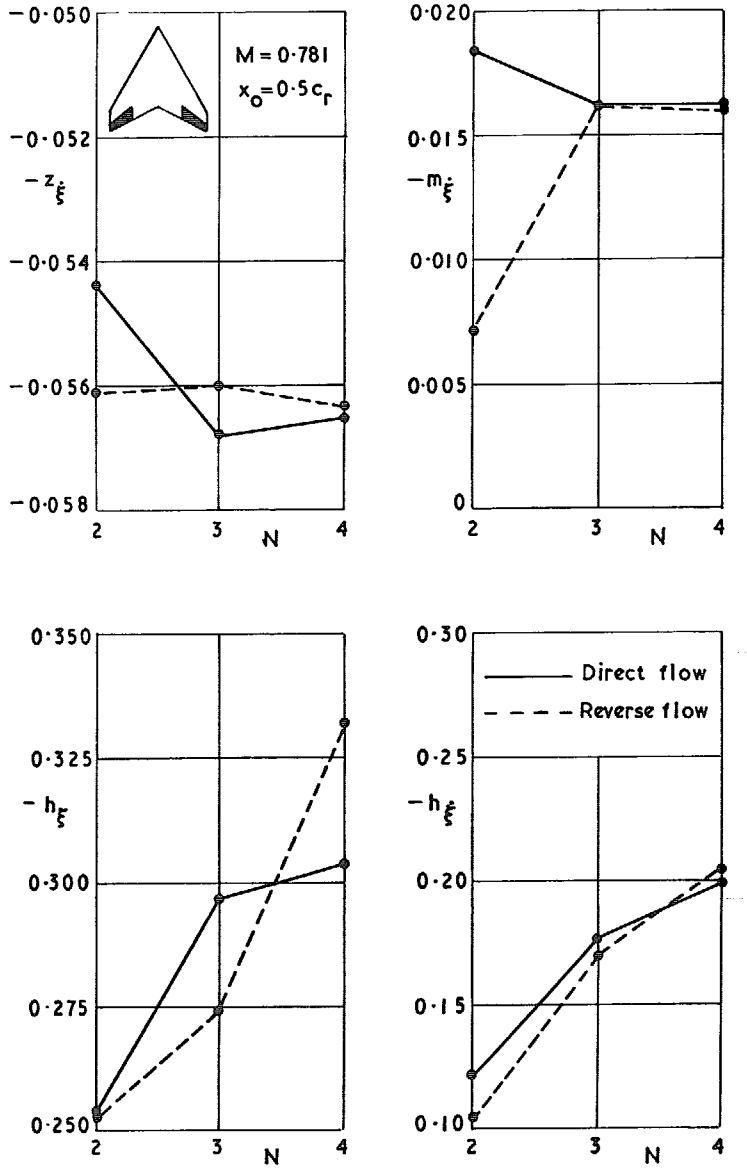

FIG. 20. Convergence with respect to N of derivatives for tapered swept wing with oscillating part-span control ($\eta_a = 0{\cdot}5$).

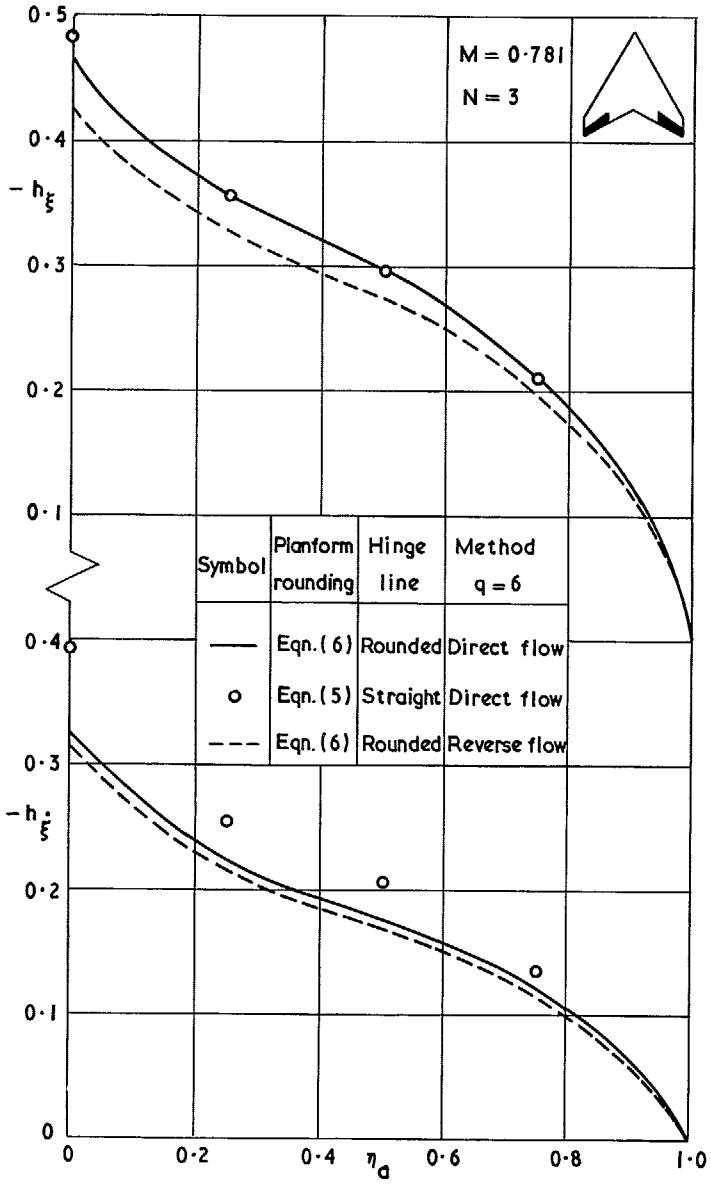

FIG. 21. Hinge moment against control span for tapered swept wing.

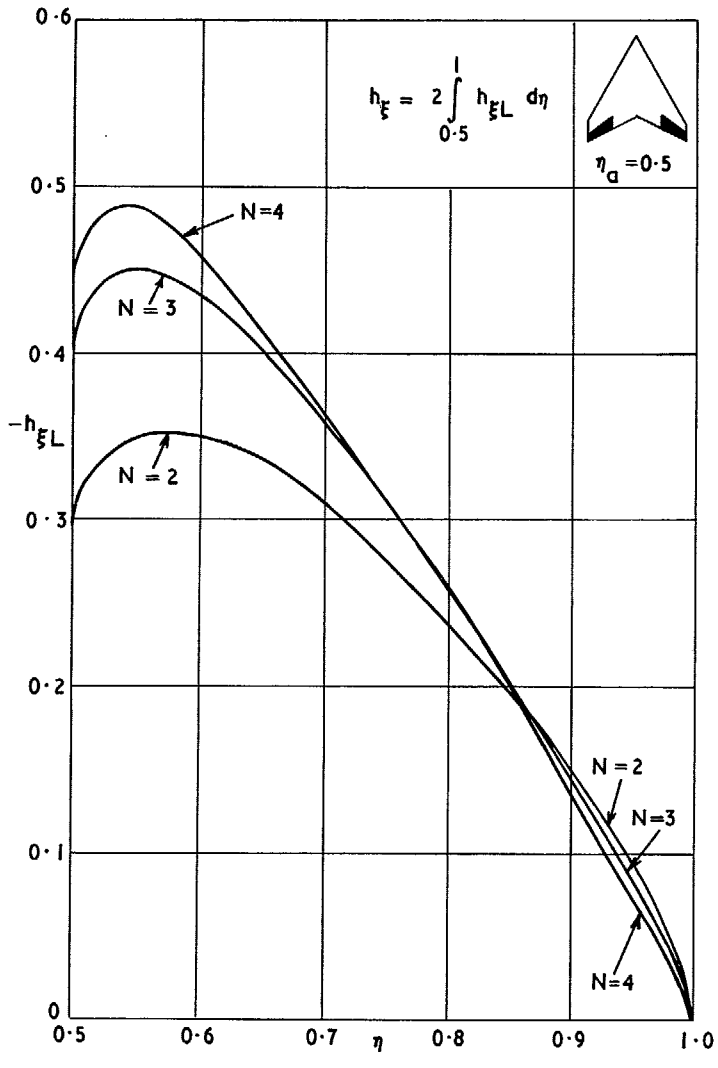

FIG. 22. Steady spanwise distribution of hinge moment on tapered swept wing with 2, 3 and 4 chordwise terms (M = 0·781).

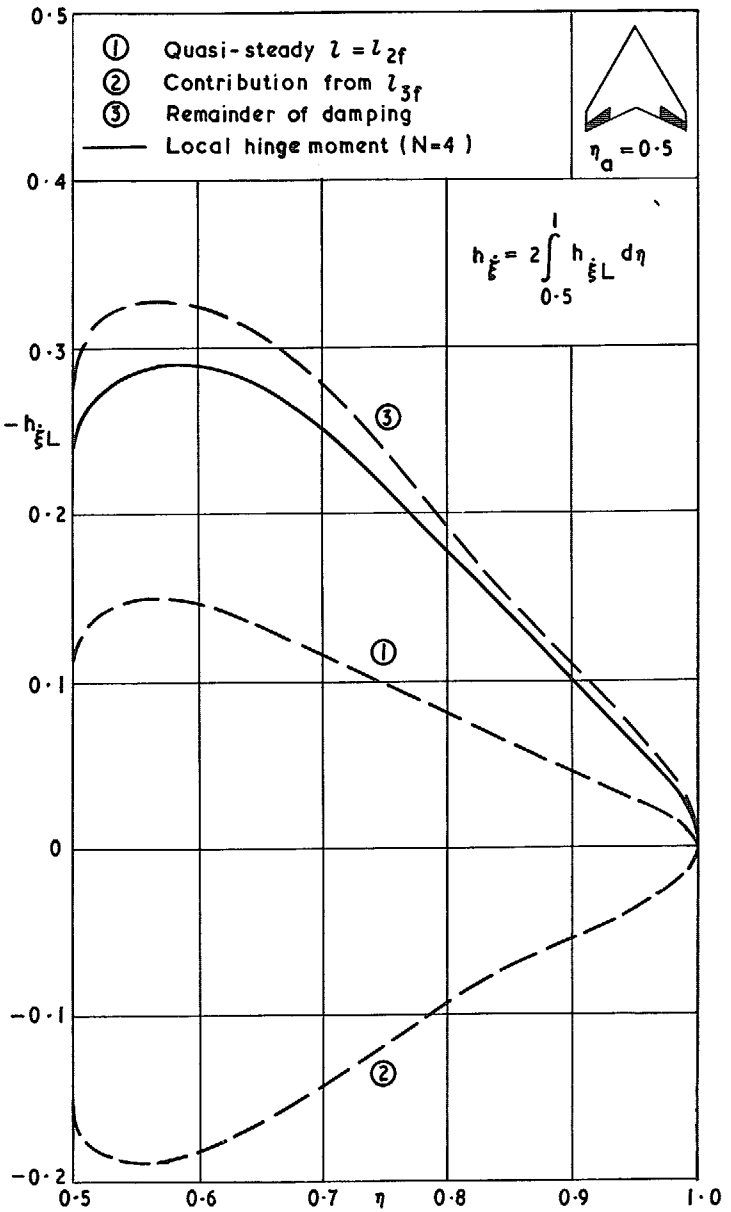

FIG. 23. Three contributions to the spanwise distribution of damping of an oscillating part-span control ($M = 0{\cdot}781$).

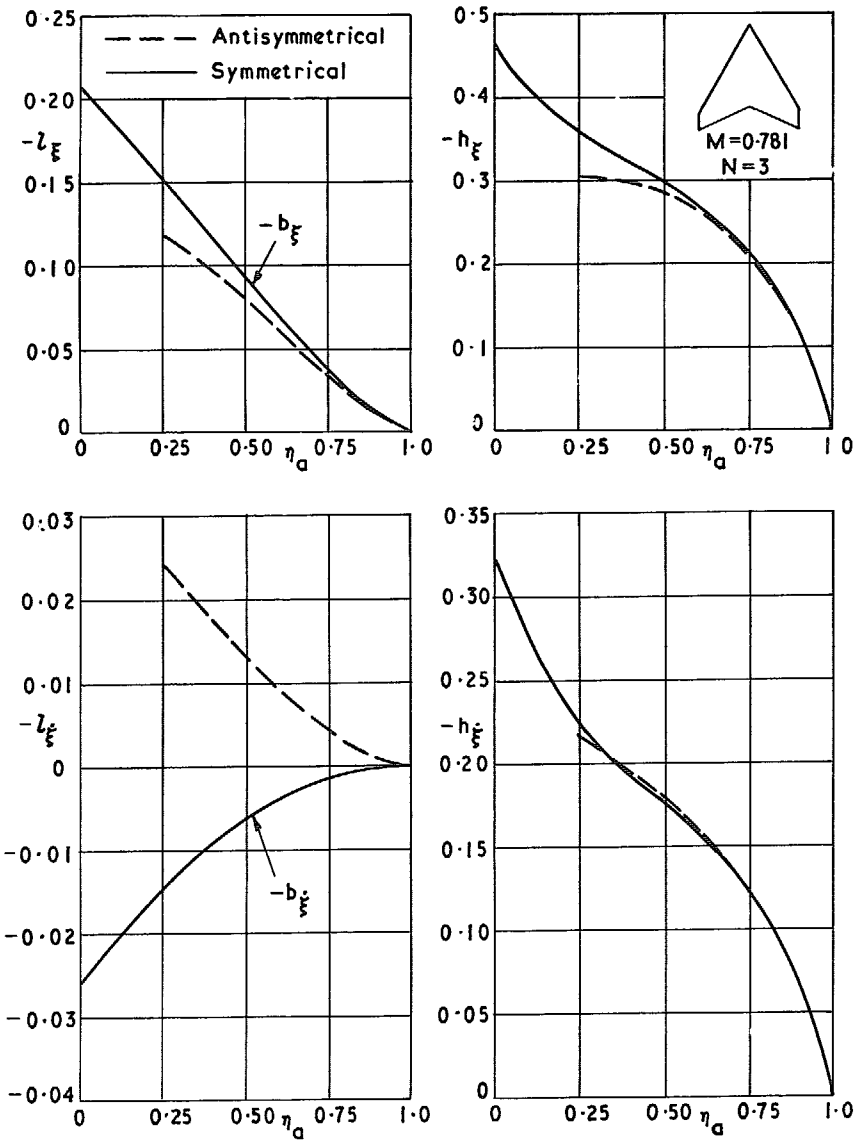

FIG. 24. Rolling and hinge moments on tapered swept wing with antisymmetrical and symmetrical part-span controls.

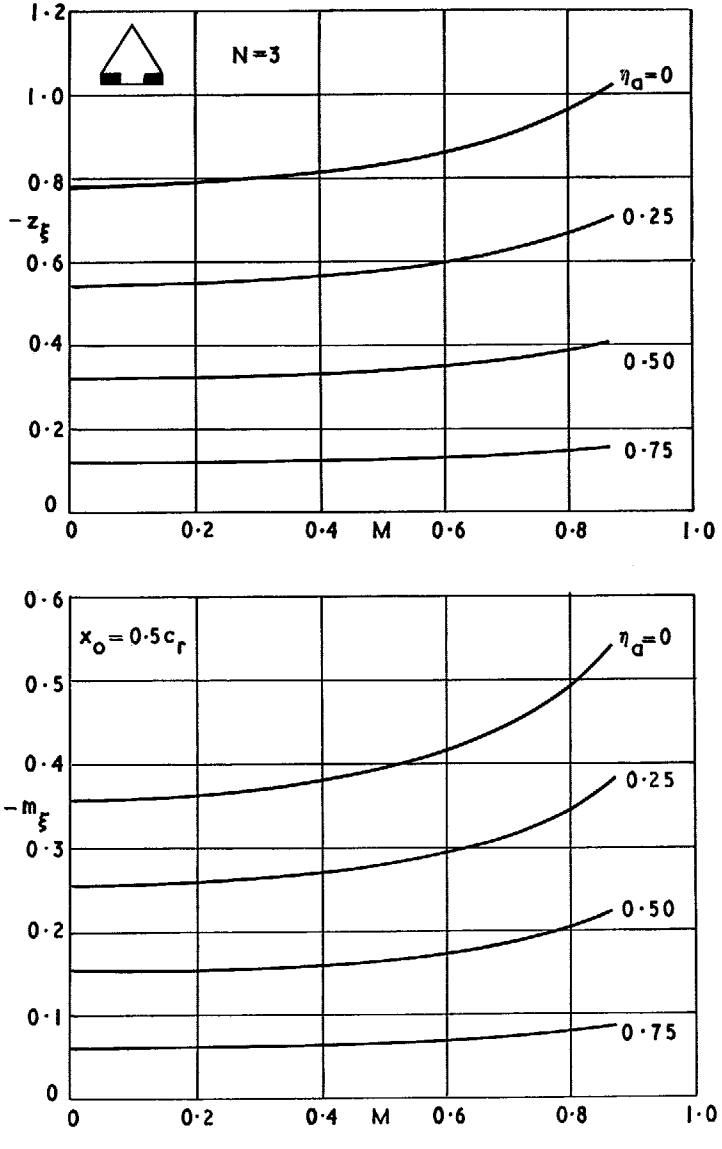

FIG. 25. $-z_\xi$ and $-m_\xi$ against M for cropped delta wing with part-span controls.

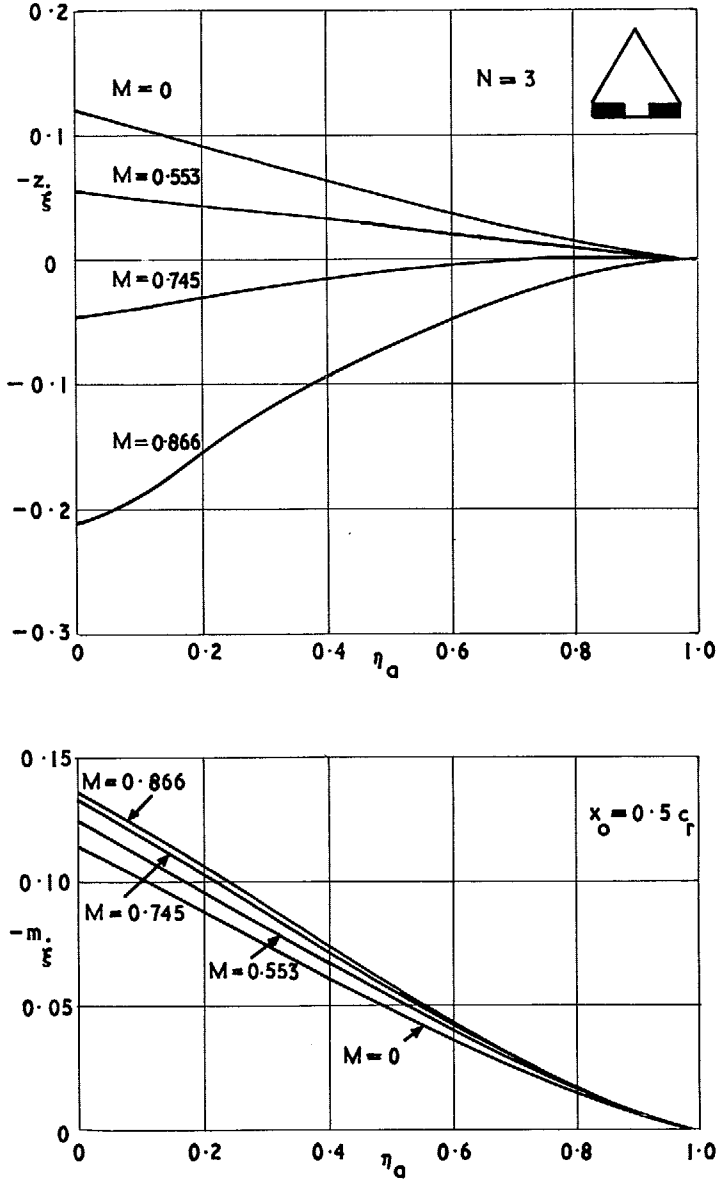

FIG. 26. $-z_\xi$ and $-m_\xi$ against η_a for cropped delta wing with part-span controls.

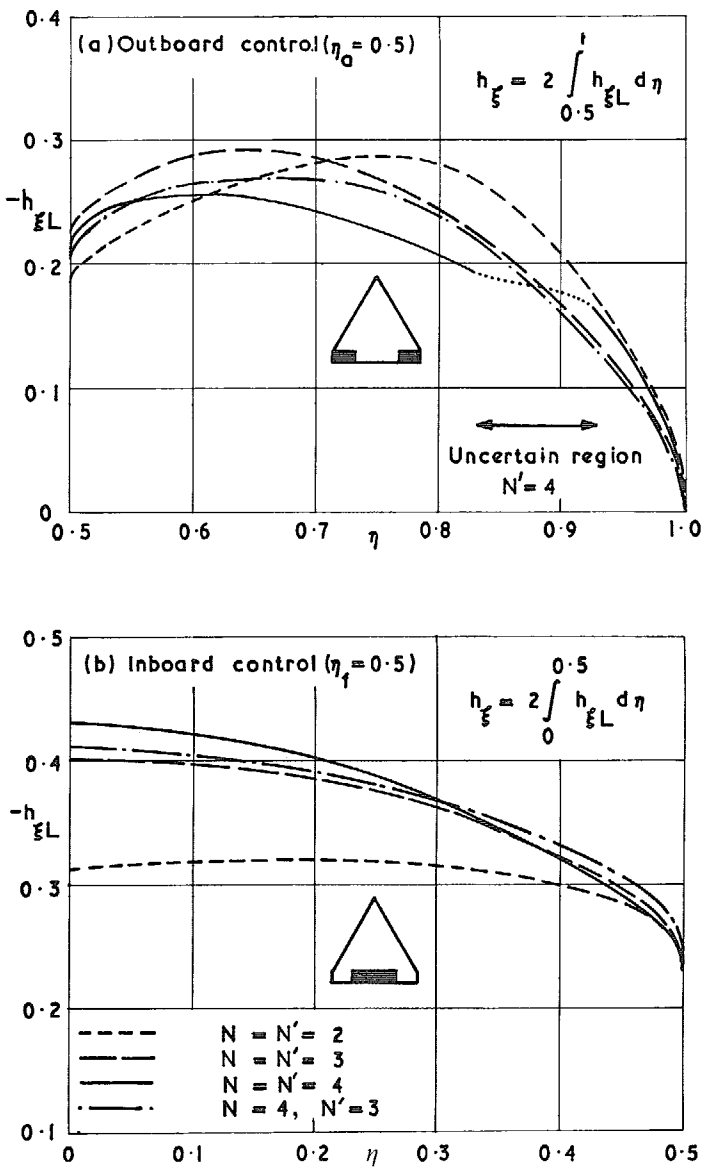

FIG. 27. Steady spanwise distributions of hinge moment on cropped delta wing with part-span controls at $M = 0.745$.

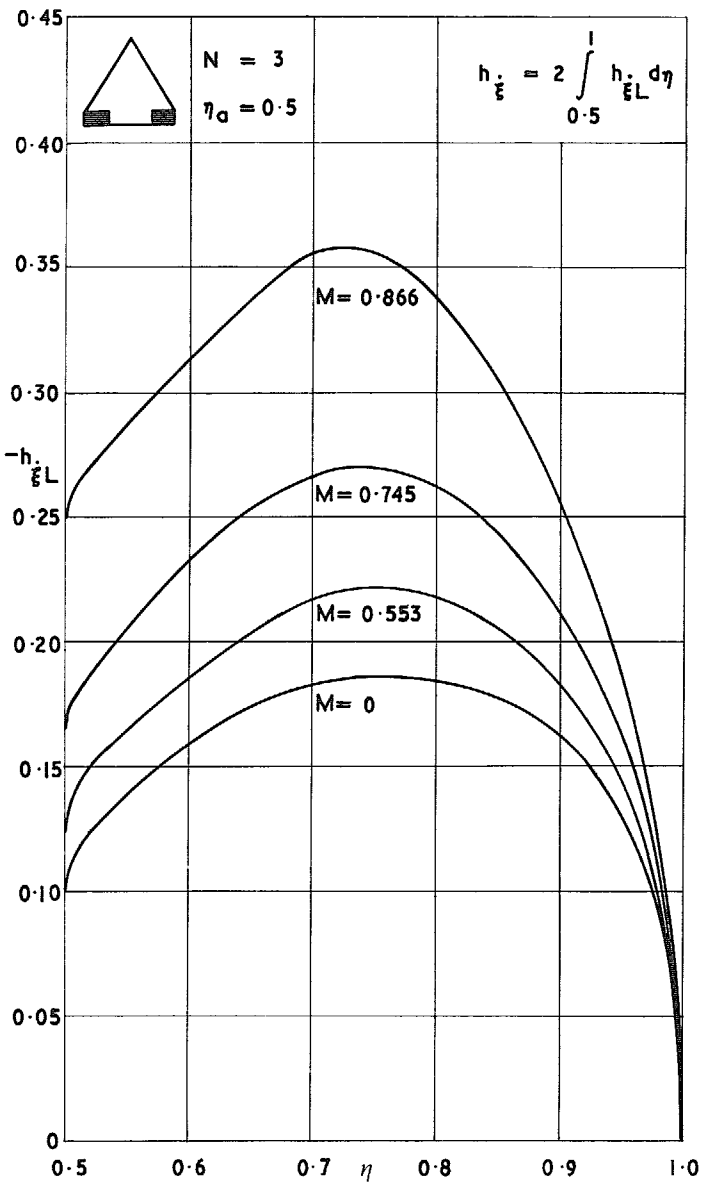

FIG. 28. Spanwise distribution of damping of an oscillating part-span control on cropped delta wing at four Mach numbers.

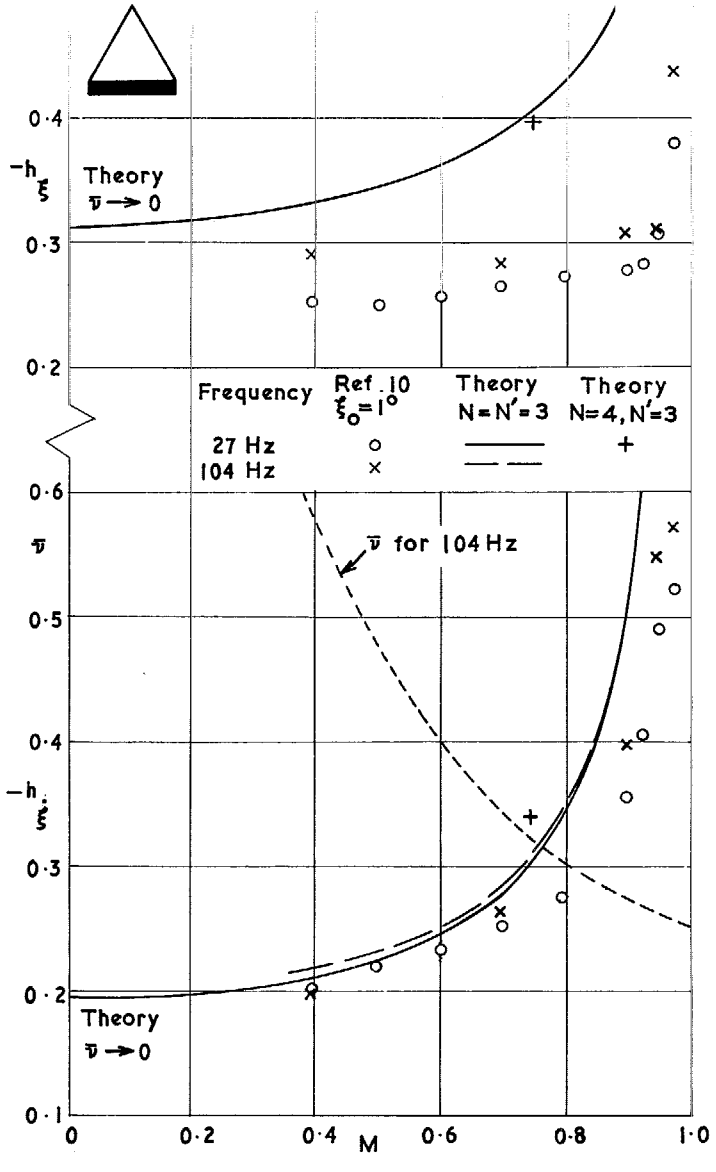

FIG. 29. Hinge-moment derivatives against M for cropped delta wing with full-span control from experiment and theory.

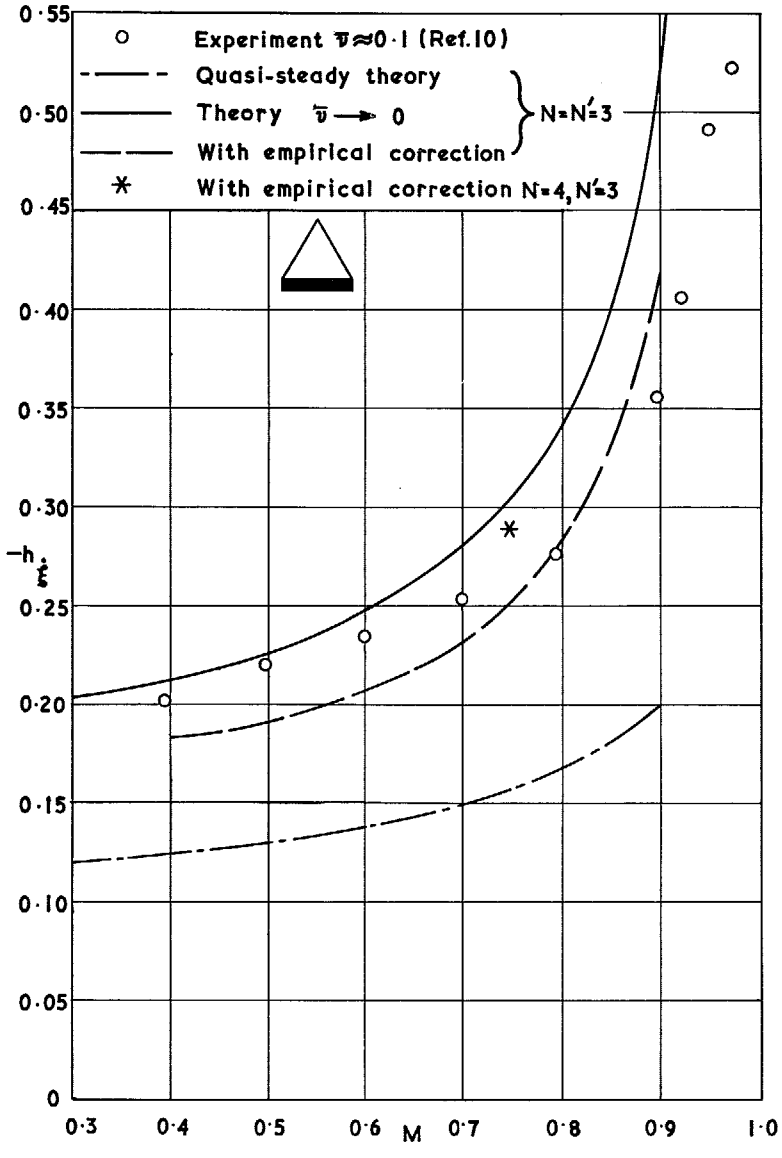

FIG. 30. Empirical correction to hinge-moment damping for cropped delta wing with full-span control.

Printed in Wales for Her Majesty's Stationery Office by Allens Printers (Wales) Ltd.
Dd. 501372 K.5.

Published by
HER MAJESTY'S STATIONERY OFFICE

To be purchased from
49 High Holborn, London WC1V 6HB
13a Castle Street, Edinburgh EH2 3AR
109 St Mary Street, Cardiff CF1 1JW
Brazennose Street, Manchester M60 8AS
50 Fairfax Street, Bristol BS1 3DE
258 Broad Street, Birmingham B1 2HE
80 Chichester Street, Belfast BT1 4JY
or through booksellers

SBN 11 470416 3*